AD NUMBER
AD360874
CLASSIFICATION CHANGES
TO: **unclassified**
FROM: **confidential**
LIMITATION CHANGES
TO: **Approved for public release, distribution unlimited**
FROM: **Distribution authorized to U.S. Gov't. agencies only; Administrative/Operational Use; 25 APR 1960. Other requests shall be referred to Director, Defense Atomic Support Agency, Washington, DC 20301.**
AUTHORITY
DNA ltr dtd 7 Nov 1980; DNA ltr dtd 7 Nov 1980

CONFIDENTIAL

CONFIDENTIAL

WT-1431

This document consists of 78 pages.

No. 147 of 170 copies, Series A

OPERATION

PLUMBBOB

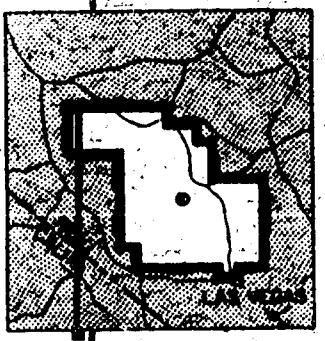

NEVADA TEST SITE

MAY-OCTOBER 1957

Project 5.2

STRUCTURAL RESPONSE AND GAS DYNAMICS OF AN AIRSHIP EXPOSED TO A NUCLEAR DETONATION (U)

Issuance Date: April 25, 1960

HEADQUARTERS FIELD COMMAND
DEFENSE ATOMIC SUPPORT AGENCY
SANDIA BASE, ALBUQUERQUE, NEW MEXICO

CONFIDENTIAL

Inquiries relative to this report may be made to

Chief, Defense Atomic Support Agency
Washington 25, D. C.

When no longer required, this document may be destroyed in accordance with applicable security regulations.

DO NOT RETURN THIS DOCUMENT

AEC Technical Information Service Extension
Oak Ridge, Tennessee

WT-1431

OPERATION PLUMBBOB–PROJECT 5.2

STRUCTURAL RESPONSE AND GAS DYNAMICS OF AN AIRSHIP EXPOSED TO A NUCLEAR DETONATION (U)

D. A. Gilstad, Project Officer
U. S. Navy Bureau of Aeronautics
Washington, D. C.

and

Christian G. Weeber
Arnold Kviljord
Gordon W. Woods
Aeronautical Structures Laboratory
U. S. Naval Air Material Center
Philadelphia, Pennsylvania

FOREWORD

This report presents the final results of one of the 46 projects comprising the military-effects program of Operation Plumbbob, which included 24 test detonations at the Nevada Test Site in 1957.

For overall Operation Plumbbob military-effects information, the reader is referred to the "Summary Report of the Director, DOD Test Group (Programs 1 to 9)," Report ITR-1445, which gives (1) a description of each detonation, including yield, zero-point location and environment, type of device, ambient atmospheric conditions, etc.; (2) a discussion of project results; (3) a summary of the objectives and results of each project; and (4) a list of project reports for the military-effects program.

ABSTRACT

Four Model ZSG-3 airships, U. S. Navy Bureau of Aeronautics Nos. 40, 46, 77, and 92, participated during Operation Plumbbob to determine the response characteristics of the Model ZSG-3 airship when subjected to a nuclear detonation in order to establish criteria for safe escape distances for airship delivery of antisubmarine warfare special weapons.

Restrained response data for 0.40-psi overpressure input were obtained during Shot Franklin with the ZSG-3 No. 77 moored tail to the blast. Unrestrained response data for 0.75-psi overpressure input were obtained during Shot Stokes with the ZSG-3 No. 40 free ballooned, tail to the blast, 300 feet aboveground.

The first airship exposed to overpressure experienced a structural failure of the nose cone when it was rammed into the mooring mast, together with a tear of the forward ballonet which necessitated deflation of the envelope. The second airship broke in half and crashed following a circumferential failure of the envelope originating at the bottom of the envelope, forward of the car. Neither airship experienced any other failure, except for damage to tail-assembly movable-surface stops from shock forces on the control surfaces. The two other project airships, Nos. 46 and 92, were torn loose from their mooring masts at the Nevada Test Site by high-intensity winds and were destroyed before participating in any shots.

In general, operation with airships within the Nevada Test Site was found to be extremely hazardous because of extreme variations in atmospheric conditions.

Histories of airship response versus time from oscillographic recording are presented for Shot Franklin. For Shot Stokes, overpressure input versus time from oscillographic ground-station recordings is presented. Unfortunately, no air-borne oscillographic recordings were obtained during Shot Stokes because of a power failure.

Primarily because of operational difficulties in the field, the scope of the data obtained was not adequate to satisfy the basic objectives of Project 5.2. However, the test results are considered to be a suitable basis for further analytical studies of airship response to nuclear blast effects beyond the scope of this report.

ACKNOWLEDGMENTS

The authors are deeply indebted to the following persons for their advice, cooperation, and active participation in the planning and in the actual execution of Project 5.2:

E. J. Jankiewicz, R. N. Nickerson, W. Turner, J. A. Holland, Jr., S. Scheindlinger, R. Lieberman, and G. Borod, all of the Aeronautical Structures Laboratory; D. D. Wallstein (CDR, USNR), Project Officer (operational phase), and personnel of the Airship Test and Development Department of the U. S. Naval Air Station, Lakehurst, New Jersey; and A. Julian (LCDR, USN), Field Command, Defense Atomic Support Agency, previously of the U. S. Navy Bureau of Aeronautics.

CONTENTS

TABLES

Chapter 1
INTRODUCTION

1.1 OBJECTIVE

The basic objective of Project 5.2 was to determine the response characteristics of the Model ZSG-3 airship when subjected to a nuclear detonation in order to establish criteria for safe escape distances for airship delivery of antisubmarine warfare (ASW) special weapons.

The results should be directly applicable to the ZSG-4 airship type and generally applicable to all other airship types.

Specifically, the test program was arranged to secure data in the following major categories: (1) dynamic response of the entire airship and its structural members to various energy input levels, (2) temperature rise and distribution in the airship envelope as a result of thermal radiation, (3) shock-wave propagation in the airship envelope, and (4) vulnerability of structural components that would restrict the weapon-delivery capabilities of the weapon system.

1.2 BACKGROUND

The ZS2G-1 and other airship models have an operational requirement for delivery of the Mark 90 and Lulu ASW weapons. The effects that define the safe escape distances for delivery of these weapons by airship are initial nuclear radiation and blast. In this regard, preliminary theoretical work, based on limited experimental data, indicated that the angle of propagation of the shock wave in air resulting from underwater detonations varies significantly with depth of burst and receiver altitude.

Studies of the response characteristics of an airship envelope have indicated the futility of attempting to predict the overall response to blast effects analytically without adequate experimental data. These data were required to substantiate the many involved assumptions and to provide information on the effects of blast which cannot be predicted at present. It was predicted that the car suspension system, in particular, would be subjected to transient loads of appreciable magnitude; and, because of the indeterminate nature of the suspension system configuration, the response characteristics would be complex. Rigid-body analyses, employing the simple relation between overpressure and the airship cross-sectional area on which the overpressure acts, yielded tremendous loads because of the large areas involved. The importance of response lag, caused by the envelope elasticity and general lack of rigidity, was also indicated. None of the sources familiar with airship characteristics offered any means of solving the overall response problem analytically.

The only feasible approach to the problem was participation in full-scale tests since it was considered essential that information be obtained as soon as possible to permit establishment of airship-delivery capabilities and response criteria.

On completion of the instrumentation of the two Model ZSG-3 airships, U. S. Navy Bureau of Aeronautics (BuAer) Nos. 46 and 77, high-explosive blast tests were conducted at the U. S. Naval Air Station, Lakehurst, N. J., with the airship moored in a manner similar to that planned for use at the Nevada Test Site (NTS). Airship response to maximum overpressures of approximately 0.15 psi was measured for 50-pound TNT blasts 750 to 1,500 feet from the airship tail. Similar response data were obtained with one of the airships in flight. High-speed motion pictures (1,000 frames/sec) were also obtained during the moored tests. In addition to checking out instrumentation functioning and test procedures, it was hoped that recorded data might be used to support data obtained at NTS. However, the positive overpressure phase (approximately $\frac{1}{60}$ second) from the small high-explosive blasts was so brief that the results had only limited qualitative value.

1.3 GENERAL DESCRIPTION OF AIRSHIP

The Model ZSG-3 airship was a two-engine nine-place nonrigid airship used primarily for antisubmarine-search missions in collaboration with other ASW air and surface craft. The airship was powered by two Pratt & Whitney R-1340-50 engines housed in nacelles outboard from the car. The airship was stabilized in flight by upper and lower vertical surfaces and two horizontal surfaces, one on each side of the envelope. Armament stores could be carried on internal and external bomb racks. Principal dimensions of the airship are shown in Figure 1.1.

The airship had a nonrigid, streamlined, helium-inflated envelope fabricated from a series of patterns cut from cotton-neoprene fabric. Each fabric pattern was identified by a gore letter and panel number, as shown in Figure 1.2. The 98 envelope panels were numbered from bow to stern as follows: 0 to 38, W, X, Y, Z, and 39 to 93. Gores extended the length of the envelope and were lettered from A, on the bottom port side, around the circumference of the envelope to L, on the starboard side. The outside envelope surfaces exposed to the weather were covered with neoprene-base aluminum paint, which protected the envelope fabric and reduced superheat (the temperature differential between the ambient air and the helium).

The envelope, which had a total volume of 527,000 ft^3, contained two air ballonets, one located forward and the other aft in the envelope. Each ballonet had a volume of approximately 62,500 ft^3. Rip panels on top of the envelope permitted quick deflation of the envelope in case of emergency.

The envelope included internal and external catenary curtains to carry the load of the airship car. The internal catenary curtain assemblies, which consisted of a 30-degree set and a 60-degree set on each side of the envelope, extended approximately from envelope Panels 20 to 61. Details of the internal suspension systems are shown in Figure 1.3. The internal catenaries, which normally carry 86 percent of the vertical car load, were sewed and cemented to the upper inside envelope surface on the opposite sides of the upper longitudinal centerline. The internal suspension cables attached to the load points on the internal catenary curtains and extended downward through cable sleeves in the air line and car cover to suspension fittings on the car.

The external catenary curtains, which extended from Panels 36 to 46, were cut from continuations of the envelope panels and were then reinforced along the cut edges. External suspension cables attached to 20 load points on the outside catenaries to carry, normally, 14 percent of the vertical car load (tie cables) and to take the longitudinal and lateral forces on the car (surge cables). Details of the external suspension system are shown in Figure 1.4.

The total design weight of the car, including fuel, crew, gas pressure, and other equipment, was 24,000 pounds. The internal and external suspension cables (all of which were adjustable) and the catenary curtains uniformly distributed on the envelope the loads imposed by car weight, gas pressure, propeller thrust, and other forces.

The empennage consisted of four fins mounted symmetrically along the vertical and horizontal planes of the envelope between envelope Panels 68 and 82. The fins, which were rigid aluminum-channel structures, were fabric covered. Brace, base, and surge cable assemblies secured the fins to the envelope. Box cable assemblies between fins added reinforcement to the fin suspension. The adjustable brace cables, which extended from suspension clips on the fin surfaces to fan patches on the envelope, held the fins in the correct angular plane.

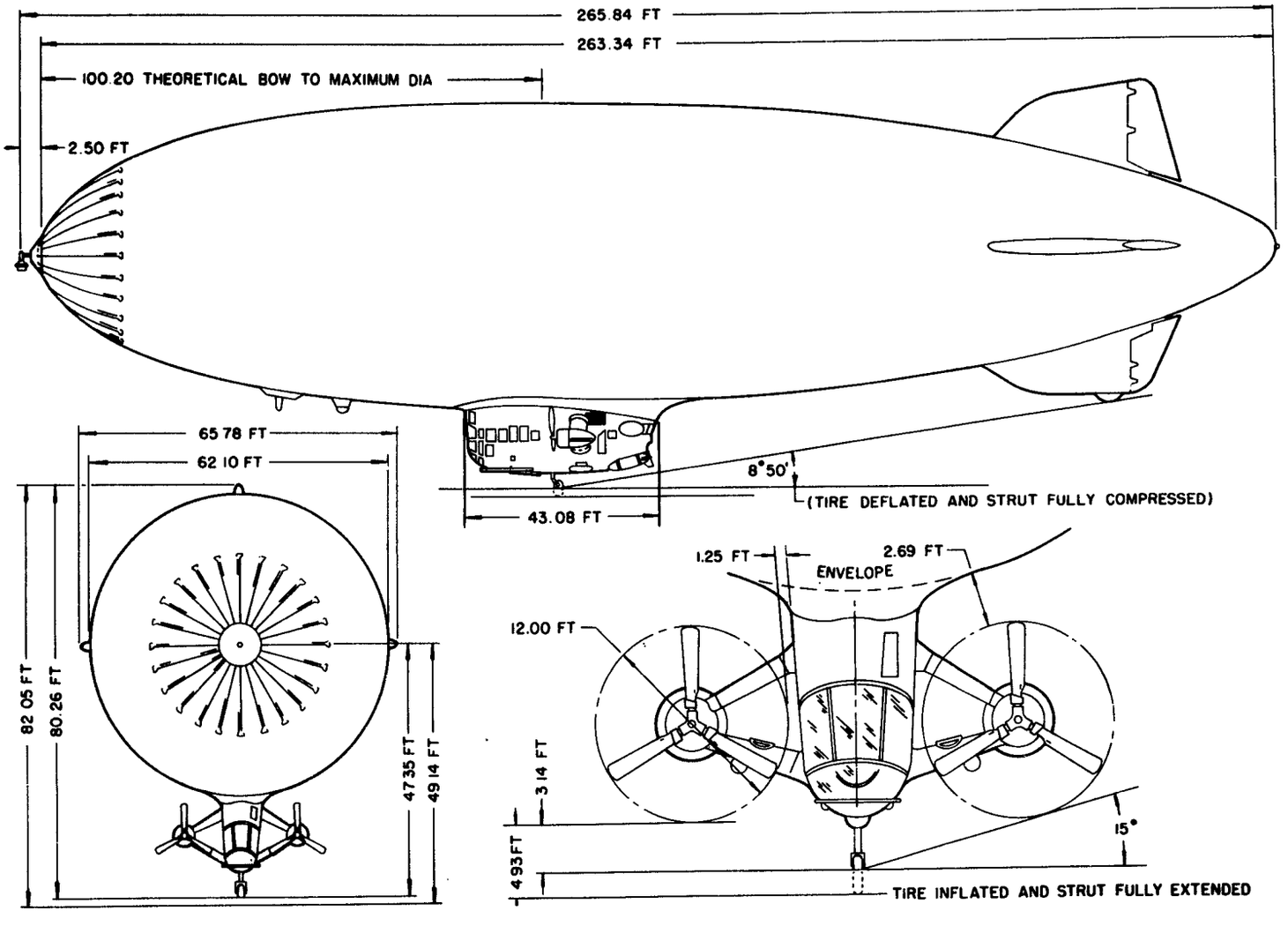

Figure 1.1 Principal dimensions of Model ZSG-3 airship.

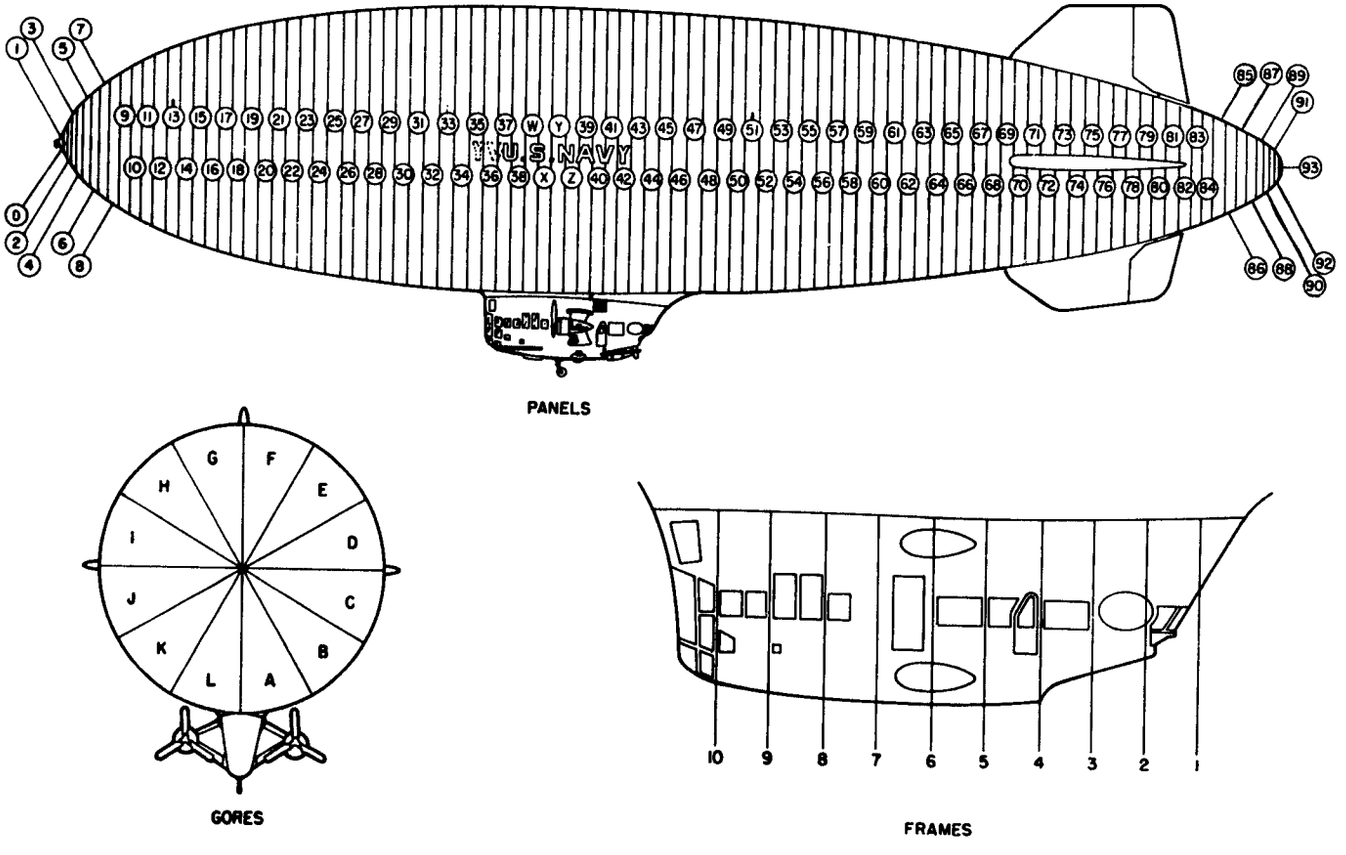

Figure 1.2 Location of frames, panels, and gores on airship.

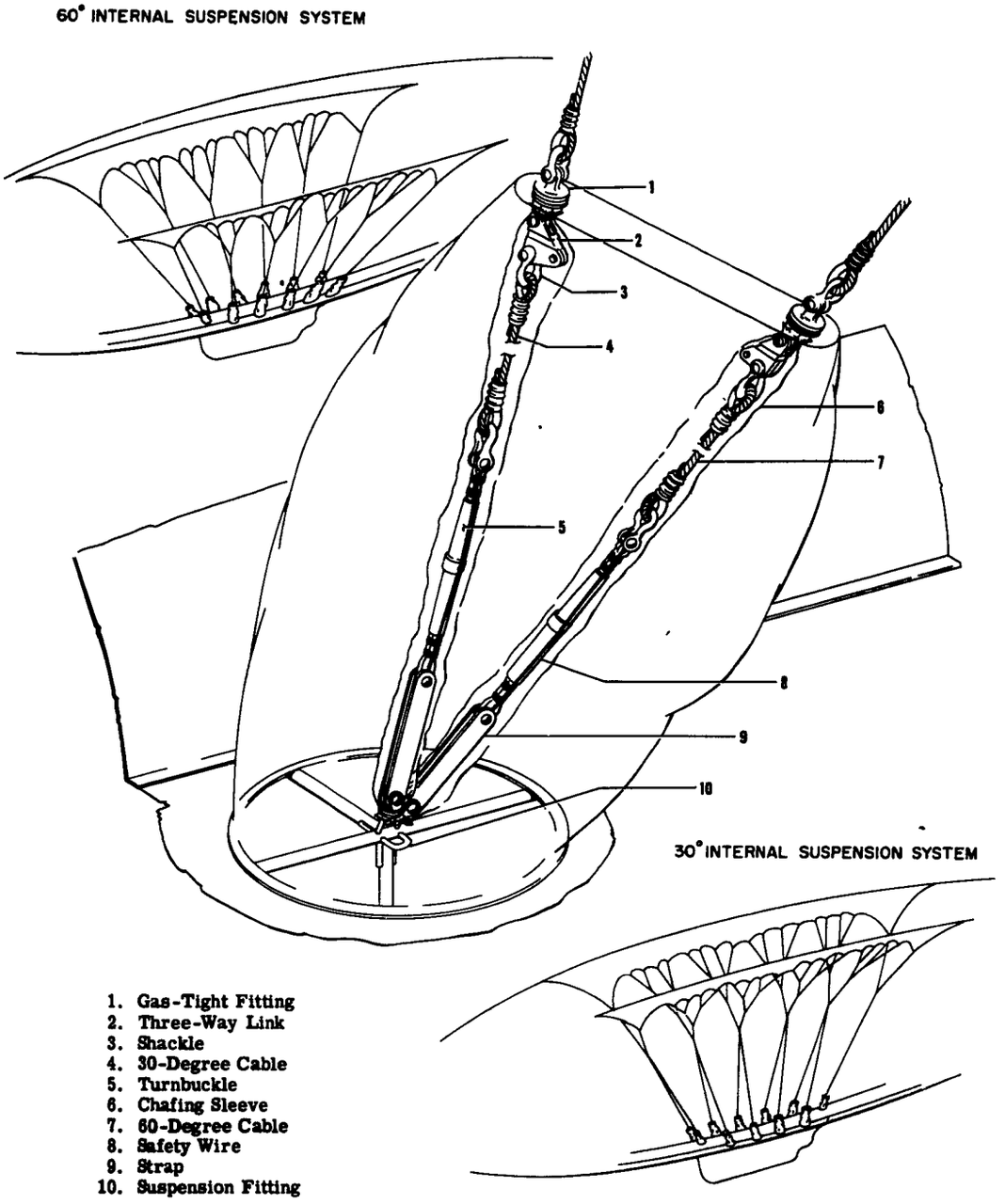

1. Gas-Tight Fitting
2. Three-Way Link
3. Shackle
4. 30-Degree Cable
5. Turnbuckle
6. Chafing Sleeve
7. 60-Degree Cable
8. Safety Wire
9. Strap
10. Suspension Fitting

Figure 1.3 Details of internal suspension systems of airships.

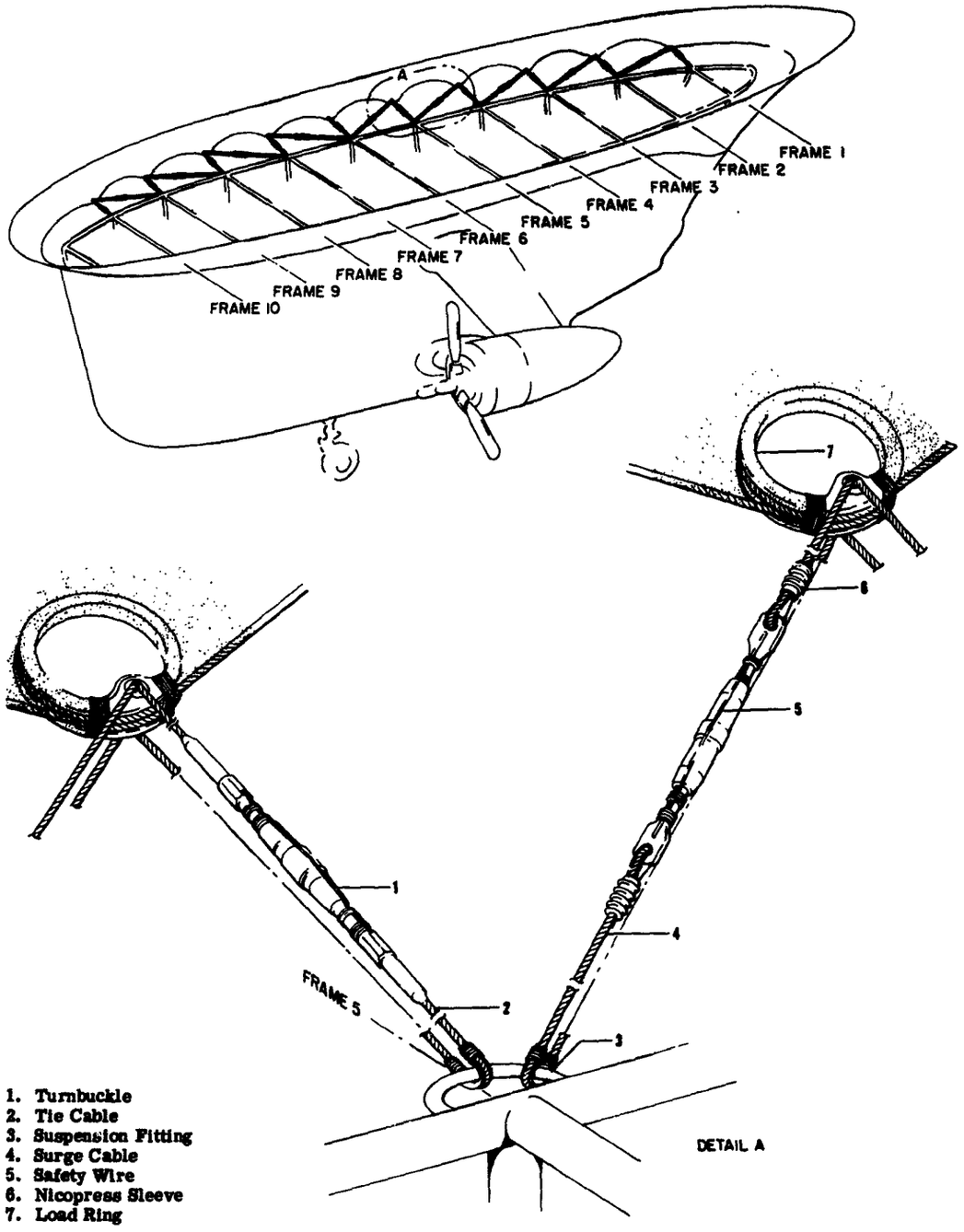

Figure 1.4 Details of external suspension systems of airships.

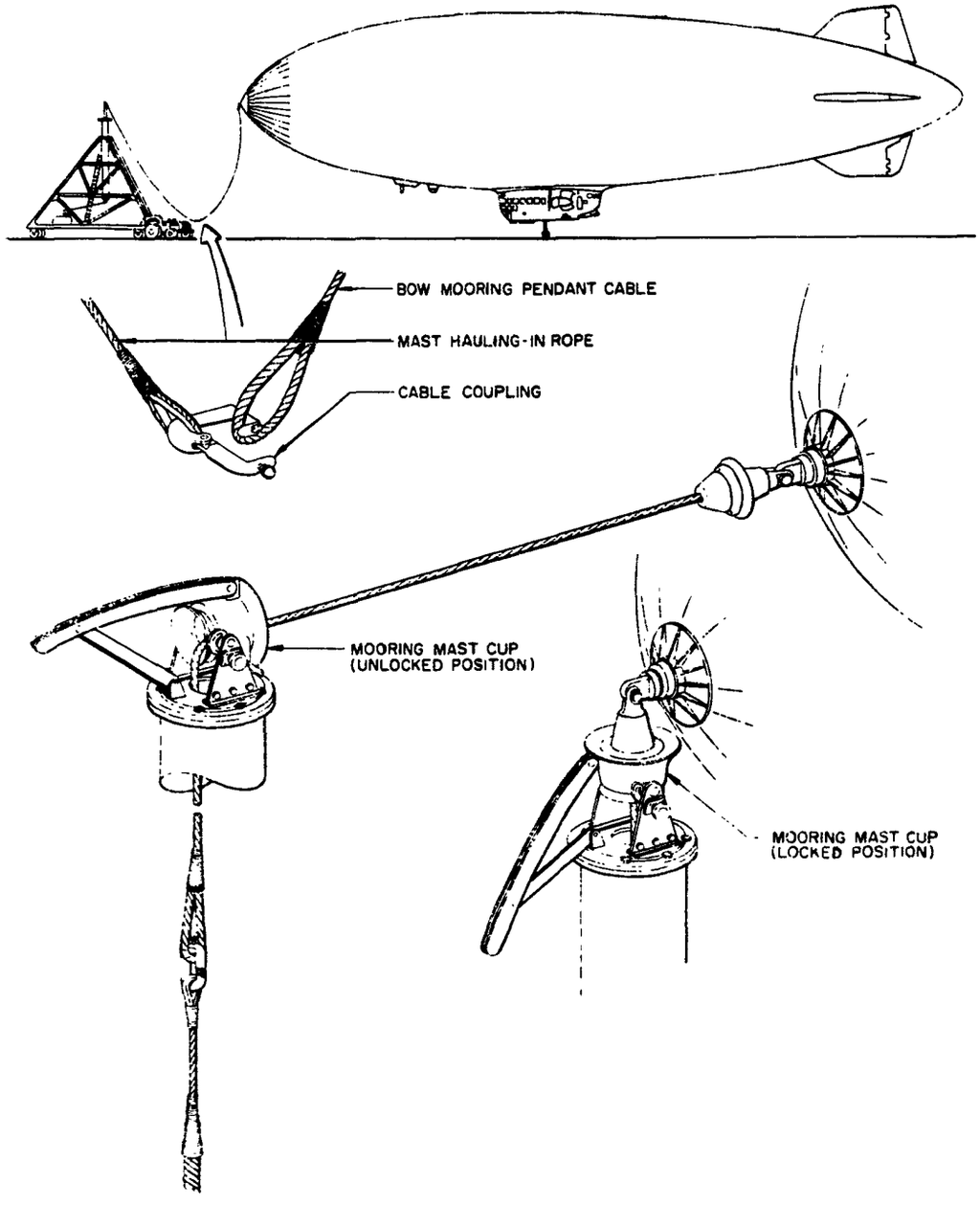

Figure 1.5 Details of mooring-mast-securing system.

Nose stiffening maintained the conformation of the nose of the envelope against air-impact pressure and distributed surge and thrust loads during ground handling and mooring. Twenty-four contoured batten assemblies, made of channel aluminum, were attached to the nose-cone assembly and secured at their aft ends by means of cables to fan patches on the envelope. The airship was secured to the mooring mast by a bow-mooring assembly located at the hub center of the airship nose cone. The bow-mooring assembly consisted of a mooring cone and pendant cable assembly bolted to a shaft turning in bearings in the nose of the airship. Details of the mooring-mast system are shown in Figure 1.5.

Chapter 2
PROCEDURE

2.1 ORIGINAL PLANS FOR SHOT PARTICIPATION

Under the original project plans, two Model ZSG-3 airships (Nos. K-46 and K-77) were fully instrumented for participation in a total of 15 shots during Operation Plumbbob. Airship K-46 was to be used only for moored tests on the ground, with the tail of the airship facing the burst. Tests were to be conducted at successively higher overpressure levels, starting about 0.20 psi, until a major failure or destruction of the airship was obtained. These series of tests were to be conducted with the longitudinal axis of the airship both horizontal and inclined tail high (20 to 30 degrees) to simulate the blast-input conditions expected from actual underwater bursts.

Between shots, it was planned to moor the ground-test airship to a KM-type mobile mast at the southern end of the Yucca Flat dry lake bed at NTS. For each test, the mast and airship would be towed to the selected test position in the area.

Airship K-77 was to be used for in-flight exposure tests only, with the airship in horizontal flight and tail toward the burst. Flight tests, at successively higher overpressure levels, were to be conducted only after sufficient data had been obtained from the moored ground tests to fulfill all requirements for safety-of-flight considerations under the planned test conditions. Between shots, the flight-test airship was to be moored to a mast located adjacent to the Desert Rock airstrip at NTS.

Based on the procedures and data contained in Reference 1, which provides data on the effects of nuclear detonations and instructions for scaling the effects to particular test environments and yields, and the yield values specified by the Defense Atomic Support Agency (DASA), calculations were made to determine the test location required (slant-range distance) to obtain a desired peak overpressure on the test airship for each shot during which participation was planned. The data given in Reference 1 was also used to determine the magnitude of other device effects (thermal and nuclear radiation, gust velocity, etc.) to be experienced at each position. A complete set of sample calculations, showing how the various effects were computed, is contained in Appendix A.

2.2 ACTUAL OPERATIONS AT TEST SITE

2.2.1 Airship Tests. In April 1957, ground-test Airship K-46 was flown from Lakehurst, N. J., to NTS, arriving 2 weeks before the first scheduled participation. Two days after arrival, the airship was destroyed when it was torn from its mooring mast on Yucca Lake bed by a violent windstorm. All instrumentation equipment was recovered without damage, and a replacement airship (No. K-92) was subsequently instrumented for use on the program.

Following the loss of Airship K-46, it was decided that the flight-test Airship K-77 (similarly instrumented) would be used for the moored ground tests but that arrival of the airship into the NTS area would be deferred until the latter part of May, when it was expected that general weather conditions would be more favorable. At the same time, the mooring site on Yucca Lake bed was moved to the northern end since it was believed that the mountainous terrain to the south might be causing some wind turbulence over the southern end of the dry lake.

At the end of May 1957, Airship K-77 was flown into NTS and subsequently participated during Shot Franklin, conducted on 2 June 1957. For this test, the airship was moored to the mast at a horizontal range of 18,200 feet from Ground Zero (GZ) with the tail toward the burst point. At this position, it was calculated that a peak overpressure of 0.20 psi would be obtained (based on a predicted yield of 2 kt). Following the passage of the shock wave, the airship became detached from the mast, owing to failure of the mooring cone, and consequently could not be remoored. In addition, the airship assumed a nose-high attitude, owing to a rip in the forward ballonet, and could not be trimmed. Since the airship was secured by a bow line only and represented a potential hazard if it broke free, it was eventually decided to deflate the envelope and lose the airship. None of the instrumentation equipment, which was removed from the airship after deflation, was damaged during this procedure.

Based on the results obtained from Shot Franklin, it was decided to attempt to free balloon Airship K-92 (replacement for Airship K-46) during the next shot to eliminate the undesirable restraining effects of the mooring mast on the dynamic response and loading of the airship. The plan was to suspend the airship in a trimmed and balanced condition approximately 300 feet aboveground, tail toward the burst. The airship would be held in this position by three quick-disconnect lines (one from the bow and two off the stern) secured to ground-handling mules and would be simultaneously released about 10 seconds before shock arrival. A slack 700-foot-long cable attached to the nose of the airship and to the mast (laterally positioned from airship), plus 500-foot-long ground-handling lines hanging free from the airship, would be used for recovery following passage of the shock wave.

Airship K-92 was flown to NTS 2 days before the scheduled date for Shot Wilson. The firing date was repeatedly postponed, and 7 days after arrival the airship was destroyed when it was torn loose from its mooring mast at Yucca Lake by a dust devil of considerable energy. All instrumentation equipment was recovered without damage.

Following the loss of this airship, an additional one (No. K-40) was assigned to the project and equipped with limited instrumentation. Utilizing the free-balloon technique planned for Shot Wilson, the airship was exposed to Shot Stokes, which was detonated on 7 August 1957. On this test, the airship was free ballooned in a level attitude approximately 300 feet aboveground, with tail toward the burst. Mooring lines holding the airship in position were released about 20 seconds before shock arrival to obtain free-body response data. Immediately following shock arrival, the envelope ruptured forward of the car, and the airship crashed but did not burn. Instrumentation equipment was salvageable with only minor damage.

2.2.2 Operational Difficulties. Airship operations in the NTS area, particularly on Yucca Flat, were conducted with extreme difficulty because of various weather phenomena peculiar to the desert. Temperature variations between the heat of the day and the cool of the evening created problems of low useful lift at night and high degree of superheat during daylight. The prevailing winds, assisted by thermally caused gustiness, posed problems of safe mooring; wind direction and velocity varied constantly through a range of 90 degrees and up to 35 knots in differential velocity. Also, the presence of dust devils (miniature whirlwinds), with the unknown velocities therein, increased the problem of safe mooring.

In attempting to position the airship for the moored tests, it was necessary to tow the airship, while masted, over 7 miles of desert terrain, with the resultant imposition on the bow-mooring assembly of unknown loadings. For proper positioning for tests, the wind conditions had to be almost ideal because of the low-lift condition at night and the requirement for orienting the aircraft tail-on to the blast.

As a result of the above factors, it was necessary to man the aircraft constantly with qualified personnel and to maintain all personnel in a full-emergency condition.

2.2.3 Overpressure Measurements. Measurements of peak free-stream overpressure made on the airship during Shot Franklin were considerably higher than the value calculated for the test position, based on the postshot yield (estimated) and the procedures specified in Reference 1. In an attempt to obtain additional data to explain or clarify the reason for the discrepancy, overpressure measurements were made using ground-mounted instrumentation at the planned airship test positions during Shots Wilson, Kepler, Owens, and Stokes. The results obtained from overpressure measurements made during these shots are discussed in Appendix B.

2.3 AIRSHIP INSTRUMENTATION

Equipment was installed in the test airships to record significant inputs and responses. Airships K-46 and K-77, which were instrumented in an identical manner, contained the most extensive instrumentation. Owing to time limitations, Airship K-92 was not so extensively instrumented, whereas Airship K-40 was the least instrumented. A summary of the instrumentation installed in each airship, listing the types of transducers used, their locations in the airship, and the purposes of the various measurements, is given in Table 2.1.

The primary system for recording the outputs of all transducers consisted of 36-channel oscillographs, Consolidated Electrodynamics Corporation (CEC) Type 5-119-P3, and associated equipment. Power for the oscillographs installed in each airship was supplied by the starboard auxiliary power unit (APU) on the airship. The transducers were powered by batteries. Installation of the recording oscillographs in the navigator's compartment is shown in Figure 2.1.

By means of photoelectric controller (Blue Box) installed in the airship car and facing the burst point, an indication was obtained on one channel of each oscillograph installed in the airship to obtain a zero-time mark and to provide means for time correlation of all records. Normally, recording equipment was remotely started 15 seconds before zero-time by a radio signal that closed a relay in the starting circuit. In the event of failure in this system, the Blue Box was connected for emergency actuation of the recorders. An electronic pulser, common to all oscillographs, was used to record pulse indications on one channel of each oscillograph as an additional means of time correlating all records.

Descriptions of the transducers used, including installation details, system-response characteristics, and calibration methods, are discussed below.

2.3.1 Strain-gage Links. Metallic links, on which strain gages were mounted in a four-arm bridge circuit, were fabricated by the Aeronautical Structures Laboratory (ASL) to measure the cable-tension loads in the airship car-suspension system. On the 30-degree and 60-degree internal suspension systems, each link was installed in the cable near its attachment point at the top of the car structure, adjacent to the turnbuckle. On the surge and the tie cable systems, which consisted of one or two continuous cable loops, the link was installed in one cable of the single or double loops. Links were installed in the horizontal fin-brace cables adjacent to the under surface of the fins. Details of a typical strain-gage link for measuring cable-tension loads are shown in Figure 2.2. General installation arrangements of these links are shown in Figures 2.3 and 2.4. Each link was calibrated throughout the expected load range in a tensile-testing machine. The overall dynamic response of the cable-tension-recording system was flat to 60 cps.

2.3.2 Bow-mooring Shaft. Strain gages, wired in a four-arm bridge circuit, were mounted internally near the aft end of the bow-mooring shaft in the nose of the airship to measure compression loads when moored. Tension loads could not be measured because of a thrust bearing at the forward end of the shaft. Load calibration of the shaft was conducted in a testing machine under compression loading. Dynamic response of the mooring-load-recording system was flat to 60 cps. Details of the mooring-shaft instrumentation are shown in Figure 2.5.

2.3.3 Differential Pressure Transducers. Type 4-312 CEC differential pressure pickups, having a range of ±1.0 psi (plus 100-percent overshoot) were used to measure the static and dynamic differential pressure changes between the outside atmosphere and the helium chamber at selected points on the airship envelope. On Airships K-46 and K-77, pickups were

TABLE 2.1 AIRSHIP INSTRUMENTATION SUMMARIES

PS: Port and Starboard. ◇ indicates inclusion of measurement. – indicates exclusion of measurement.

Type of Transducer	Location of Measurement	Purpose of Measurement	Airship Number K-46	K-77	K-92	K-40
30-Degree Internal Suspension System:						
Strain-gage links	Car Frame No. 1 (Center)	Tension load in cables	◇	◇	◇	◇
do	do 3 (PS)	do	◇	◇	◇	◇
do	do 5 (PS)	do	◇	◇	◇	–
do	do 7 (PS)	do	◇	◇	◇	◇
do	do 9 (PS)	do	◇	◇	◇	–
do	do 11 (PS)	do	◇	◇	◇	◇
60-Degree Internal Suspension System:						
Strain-gage links	Car Frame No. 1 (PS)	Tension load in cables	◇	◇	◇	◇
do	do 3 (PS)	do	◇	◇	◇	–
do	do 5 (PS)	do	◇	◇	◇	◇
do	do 7 (PS)	do	◇	◇	◇	◇
do	do 9 (PS)	do	◇	◇	◇	–
do	do 11 (PS)	do	◇	◇	◇	◇
Port and Starboard Horizontal Fin-Brace Cables, Lower Set:						
Strain-gage link	Fin-brace cables 1 to 5	Tension load in cable	◇	◇	◇	–
External Suspension System, Surge Cables:						
Strain-gage links	Car Frame No. 1 (PS)	Tension load in cables	◇	◇	◇	◇
do	do 2 (PS)	do	◇	◇	◇	◇
do	do 3 (PS)	do	◇	◇	◇	–
do	do 4 (PS)	do	◇	◇	◇	◇
do	do 5 Aft (PS)	do	◇	◇	◇	◇
do	do 6 Fwd (PS)	do	◇	◇	◇	◇
do	do 7 (PS)	do	◇	◇	◇	–
do	do 8 (PS)	do	◇	◇	◇	◇
do	do 9 (PS)	do	◇	◇	◇	◇
External Suspension System, Tie Cables:						
Strain-gage links	Car Frames 1 to 10 (PS)	Tension load in cables	◇	◇	◇	–
Car Accelerations						
NAES Linear Accelerometers	Center of gravity of airship car	Vertical, longitudinal, and transverse accelerations of car	◇	◇	◇	◇
Statham angular accelerometers	Center of gravity of airship car	Pitch, roll, and yaw accelerations of car	◇	◇	◇	◇
Envelope Differential Pressures:						
CEC differential pressure pickups	Panel 92 (tail of airship)	Dynamic impact pressure on tail of airship	◇	◇	◇	–
do	51, Gore B	do	◇	◇	◇	–
do	51, Gore E	do	◇	◇	◇	–
do	51, Gore H	do	◇	◇	◇	–
do	51, Gore K	do	◇	◇	◇	–
do	33, Gore B	do	◇	◇	◇	–
do	33, Gore E	do	◇	◇	–	–
do	33, Gore H	do	◇	◇	–	–
do	33, Gore K	do	◇	◇	◇	–
do	13, Gore B	do	◇	◇	◇	–
do	13, Gore E	do	◇	◇	–	–
do	13, Gore H	do	◇	◇	–	–
do	13, Gore K	do	◇	◇	◇	–

TABLE 2.1 CONTINUED

Type of Transducer	Location of Measurement	Purpose of Measurement	Airship Number K-46	K-77	K-92	K-40
Absolute Pressures:						
CEC absolute pressure pickup	Panel 92 (inside tail)	Fluctuation of absolute pressure within helium chamber	◇	◇	–	–
do	51 inside helium		◇	◇	◇	–
do	31 chamber on		◇	◇	–	–
do	13 longitudinal axis of envelope		◇	◇	◇	–
do	Mounted with superheat indicator, Panel 35, Gore A		–	–	–	◇
do	Fwd ballonet air tunnel just fwd of access manhole in car	Fluctuation of absolute pressure within fwd ballonet	–	–	–	◇
do	Aft ballonet air tunnel just aft of access manhole in car	Fluctuation of absolute pressure within aft ballonet	–	–	–	◇
Side-on Overpressures:						
CEC differential pressure pickup	On horizontal boom or probe projecting aft from car	Free-stream side-on overpressure at aft end of car	◇	◇	◇	◇
do	On horizontal boom or probe projecting fwd from car	Free-stream side-on overpressure at fwd end of car	◇	◇	◇	–
Shock-Wave Passage Indicators:						
CEC absolute pressure pickup	Panel 92 (mounted side-on at tail of envelope)	Indication on all records when shock wave reaches tail	–	–	–	◇
do	Panel 0 (mounted side-on at nose of envelope)	Indication on all records when shock wave reaches nose	–	–	–	◇
Gianinni pressure switch	Panel 92 (at tail of envelope)	Indication on all records when shock wave reaches tail	–	–	–	◇
do	Panel 0 (at nose of envelope)	Indication on all records when shock wave reaches nose	–	–	–	◇
Car Attitude:						
Gianinni Gyro	Center of gravity of airship car	Pitch and roll	◇	◇	◇	–
do	do	Yaw	◇	◇	◇	–
Mooring Load:						
Strain gages	Mooring spindle in nose of airship	Measure compression loads when moored	◇	◇	◇	–
Position Indicators:						
Potentiometers	Port elevator hinge fitting	Record control surface displacements	◇	◇	◇	–
do	Apex of mooring mast	Record pitching motion of airship when moored	◇	◇	◇	–
do	do	Record yawing motion of airship when moored	◇	◇	◇	–

TABLE 2.1 CONTINUED

Type of Transducer	Location of Measurement	Purpose of Measurement	Airship Number K-46	K-77	K-92	K-40
Calorimeters:						
NRDL Calorimeters (two)	Lower aft end of car in special rack facing burst point	Record total incident thermal radiation	◇	◇	◇	–
Radiometers:						
NRDL Radiometer	Lower aft end of car in special rack facing burst point		–	–	–	–
Cameras:						
GSAP Cameras, 32 fps (two)	Adjacent to and aligned with axes of calorimeters and radiometers	Posttest check on degree of alignment of calorimeters and radiometers on fireball	◇	◇	◇	–
Zero-Time Indicator:						
Photoelectric controller (Blue Box)	Aft end of airship car facing burst point	Indicate zero time on all records and/or emergency start of recorders if radio signal fails	◇	◇	◇	◇
Envelope Temperatures:						
Thermocouple	Panel 92 (tail of airship)	Record temperature change in envelope fabric	◇	◇	◇	–
do	51, Gore B	do	◇	◇	◇	–
do	51, Gore E	do	◇	◇	–	–
do	51, Gore H	do	◇	◇	–	–
do	51, Gore K	do	◇	◇	◇	–
do	33, Gore B	do	◇	◇	◇	–
do	33, Gore E	do	◇	◇	–	–
do	33, Gore H	do	◇	◇	–	–
do	33, Gore K	do	◇	◇	◇	–
do	13, Gore B	do	◇	◇	◇	–
do	13, Gore E	do	◇	◇	–	–
do	13, Gore H	do	◇	◇	–	–
Helium Temperatures:						
Thermocouple	Panel 92 inside helium chamber on longitudinal axis of envelope	Record temperature change in helium gas	◇	◇	–	–
do	51 do	do	◇	◇	◇	–
do	33 do	do	◇	◇	–	–
do	13 do	do	◇	◇	◇	–
Oscillograph Time Synchronizer:						
Pulse generator	Mounted with recording equipment in airship car	Synchronize all oscillograph records on a common time basis for time correlation of data	◇	◇	◇	◇
		Total number of active channels:	133	133	119	50
		Total number of oscillographs used:	4	4	4	2

Figure 2.1 Installation of instrumentation recording equipment in airship.

installed at three longitudinal panel stations, with four pickups at each station located 90 degrees apart and 45 degrees from the vertical centerline. The diaphragms were flush with the envelope surface. One pickup was located in the tail of the envelope, with the plane of the diaphragm normal to the longitudinal axis. Location of the pickups on the envelope are shown in Figure 2.6, and details of a typical installation are shown in Figure 2.7. No pickups were installed on the envelope of Airship K-40.

The differential pressure pickups were calibrated statically by the use of a water manometer. Dynamic response of the recording systems was flat to 60 cps.

2.3.4 Overpressure Transducers. Differential pressure pickups, similar to those used on the airship envelope, were installed inside booms or probes to measure free-stream or side-on overpressures. The probes were 1¾ inches in diameter. One probe was attached to the handrail of the airship car at Frame 11 and extended forward 12 feet in a horizontal position. The other probe was attached to the car at Frame 3 and extended aft 2 feet in a horizontal position. An orifice, 0.07 inches in diameter, was located approximately 10½ inches aft of the tip on one side of each probe. A right-angled pressure tube inside the probe extended from the orifice to the diaphragm of the pickup, which was vented at ambient pressure into a reference chamber that was automatically sealed prior to shock arrival. Installation of both probes on the airship car is shown in Figure 2.8.

The pickup system was calibrated statically by the use of a water manometer and checked dynamically by the instantaneous release of pressure. The overall dynamic response of the overpressure-measuring systems was flat to 135 cps.

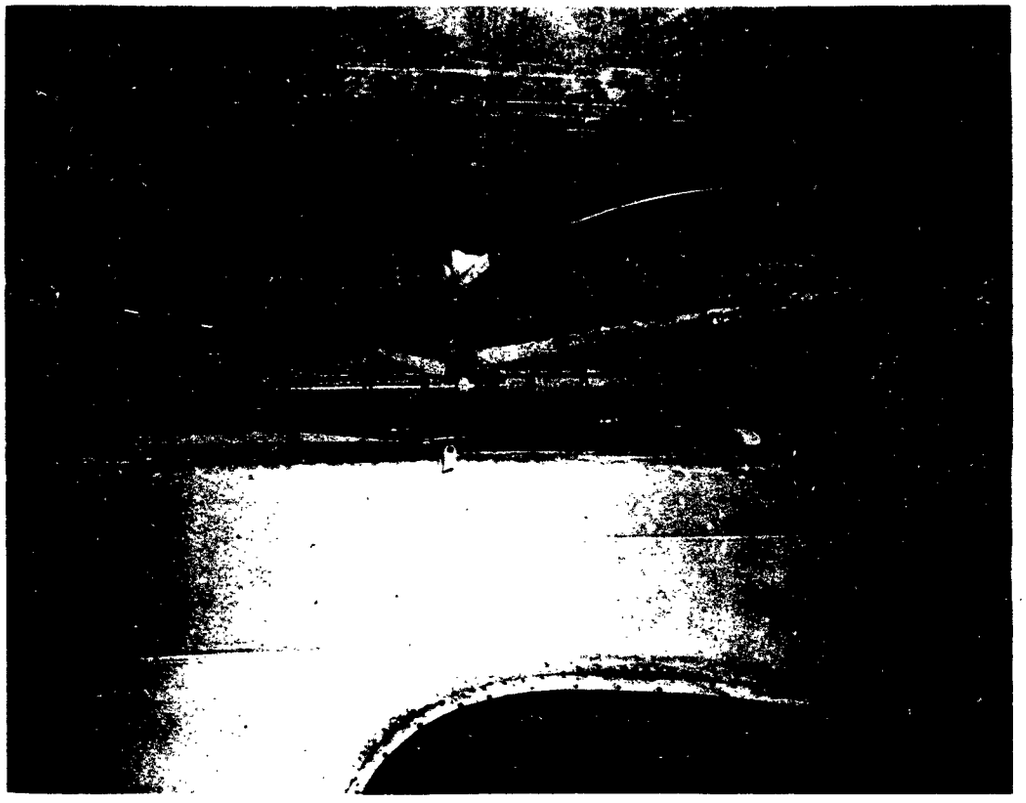

Figure 2.2 Details of ASL strain-gage link for measuring cable-tension loads.

2.3.5 Absolute Pressure Transducers. Type 4-312 CEC absolute pressure pickups, having a range of 0 to 15 psi, were used to measure the absolute gas pressure in the helium chamber. On Airships K-46 and K-77, pickups were suspended at the centerline of the envelope at four different panel stations by means of vertical cables spanning the interior. Diaphragms of the pickups were facing upward. Locations of the pickups in the envelope are shown in Figure 2.6.

No pickups were similarly installed in Airship K-40. However, one absolute pressure pickup was installed in the forward ballonet (in the air tunnel), in the helium chamber (at the superheat indicator), and in the aft ballonet (in the air tunnel).

Absolute pressure pickups were calibrated statically with a water manometer. Response of the recording systems was flat to 30 cps.

2.3.6 Linear Accelerometers. Type D-3 ASL linear accelerometers, having a 3-gram range, were installed near the center of gravity of the airship car to record vertical, longitudinal, and transverse accelerations. The accelerometers were calibrated on a centrifuge, and the frequency-response characteristics were checked on a vibration table. Response of the accelerometers was flat to 6 cps.

2.3.7 Angular Accelerometers. Type AA17b Statham angular accelerometers, having a range of $1\frac{1}{2}$ radians/sec^2, were installed in the airship car to record pitch, roll, and yaw accelerations. The accelerometers were calibrated on a compound pendulum.

2.3.8 Attitude Gyros. Two Gianinni gyros were installed on a rigid structure near the center of gravity of the airship car to record changes in car attitude or displacement. One gyro recorded pitch and roll displacements, and the other gyro recorded yaw displacements.

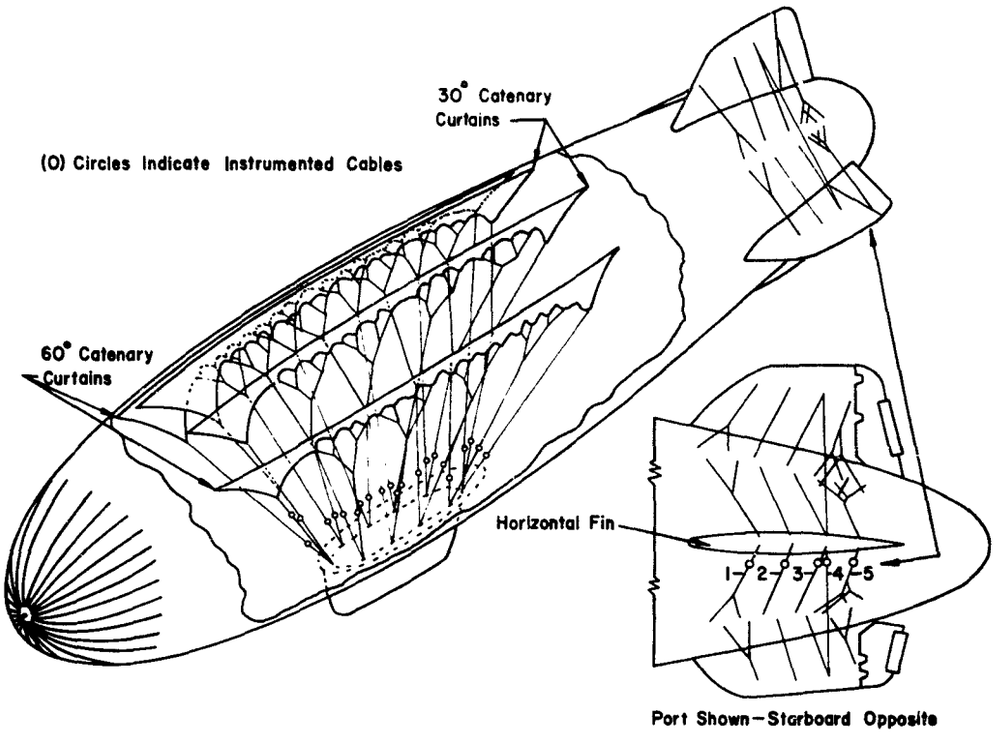

Figure 2.3 Location of the strain links in the internal suspension system and fin-brace cables.

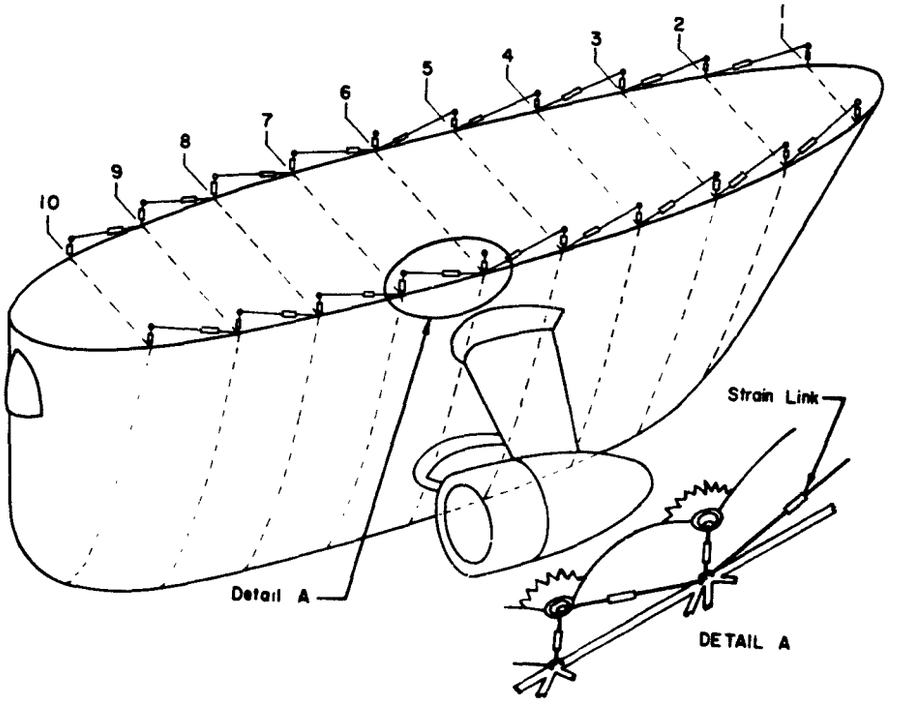

Figure 2.4 Location of the strain links in the external suspension system.

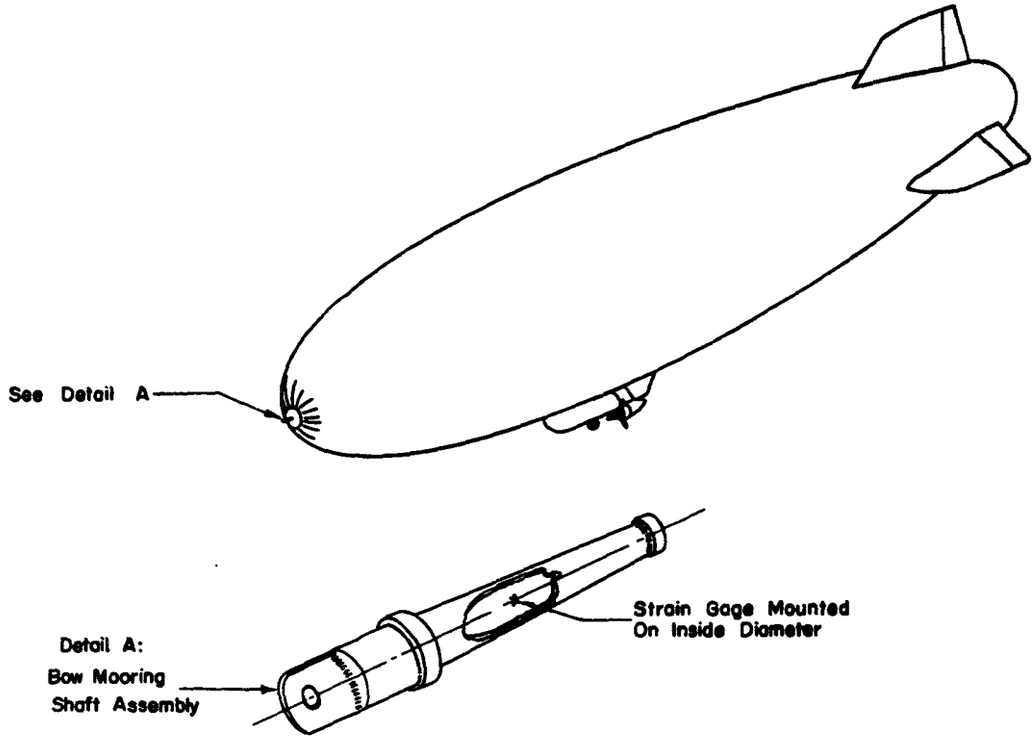

Figure 2.5 Details of bow-mooring-shaft instrumentation.

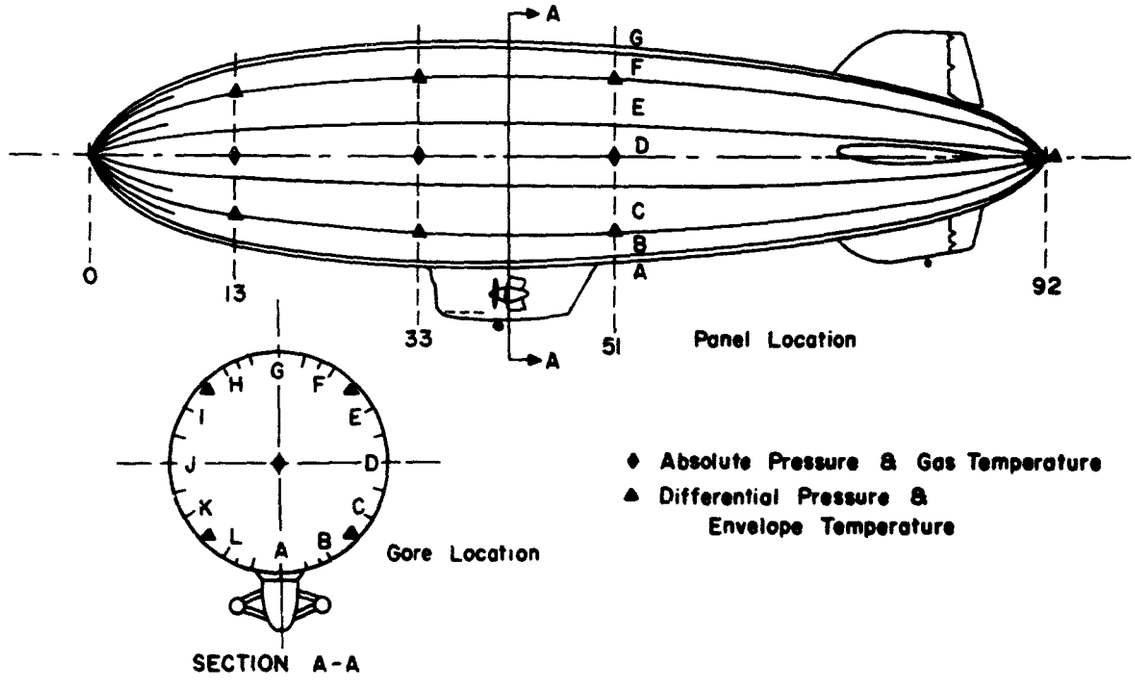

Figure 2.6 Location of pressure and temperature pickups on airship.

The gyros were calibrated on a gyro table to the following ranges: pitch and roll, 45 degrees; yaw, 90 degrees.

2.3.9 Shock-arrival Indicators. On Airship K-40, one Gianinni pressure switch (air speed) and one CEC absolute pressure pickup were installed at the tail and at the nose of the airship envelope to indicate arrival of the shock wave at these respective stations. The pressure switches were set to actuate at 0.25 psi.

2.3.10 Position Indicators. One position indicator was installed on a hinge fitting of the port elevator to record control-surface displacements. Two potentiometers were mounted at the apex of the ground mooring mast to record displacements in pitch and azimuth of the airship while moored.

2.3.11 Thermocouples. On Airships K-46, K-77, and K-92, copper-constantan thermocouples, using a 250°F Arnoux reference junction, were attached to the envelope fabric at each differential pressure pickup location. In addition, thermocouples were mounted with each absolute pressure pickup installed inside the helium chamber. The thermocouples were installed to measure temperature rise in the envelope fabric and helium gas during the thermal phase of weapon detonation.

2.3.12 Calorimeters and Radiometers. Provisions for installing U. S. Naval Radiological Defense Laboratory (NRDL) calorimeters and radiometers in a special rack at the aft end of the airship car at Frame 2 were made for each airship for thermal-radiation measurements. The rack could swivel so that the axes of the instruments as installed would be aligned on the burst point. Calorimeters having suitable sensitivities were provided and calibrated by NRDL. Two gun-sight-aiming-point (GSAP) cameras, operating at 32 frames/sec, were also installed in the calorimeter mount with their axes aligned with the instrument axes. In this manner,

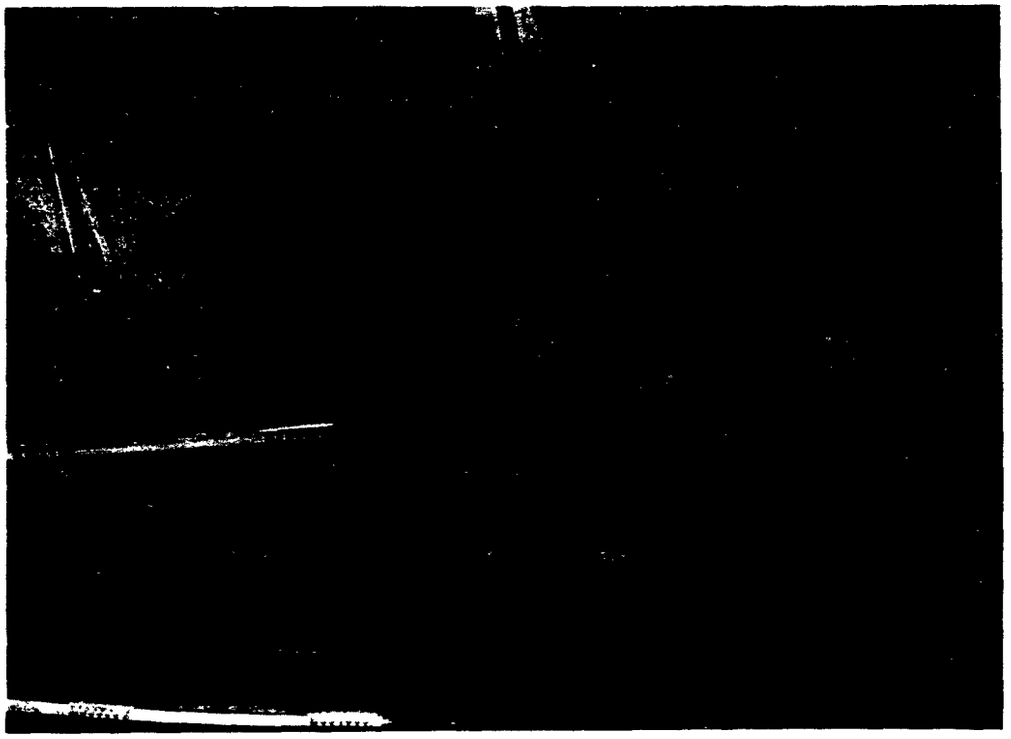

Figure 2.7 Typical installation of differential pressure pickup on envelope.

Figure 2.8 Installation of free-stream overpressure probes on airship car.

means were provided whereby a postshot check could be made to ascertain that the fireball was on the field of view of the instruments.

Dimensional locations of principal instrumentation stations on the airship are shown in Figure 2.9.

2.4 MOTION-PICTURE PHOTOGRAPHY

In addition to the instrumentation equipment contained in the airship, high-speed motion-picture cameras were set up on the ground adjacent to the test position to photograph the dynamic behavior and response of the airship during passage of the shock wave.

Three high-speed Eastman cameras, rated at 1,000 frames/sec, were used to photograph the airship. The cameras were set up approximately 300 feet abeam the airship. One camera was focused on the nose area of the envelope, the second camera was focused on the midsection of the envelope (including the car), and the third camera was focused on the tail section. The fields of view of the different cameras overlapped for complete coverage. Timing marks at the rate of 200 per second were placed on the edge of each film.

In addition to the Eastman cameras, two GSAP cameras, operating at 32 frames/sec, were utilized to photograph the complete airship.

Start-up of the cameras was accomplished through the closure of a relay immediately before shock arrival since the total running time of the Eastman cameras was approximately 6 seconds. Since lighting for predawn shots was critical, magnesium flares backed by reflectors were used for illumination of the complete envelope.

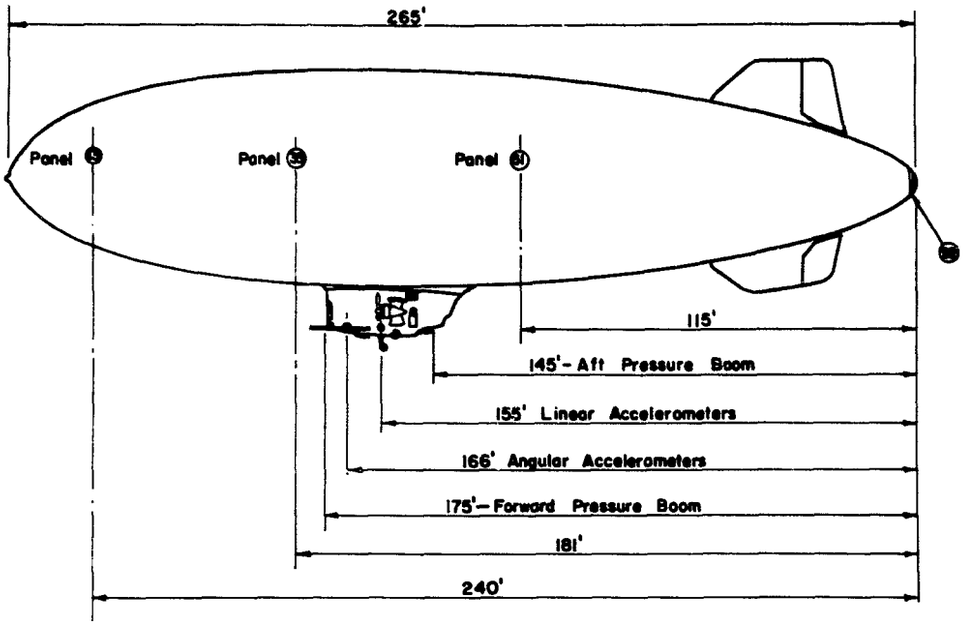

Figure 2.9 Dimensional locations of principal instrumentation stations on airship.

2.5 DATA REQUIREMENTS

To establish limits governing the special-weapon-delivery capabilities of lighter-than-air craft, complete time histories describing the dynamic behavior and response of the airship to known weapon-effect inputs were required. Under the test conditions of this project, the primary input parameter requiring definition, before the dynamic-response data on the airship could be adequately interpreted, was the overpressure resulting from the blast. Of lesser importance were nuclear and thermal radiations, as considered from the standpoint of effects expected from underwater bursts during airship ASW operations.

In terms of the dynamic response and loads imposed on the complete airship and major components during blast inputs, time histories of the linear and angular accelerations of the airship car, dynamic loads in the suspension systems, envelope pressure fluctuations and loads, and tail surface loads were required. Inasmuch as the airship represented a complex arrangement of interacting elastic and inelastic masses, a considerable quantity of experimental data from blast-effect tests was required to provide a valid basis for extended analytical treatment of the problem. The instrumentation described in Section 2.2 was designed to yield the required experimental data.

Chapter 3
RESULTS

3.1 SHOT FRANKLIN

Figure 3.1 shows the arrangement and test setup for Shot Franklin. The airship was restrained only by the mast secured to the mooring attachment. The blast wave forced the airship forward abruptly, resulting in a failure of the nose-cone fitting (Figure 3.2). This failure allowed the airship to separate from the mast and float free until restrained by the handling lines. Shortly afterward, the airship assumed a nose-high attitude, and deflation of the envelope was necessary for recovery. Subsequent inspection revealed that the forward ballonet had been torn for a length of more than 10 feet (Figure 3.3).

The instrumentation performed satisfactorily, and the time histories of the data recorded are given in Figures 3.4 and 3.13. The data are plotted against a common time scale; zero time for these traces is approximately the time of incident shock arrival at the tail of the airship as determined by the initial deflection of the trace for differential pressure at Station 92. Figure 3.4 shows the variation of the external overpressures, incremental pressures in the helium chamber, and the differential pressure at Station 92. The peak external overpressures recorded were 0.40 psi at the aft boom and 0.30 psi at the forward boom. The predicted peak overpressure for the nominal expected yield of 2 kt was 0.19 psi. As shown in Figure 3.4, the maximum positive incremental pressure inside the envelope at the centerline was 0.20 psi.

The linear and rotational accelerations of the airship car are shown in Figure 3.5, together with the bow-mooring-shaft load trace which cannot be followed during the time of maximum loads but which does indicate the times that the nose of the airship was forced against the mast. It is evident that the response of the car was violent in comparison to more normal airship operating conditions, where incremental accelerations were but a small fraction of the peak values shown in Figure 3.5.

The loads in the internal suspension systems are shown in Figures 3.6 and 3.7. Also shown are the violent oscillations of loads, but the load variations with time were relatively smooth even though the trace excursions are large. The external suspension system loads shown in Figures 3.8 to 3.12 were high in magnitude, but the surge cables (which respond primarily to longitudinal loads) displayed less oscillatory characteristics than either the tie cables or the internal cables.

In Figure 3.13, the recorded differential pressures on the envelope surface exhibited extremely violent transient behavior. The pressure values from these traces were highly questionable since it was known that the pressure gages were sensitive to acceleration as well as to pressure. The motion pictures show that transient wrinkling of the envelope occurred, which undoubtedly introduced accelerations of the envelope fabric.

Table 3.1 gives a summary of the recorded peak suspension cable loads and the corresponding percentages of design breaking strength. Also given in Table 3.1 are the peak cable

loads recorded for the first 0.25 second after shock arrival at the tail. These loads at the early times up to 0.25 second were considered to be more significant than those at subsequent times, when such factors as the reaction of the mooring mast caused the airship response to deviate from that of a free-flight condition. The probable influence of the mooring mast on the recorded response is discussed in Chapter 4.

Figure 3.14 shows a sequence of frames from the motion pictures taken during the test. The frames have been approximately correlated in time with the time scales of the preceding figures. Indentation of the envelope caused by the internal suspension loads can be clearly seen, as well as a diagonal wrinkle forward of the car as the peak longitudinal loads developed.

Thermal inputs, envelope fabric temperatures, and helium temperatures were recorded in the event that these factors might influence the other results. These thermal measurements were all of negligible magnitude; consequently, they are not reported.

3.2 SHOT STOKES

The relative location and test setup of the airship for Shot Stokes are shown in Figure 3.15. The airship was free ballooned in a trimmed level attitude at shock arrival, as described in Section 2.2.1. The blast wave apparently induced a response of the airship similar to that of Shot Franklin. The incident overpressure was much higher than expected, and a circumferential failure of the envelope immediately forward of the car occurred within a fraction of a second after shock arrival. The initiation of the envelope failure and the progression of the tear around the circumference are clearly shown in the motion-picture sequence of Figure 3.16. Figure 3.17 shows the outline of the envelope rupture determined from measurements of the envelope sections after they had fallen and collapsed. Figure 3.18 shows the area at the bottom of the envelope where the failure initiated.

Unfortunately, no measurements were obtained in the airship because of failure, prior to shock arrival, of the APU that supplied power to the oscillographs. An overpressure time-history measurement was obtained from a pressure probe, with an independent oscillograph, mounted on the ground near the airship. The recorded overpressure traces are shown in Figure B.6. The peak overpressure from this record was 0.75 psi, compared with the expected peak overpressure of 0.13 psi, based on the nominal expected yield of 10 kt. Accordingly, the blast effects of Shot Stokes were approximately twice as severe as those of Shot Franklin, and a failure was to be expected at such an overpressure level.

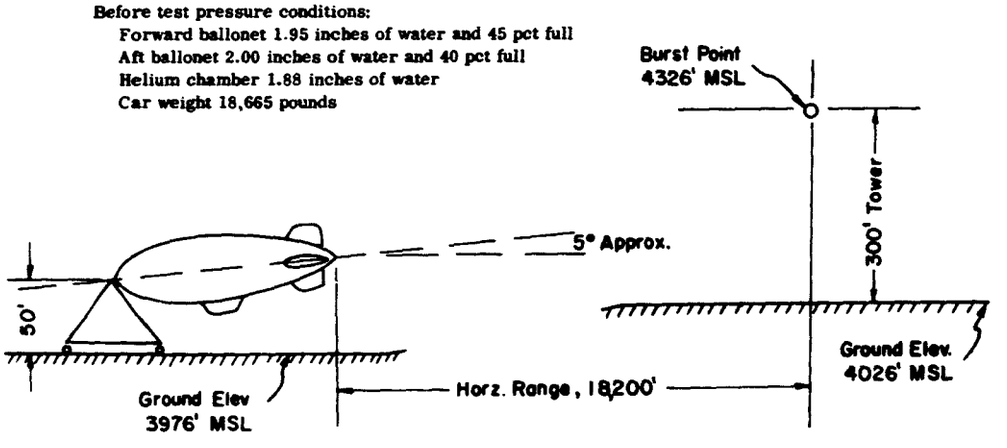

Figure 3.1 Airship test setup, Shot Franklin.

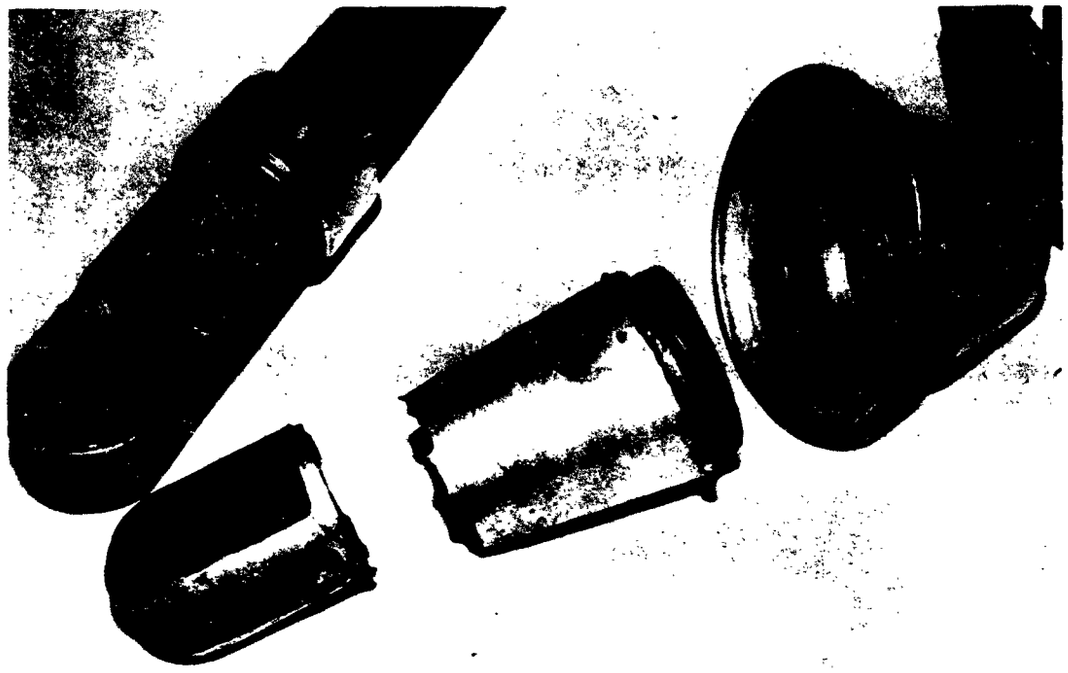

Figure 3.2 Airship nose-cone failure.

Figure 3.3 Tear in forward ballonet of airship.

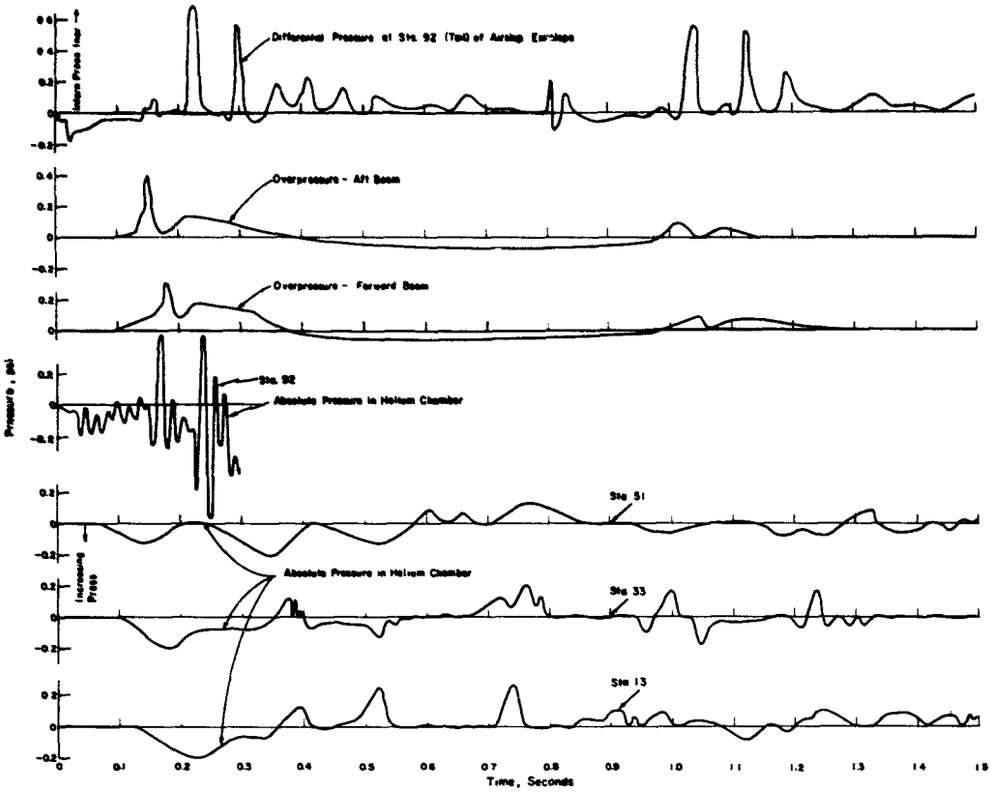

Figure 3.4 Time histories of pressures, Shot Franklin.

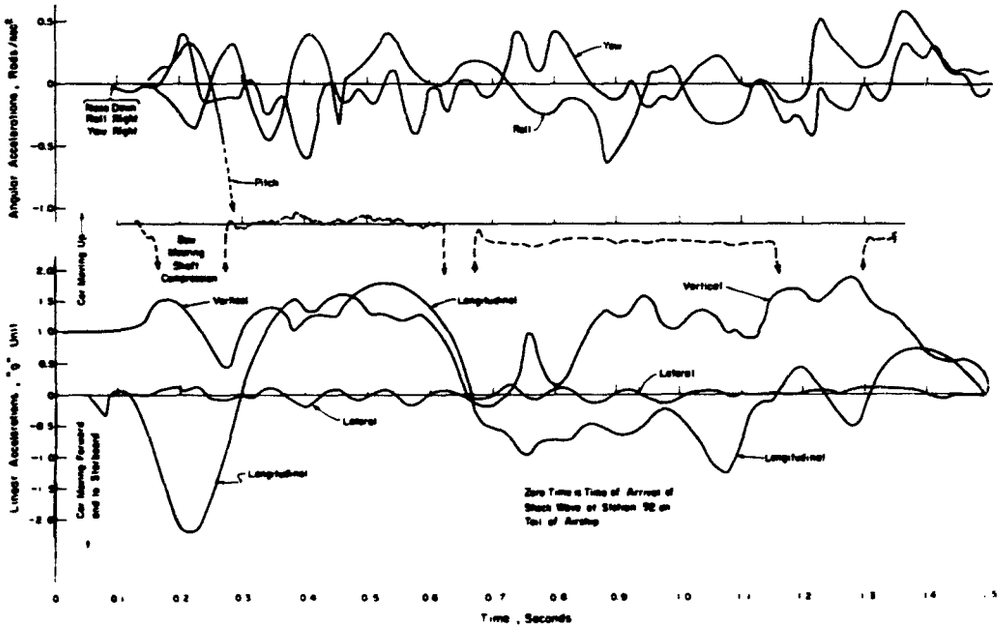

Figure 3.5 Time histories of linear and angular accelerations of airship car, Shot Franklin.

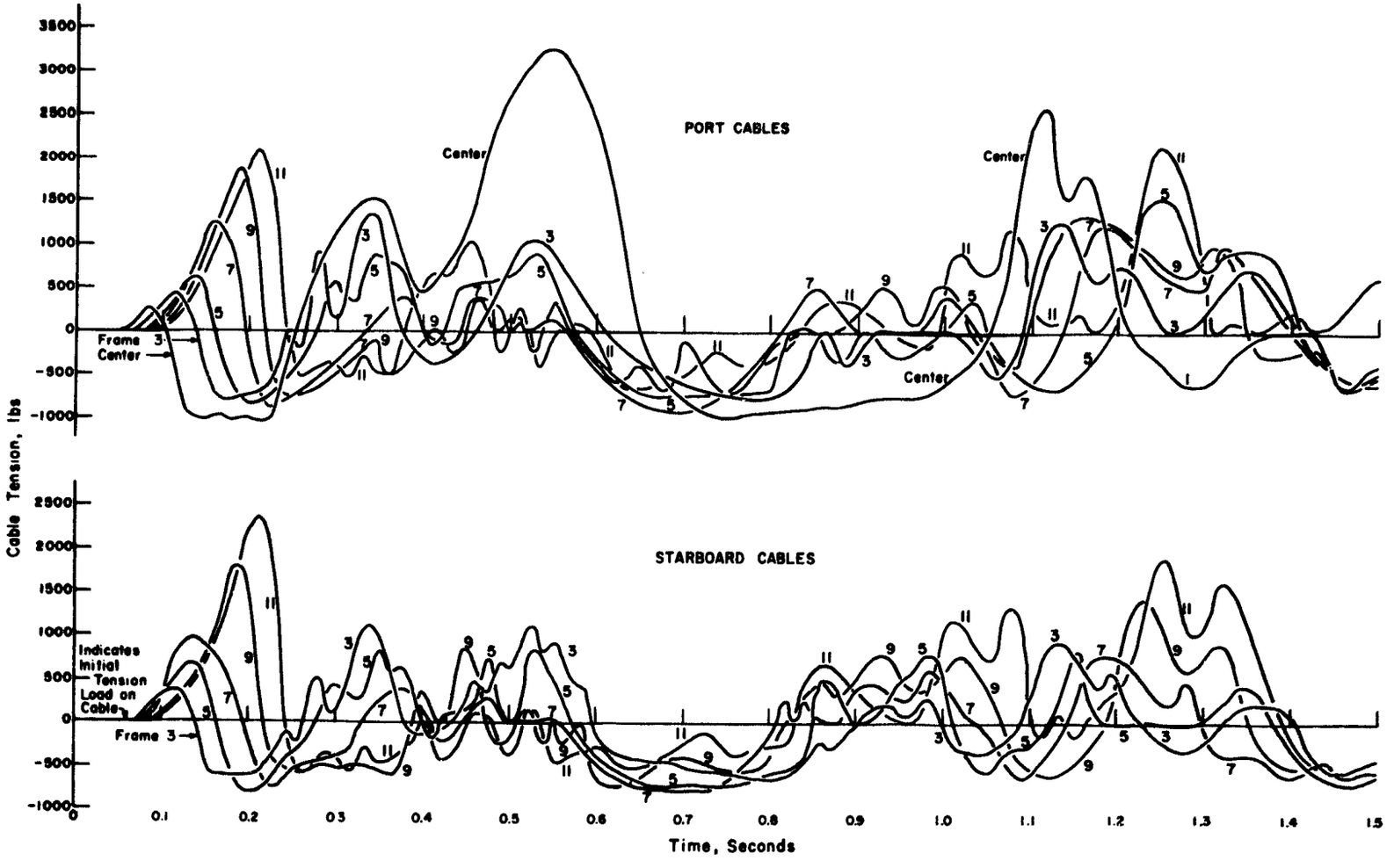

Figure 3.6 Time histories of loads in 30-degree internal suspension system, Shot Franklin.

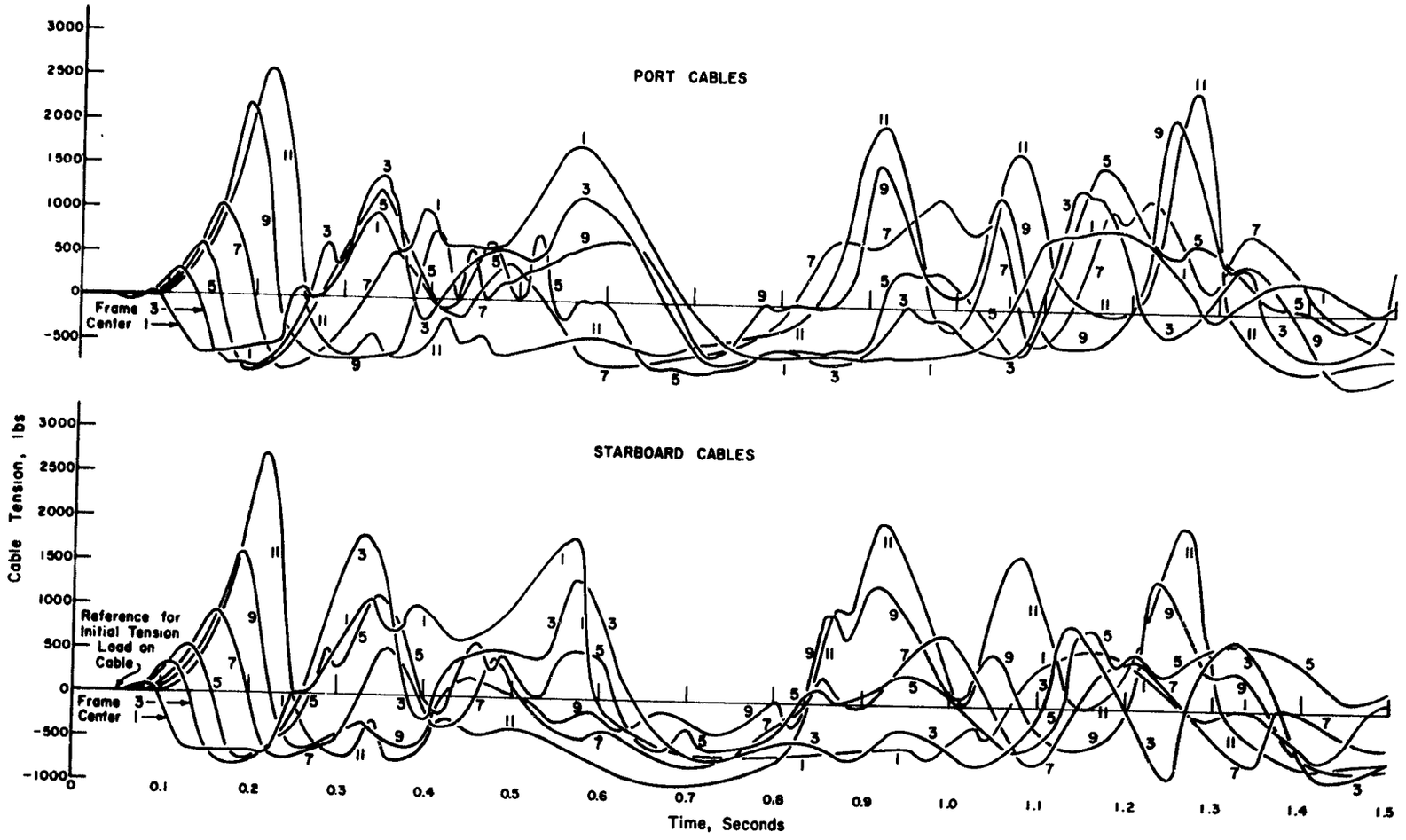

Figure 3.7 Time histories of loads in 60-degree suspension system, Shot Franklin.

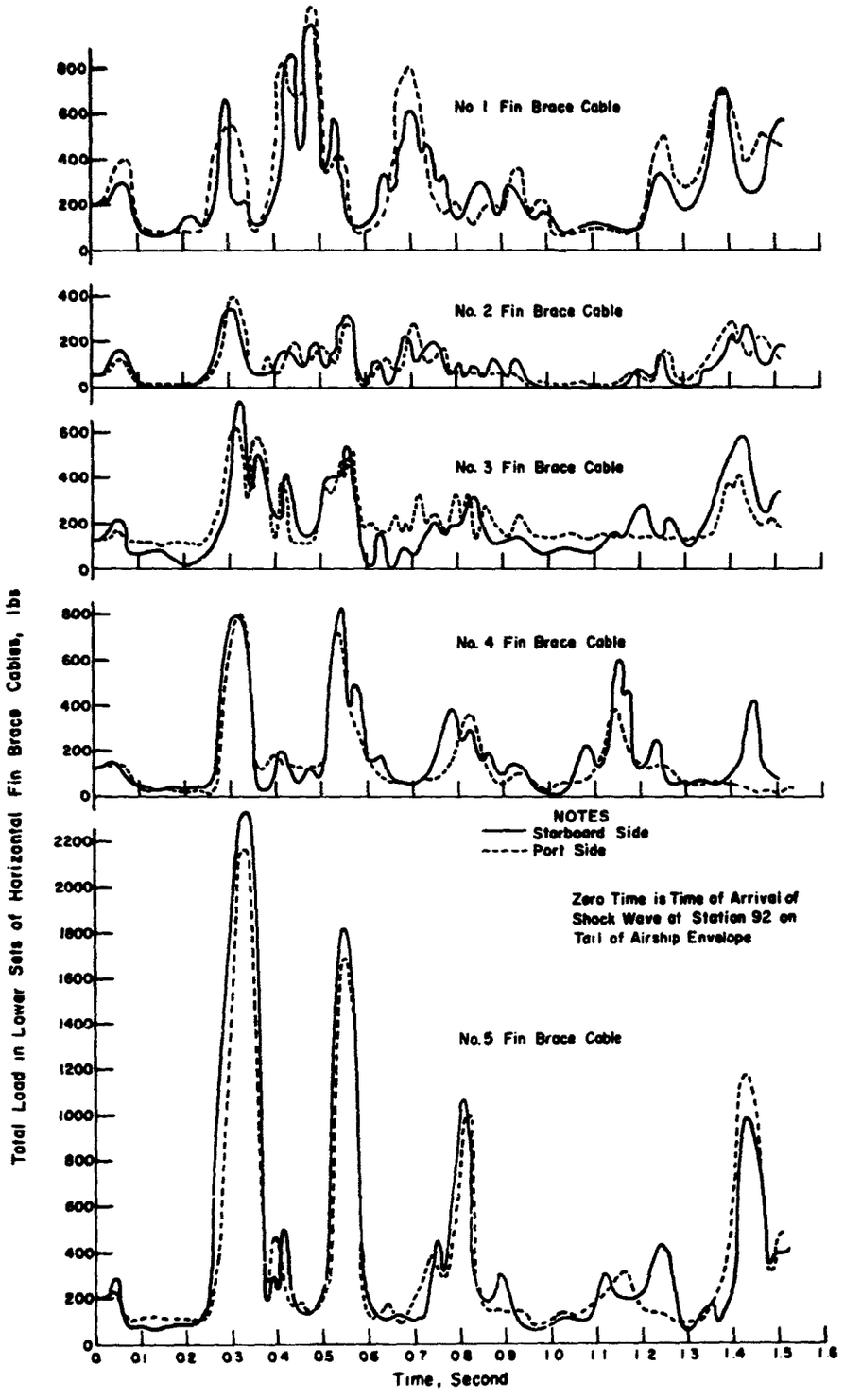

Figure 3.8 Time histories of loads in fin-brace cables, Shot Franklin.

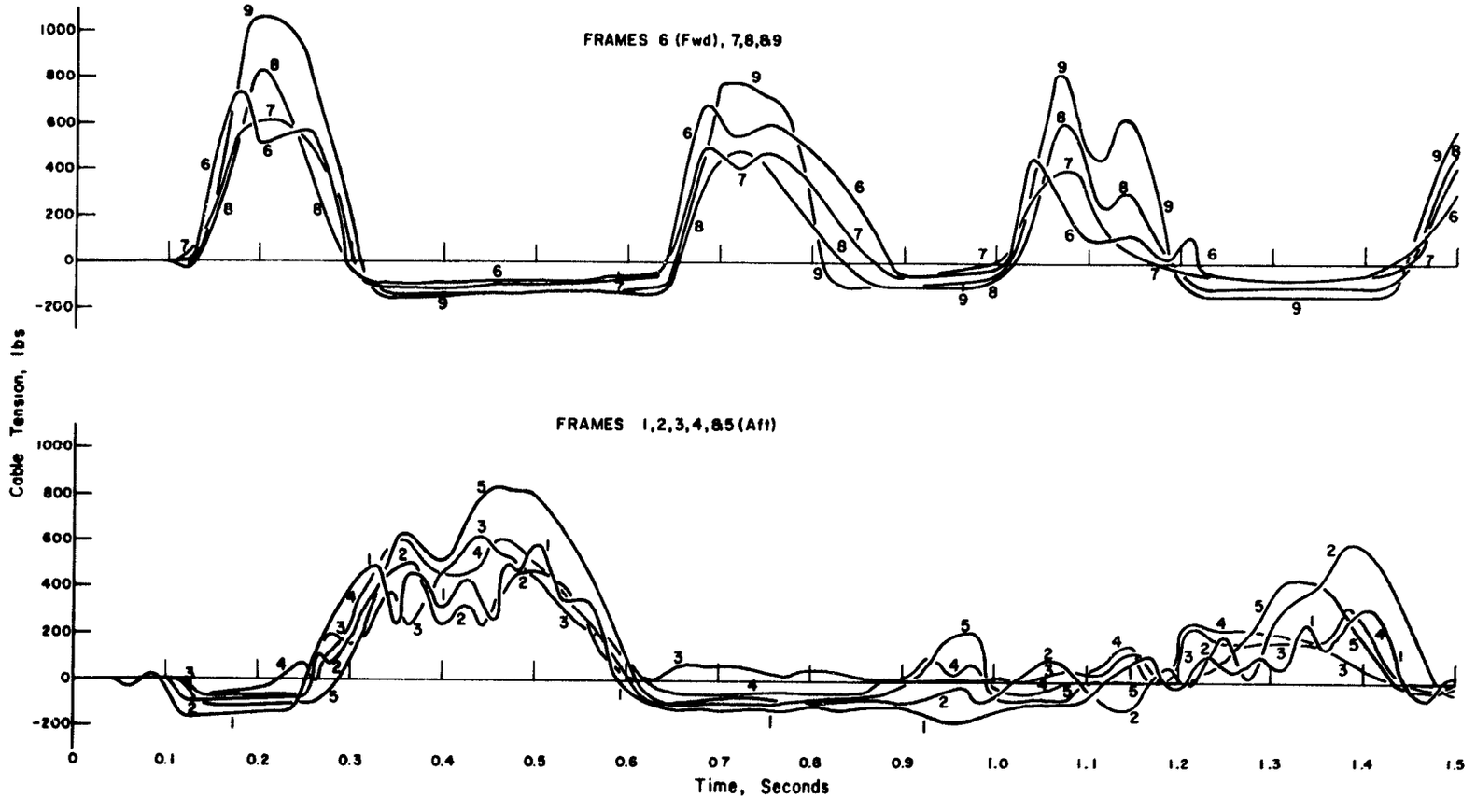

Figure 3.9 Time histories of loads in port surge cables, Shot Franklin.

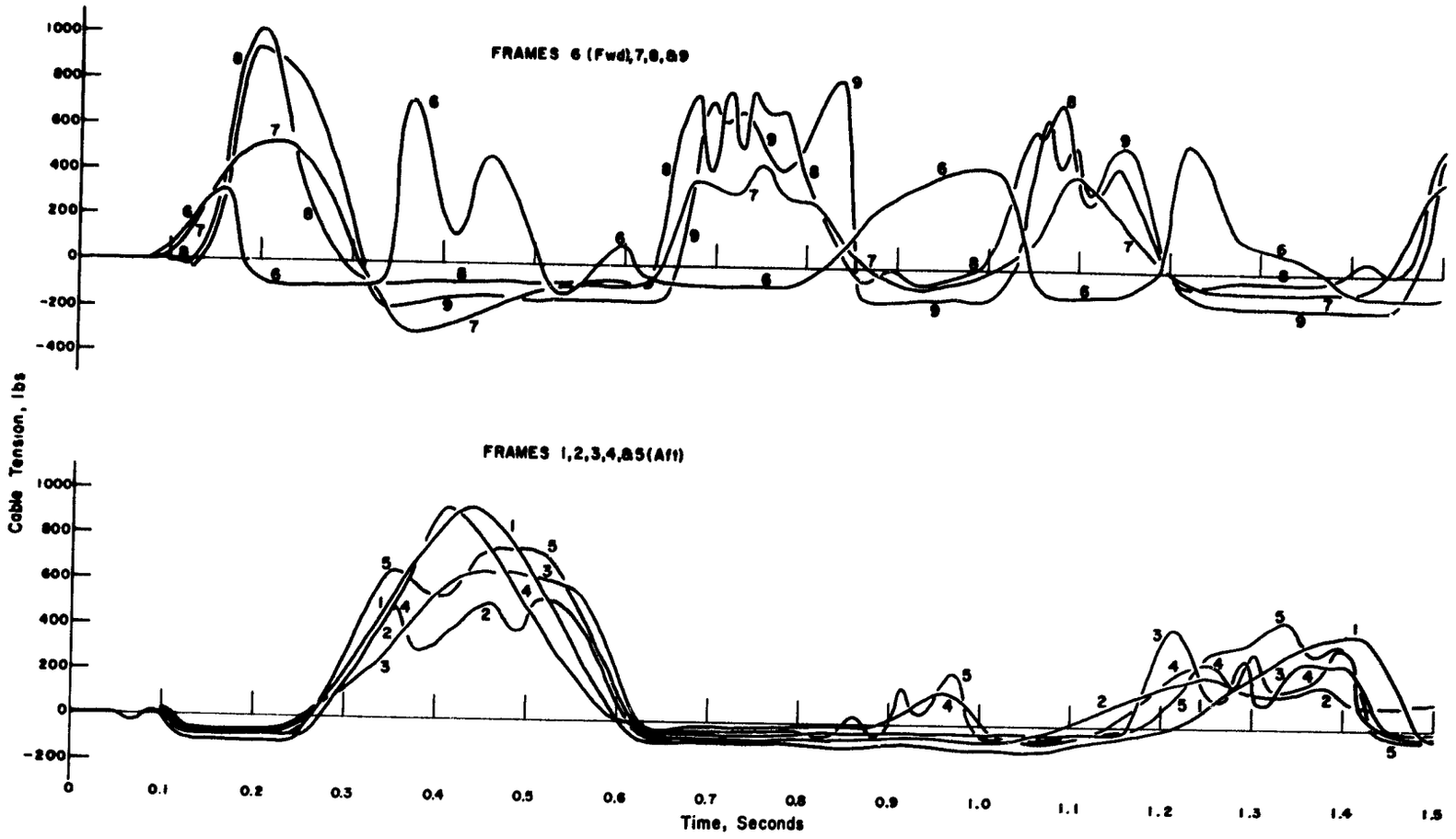

Figure 3.10 Time histories of loads in starboard surge cables, Shot Franklin.

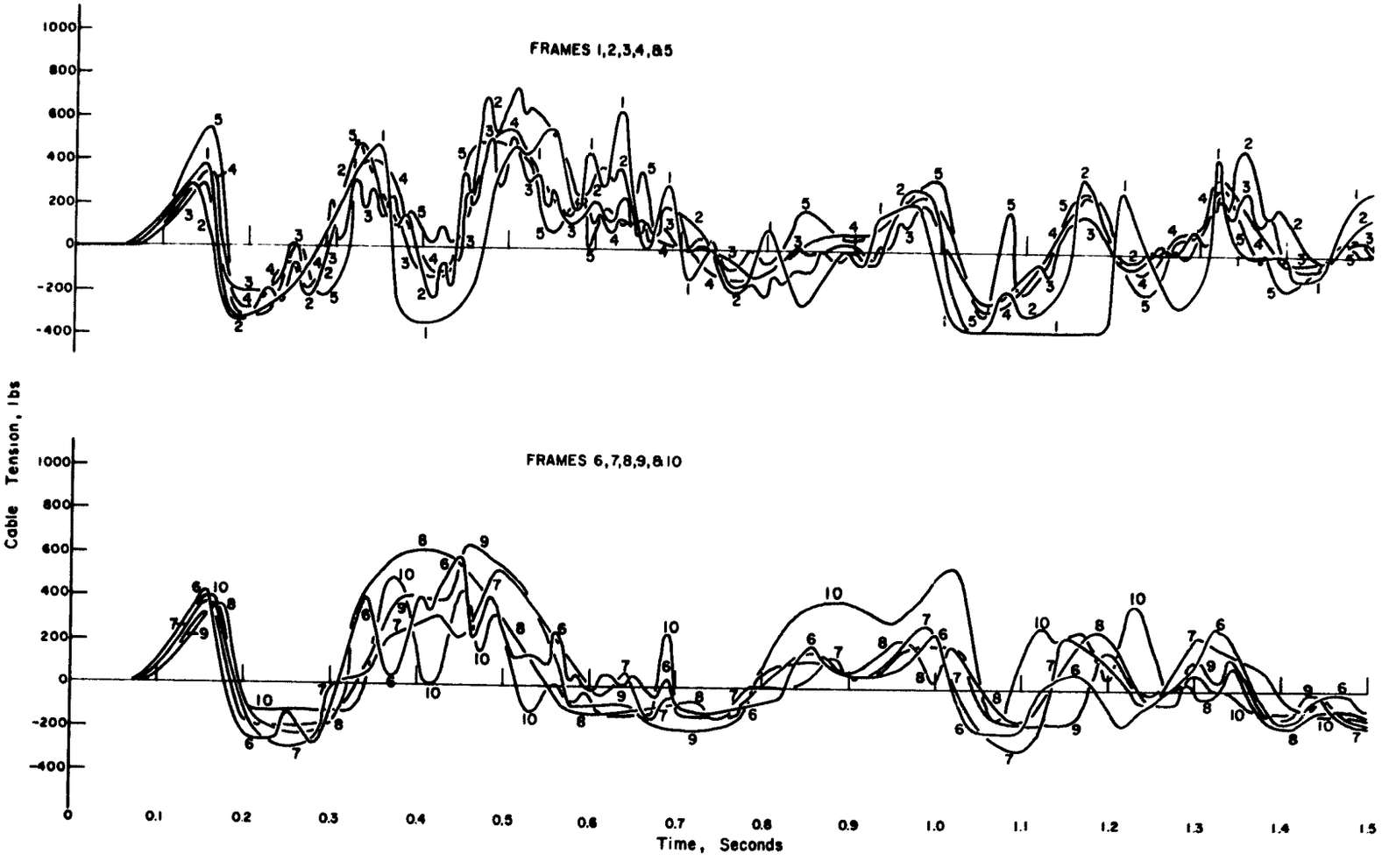

Figure 3.11 Time histories of loads in port tie cables, Shot Franklin.

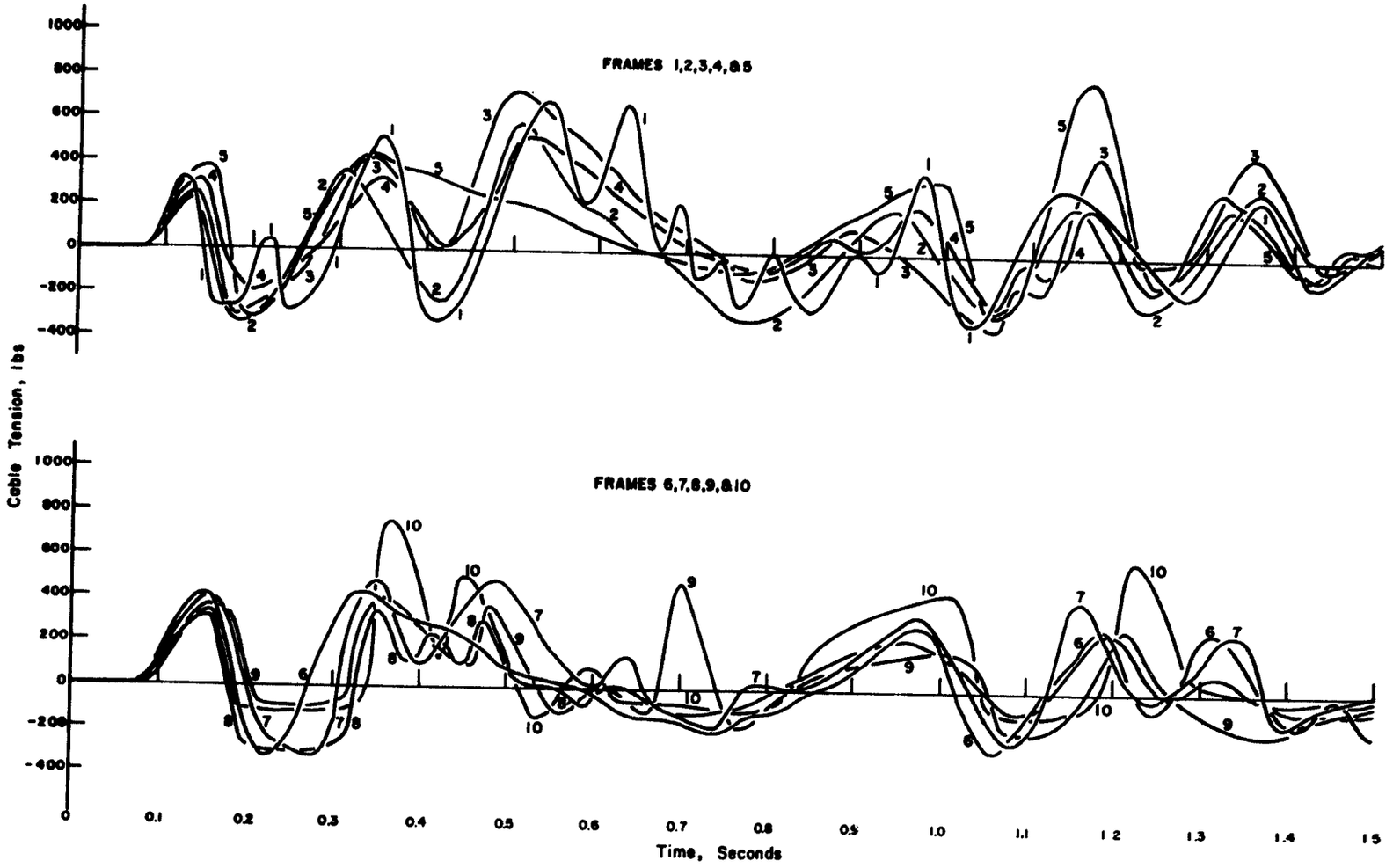

Figure 3.12 Time histories of loads in starboard tie cables, Shot Franklin.

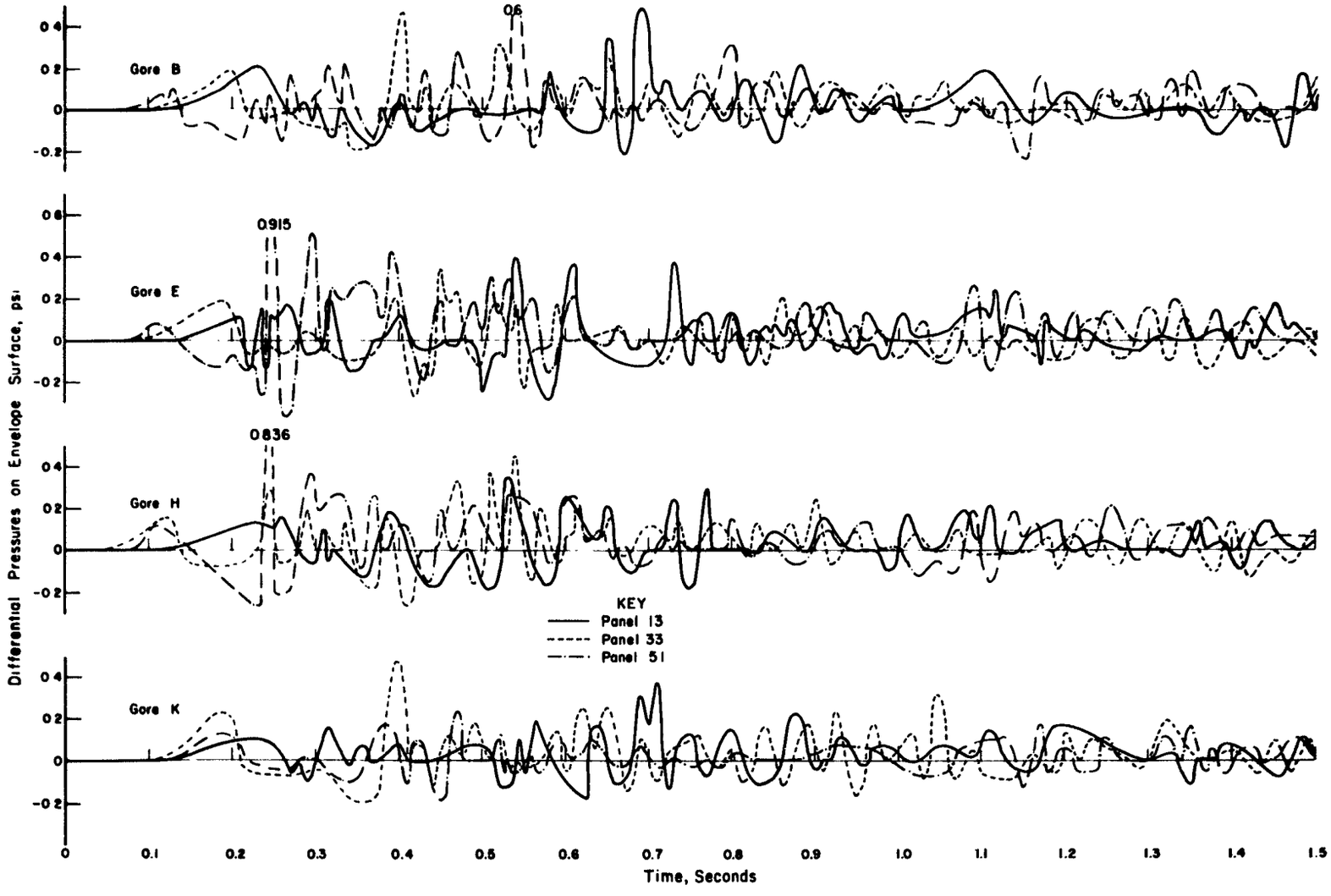

Figure 3.13 Time histories of differential pressures on airship envelope, Shot Franklin.

TABLE 3.1 SUMMARY OF RECORDED PEAK CABLE LOADS, SHOT FRANKLIN
(Internal and external suspension and fin-brace cable loads).

Columns 3, 4, and 6 represent loads for times up to 0.25 second; Columns 7, 8, and 9 represent peak loads for the total recording time.

(1)	(2)		(3)		(4)		(5)	(6)		(7)		(8)		(9)	
Frame Number	Initial Tension Load per Cable		Maximum Measured Incremental Tension Load per Cable t ≤ 0.25 sec.		Maximum Total Tension load Per Cable t ≤ 0.25 sec.		Design Breaking Strength Per Cable	Percent of Design Breaking Strength Attained t ≤ 0.25 sec.		Maximum Measured Incremental Tension Load per Cable		Maximum Total Tension Load per Cable		Percent of Design Breaking Strength Attained	
	Port	Stbd	Port	Stbd	Port	Stbd		Port	Stbd	Port	Stbd	Port	Stbd	Port	Stbd
	pounds		pounds		pounds		pounds	pct		pounds		pounds		pct	
30-Degree Internal Suspension System:															
1	1020		250		1270		7000	18		3250		4270		61	
3	797	580	412	372	1209	952	3570	34	27	1350	1120	2147	1700	60	48
5	911	825	632	668	1543	1493	4760	32	31	1525	790	2436	1615	51	34
7	1085	724	1160	965	2265	1689	4420	51	38	1250	950	2235	1674	53	38
9	1400	886	1850	1725	3250	2611	4420	74	59	1675	1600	3275	2686	74	61
11	610	680	2050	2320	2660	3000	4420	60	68	2150	2340	2760	3020	62	68
60-Degree Internal Suspension System:															
1	866	795	100	170	966	965	3570	27	27	1750	1600	2616	2595	73	73
3	935	978	302	322	1237	1300	3570	35	36	1400	1770	2335	2746	65	77
5	1172	910	576	512	1748	1422	4760	37	30	1600	1125	2772	2035	58	43
7	1115	958	1040	917	2155	1872	4420	49	42	1250	975	2335	1839	53	41
9	1000	567	2100	1580	3100	2167	3315	94	65	2175	1650	3175	2237	96	67
11	1002	720	2560	2690	3562	3410	4420	81	77	2600	2700	3602	3420	81	77

Horizontal Fin-brace Cables, Lower Set:

1	130	130	400	300	530	430	5610	9	8	945	870	1075	1000	19	18
2	90	90	130	160	210	250	2210	10	11	310	260	400	350	16	16
3	90	90	170	210	260	300	3315	8	9	530	660	620	740	19	22
4	80	80	140	180	190	200	2210	9	9	670	780	720	830	33	36
5	140	140	230	290	370	430	6800	5	6	2035	2200	2175	2340	32	34

External Suspension System, Surge Cables:

1	80	80	0	20	80	100	2360	2	3	565	920	665	1000	20	30
2	40	0	20	0	60	0	2520	2	0	590	530	630	530	25	21
3	40	72	0	0	40	72	1660	2	4	610	650	650	722	39	43
4	40	48	0	0	40	48	1200	3	4	600	930	640	978	53	62
5 (Aft)	40	8	0	0	40	8	1200	3	1	830	750	870	758	73	63
6 (Fwd)	40	32	690	--*	730	--*	1200	61	--*	730	--*	770	--*	64	--*
7	32	40	586	523	718	563	1200	60	47	610	530	642	570	54	48
8	120	136	819	1013	939	1149	1680	56	68	830	1020	950	1156	57	69
9	48	160	1093	938	1141	1098	3360	34	33	1050	940	1098	1100	33	33

External Suspension System, Tie Cables:

1	112	144	361	320	473	464	2520	19	18	630	690	742	834	29	33
2	48	72	273	238	321	310	2520	13	12	740	380	788	452	31	18
3	16	0	273	271	289	271	2520	11	11	510	730	526	730	21	29
4	88	0	328	315	416	315	2520	17	13	540	530	622	530	25	21
5	16	0	547	400	563	400	2520	22	16	550	820	566	820	22	33
6	8	8	417	388	425	396	2520	17	16	580	430	588	438	23	17
7	40	56	360	399	400	455	2520	16	18	520	490	560	546	22	22
8	16	24	355	311	371	335	2520	15	13	610	320	626	344	25	14
9	72	16	323	372	395	388	2520	16	15	630	460	702	496	28	20
10	144	112	375	318	519	430	2520	21	17	550	760	694	872	28	35

*Measurement of starboard surge cable load at Frame 6 was unreliable (see Section 4.4).

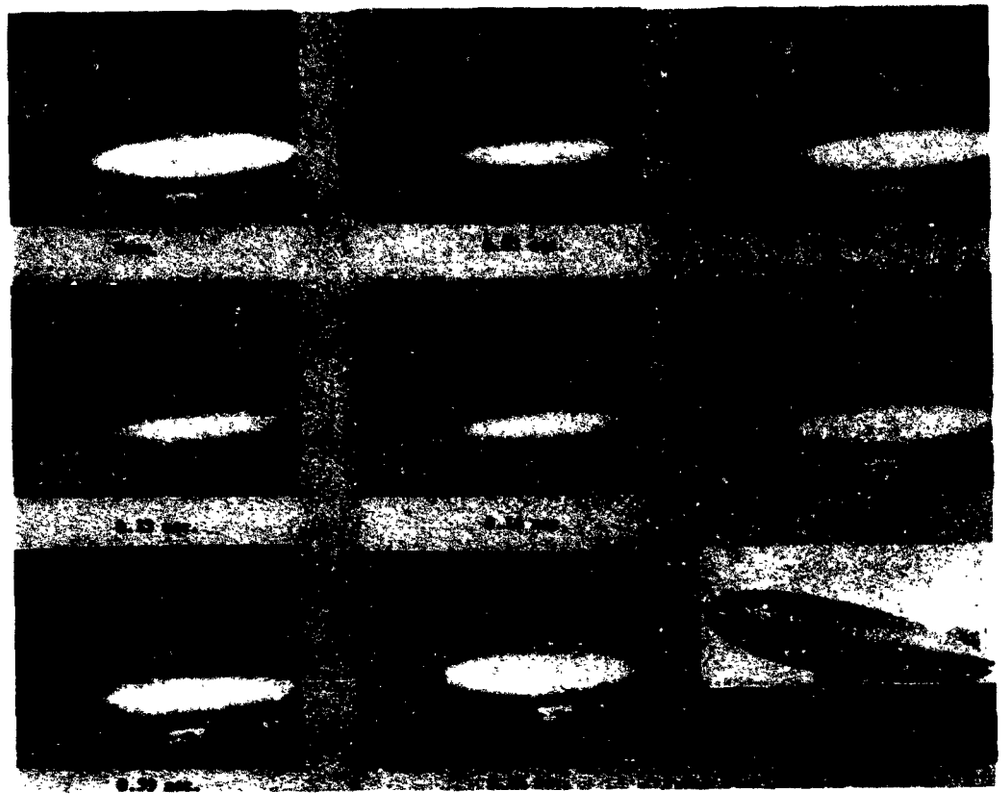

Figure 3.14 Motion-picture time sequence, Shot Franklin.

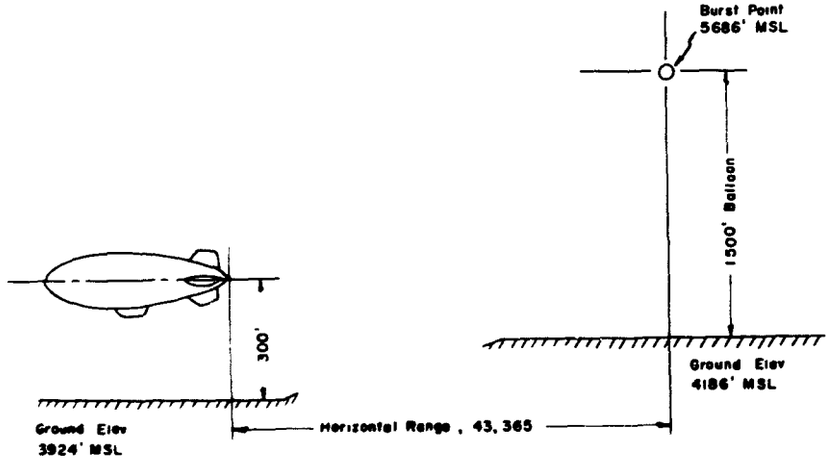

Figure 3.15 Airship test setup, Shot Stokes. It is estimated that longitudinal axis of airship was aligned within 5 degrees of vertical plane passing through burst point and airship position. Before test pressure conditions: Forward ballonet, 1.95 inches H_2O and 25 pct full: aft ballonet, 2.00 inches H_2O and 30 pct full; helium chamber, 1.88 inches H_2O. Car weight, 18,500 pounds.

Figure 3.16 Motion-picture time sequence, Shot Stokes.

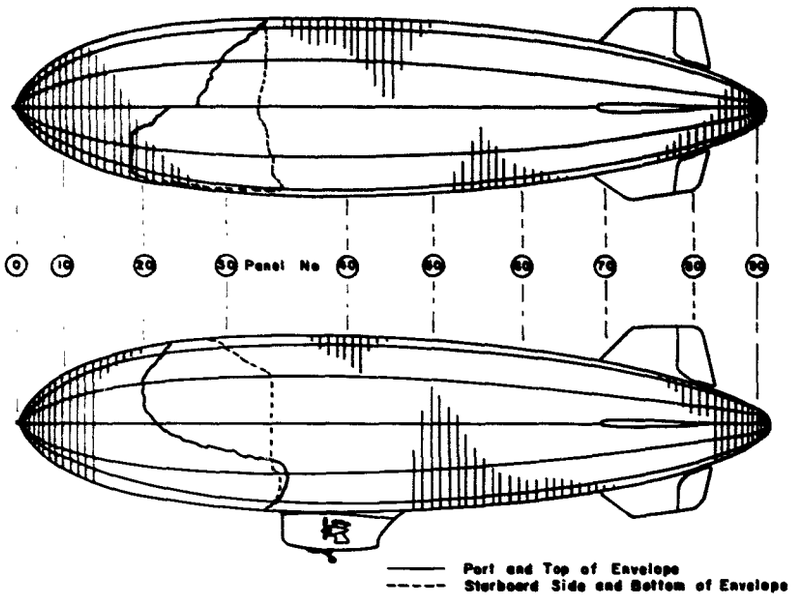

Figure 3.17 Diagram of ruptured section of envelope, Shot Stokes.

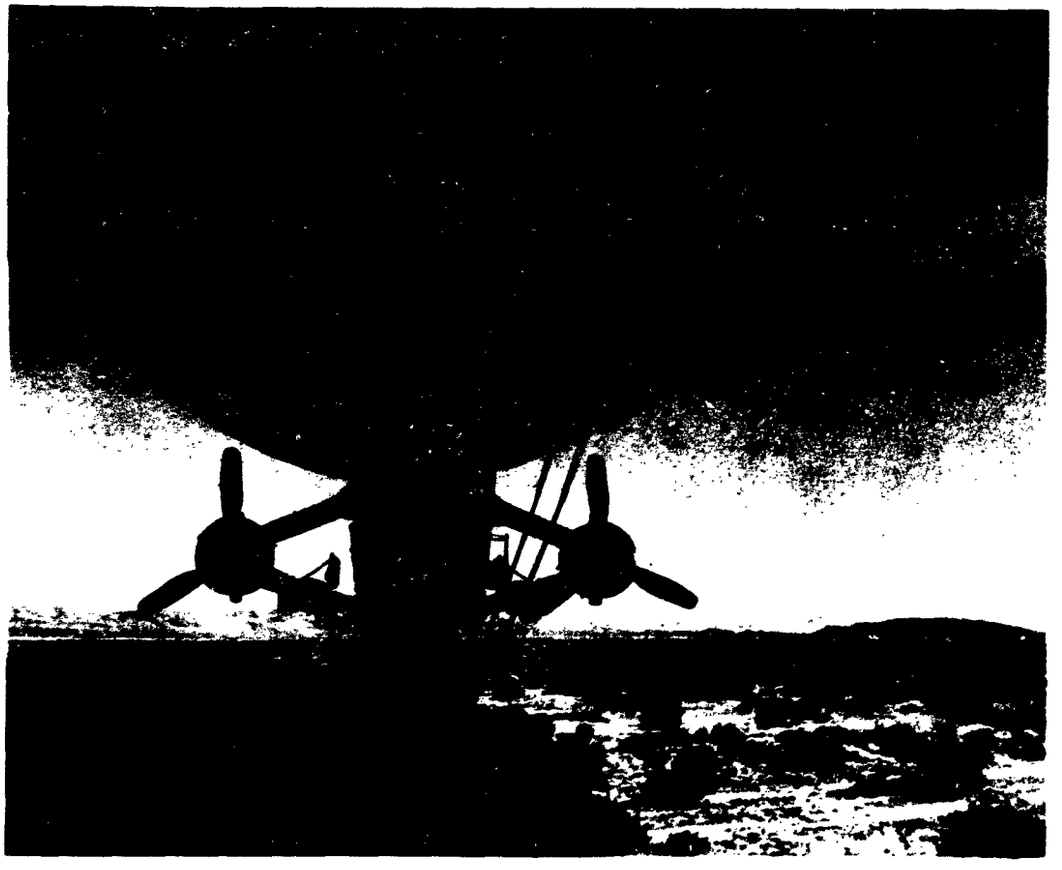

Figure 3.18 Area where envelope failure originated, Shot Stokes.

Chapter 4
DISCUSSION

4.1 FREE-FIELD OVERPRESSURE DATA

Following the anomalous external overpressure readings obtained by Project 5.2 during Shot Franklin, free-field overpressure measurements were made during several subsequent shots with pressure gages independent of the airship instruments. These data are discussed in Appendix B. The likelihood of certain envelope shock-refraction influences on the external overpressure measurements during Shot Franklin is discussed in Section 4.2. The overpressure anomalies, which resulted in consistently higher pressures than those predicted (using the generally accepted pressure-distance relations), were partially responsible for the inadequate participation of the project.

4.2 SHOCK-REFRACTION EFFECTS

In Appendix C the application of available theories and shock-tube experiments to the interaction of the air shock and the airship envelope is discussed.

The hypothesis discussed in Appendix C regarding the characteristics of the shock-refraction phenomena may be at least partially evaluated in view of the pressure data obtained during Shot Franklin. Referring first to the external overpressure records, there are certain atypical characteristics in the overpressure time histories, in addition to the lack of correlation of peak magnitudes. In Figure 3.4, the time-wise variation of overpressure recorded by both booms exhibits a rather gradual initial pressure rise with an abrupt peak, followed by a decay that is much greater than the classical form, and a subsequent pressure rise, followed by a more normal pressure decay. From the discussion of shock patterns in Appendix C, it would be expected that an irregular refraction configuration would occur in the vicinity of the airship car and that the locations of the shocks relative to the overpressure booms would be such that the booms would be between the interface and the intersection of the incident and reflected shocks shown in Figure A.2. Thus, there appears to be a qualitative correlation between the external overpressure time histories and the irregular refraction configuration anticipated. The magnitude of the peak overpressure was not considered to be strongly affected by the refraction phenomena since the reflected shock wave from the envelope should have been outside the boom position, but the peak magnitudes may have been affected by interaction with the ground.

The absolute pressures recorded at the envelope centerline and the differential pressures on the envelope surface appear to further support the qualitative descriptions of the refraction conditions discussed in Appendix C. The differential pressure measurements are considered less reliable because of the local transverse accelerations of the fabric and the known sensitivity of the pressure gages to acceleration forces. Also, local shock reflections within the en-

velope, particularly at times following the transit of the external shock wave, may have been responsible for some of the rapid pressure fluctuations recorded. Most of the maximum loads of significance, however, occurred during the early times up to approximately 0.25 second after shock arrival at the tail; thus, it is considered reasonable to concentrate on these phenomena. Both the differential and absolute pressures measured during the initial pressure rises exhibited the characteristics of compression waves, as would be expected for the transmitted waves during the phases of irregular refraction. No immediate rarefaction was evident in the absolute pressures at the centerline; this may have been caused by the interaction at the centerline between the rarefaction waves from the envelope surface, which could have resulted in a delayed reaction during mutual penetration or a more complex phenomenon because of the convergence of the waves.

Perhaps a more useful correlation between the measured pressures and the characteristics discussed in Appendix C is a comparison of the magnitudes of the peak internal pressures. The helium purity of Airship K-77 was estimated at 96.5 percent for Shot Franklin, and the maximum incremental pressure recorded at the centerline during the initial pressure buildup was 0.20 psi (Figure 3.4). The maximum differential pressure at the envelope surface was also of the same order. The ambient pressure was 12.77 psi, and the initial pressure in the envelope was 12.84 psi. For a transmitted pressure ratio of $0.20/12.84 = 0.0156$, Figure A.4 gives an incident pressure ratio of 0.0280. The incident peak overpressure thus derived would be $0.0280 \times 12.77 = 0.357$ psi, compared with the measured overpressure of 0.40 psi aft and 0.30 psi forward. It is considered that this indicates reasonable agreement between the measured values and the method discussed in Appendix C.

By the same technique, the peak internal pressure for Shot Stokes can be estimated. The external overpressure recorded was 0.75 psi; the helium purity, 97 percent; and the ambient atmospheric pressure, 12.76 psi. As shown in Figure A.4, the peak incremental transmitted pressure for these conditions is approximately 0.44 psi. The total internal excess pressure would have been $0.44 + 0.07 = 0.51$ psi.

4.3 AIRSHIP RESPONSE

The airship response to the blast effects is discussed in terms of the forcing functions and accelerations affecting the airship as a whole, the loads in the suspension systems, and the critical aspects of the loads in the envelope fabric. The theoretical response characteristics are correlated in so far as feasible with the data obtained in Shot Franklin, and the implications of these characteristics as they relate to the envelope failure in Shot Stokes are discussed.

The structural responses of the airship components which were recorded at times subsequent to the first load peaks in the more important systems were believed to have been strongly influenced by the presence of the mooring mast. Since quantitative data was lacking on the resultant mast reactions, it was not considered feasible to interpret the response measurements in terms of free-flight conditions beyond 0.25 second after shock arrival at the tail. Consequently, the following discussion of the response characteristics is limited to the initial 0.25 second, and consideration of the airship behavior for free-flight conditions at later times is beyond the scope of the data obtained by Project 5.2.

4.3.1 Accelerations. The primary response of the airship to the blast wave should have been a translational acceleration resulting from the pressure force, as discussed in Section C.3. It is believed that the total pressure force resulted from two primary sources: One was the overpressure transmitted inside the envelope which advanced ahead of the incident shock for irregular refraction, and the other was caused by the external overpressure behind the incident shock being greater than the internal pressure. The leading transmitted pressure produced a thrust against the inside of the envelope while the greater external pressure relieved the initial envelope tensions, producing a thrust that was limited to the initial tension force.

The internal and external overpressures recorded in Shot Franklin (Figure 3.4) were evaluated in terms of time and distance, resulting in a conclusion that the maximum longitudinal

force could be approximated by the peak internal overpressure multiplied by the cross-sectional area of the envelope at the station where the peak incident pressure was located at the time of maximum longitudinal acceleration. This was determined to be approximately 50 feet aft of the theoretical bow, where the area was 2,550 ft^2. The initial envelope pressure corresponded to 1.88 inches of water, or 0.068 psi. The total overpressure was 0.20 + 0.068 = 0.268 psi, and the maximum pressure force was 98,000 pounds.

The mast-force oscillograph trace was off scale at the time the maximum longitudinal acceleration was recorded, and the nose-cone fitting failed at some time during the blast-loading sequence. The horizontal force required to break the fitting was about 18,000 pounds, according to static test results. If it is assumed that the mast was reacting with a longitudinal force of 15,000 pounds at the time of maximum pressure forces, the net longitudinal force would have been 83,000 pounds.

To correlate the calculated forces with the measured accelerations, the effective weight of the test airship was determined to have been 38,000 pounds from the weight of the air displaced, increased by an additional mass coefficient of 0.07 determined from Reference 2, page 84. The peak longitudinal acceleration, based on the pressure forces with an assumed mast reaction of 15,000 pounds, is then a = 83,000/38,000 = 2.18 grams. This compares well with the recorded peak acceleration of 2.20 grams and indicates that, had there been no mast reaction, the maximum longitudinal acceleration might have been a = 98,000/38,000 = 2.58 grams.

The peak forces and accelerations for Shot Stokes may also be estimated in a similar manner, neglecting the probability that the envelope rupture occurred before these peak forces developed. As stated in Section 4.2, the estimated peak internal total pressure was 0.51 psi. Thus, the maximum pressure force would be 187,000 pounds and the peak longitudinal acceleration would be 4.93 grams.

4.3.2 Suspension Systems. Since the airship car was attached to the envelope by means of internal and external cable suspensions, the car acceleration forces had to be transmitted through these cables. The suspension systems and their normal functions are described in Section 1.3. Owing to the multiplicity of the cable systems, it was difficult to accurately determine the load distributions for any but the simplest loading conditions. A method of static analysis of typical airship suspension systems, based on the elastic characteristics, is discussed in Appendix D. The normal design conditions for an airship involve relatively small longitudinal and lateral loads. Consequently, vertical loads and pitching moments, as well as the elastic properties associated with these factors, are given primary emphasis in the elastic analysis.

As discussed in Appendix D, the elastic properties of the external systems have not been determined for the ZSG-3 airship. It was therefore possible to calculate only the cable loads for the internal systems, using the equilibrium equations for vertical loads and moments and neglecting the longitudinal equilibrium. In the ZSG-3 system, this technique should not be too seriously in error since the external systems should be far stiffer than the internal systems for longitudinal loads. The major effect of neglecting the distribution of longitudinal cable forces is to define the proportion of longitudinal force carried by the internal system as that resulting from the vertical force and pitching moment applied to the car without considering interaction between the internal and external systems.

The internal suspension system loads are calculated in Appendix D for t = 0.20 second, assuming a quasi-static condition. The resulting cable loads are compared with the measured loads from Shot Franklin in Figure 4.1, and the agreement is considered quite good. Similar calculations for other times have also resulted in fair agreement, and it is concluded that this method of determining the internal cable loads is satisfactory for the ZSG-3 airship when subjected to a blast wave traveling essentially parallel to the longitudinal axis.

No calculation of individual cable loads in the external systems has been attempted since the necessary elastic properties of the cables and catenary systems were not available. The total longitudinal load in the Shot Franklin surge system, derived from the recorded data, did not agree well with that estimated from the longitudinal components of the internal cable loads and the longitudinal acceleration forces on the car. It is suspected that the measured external cable loads are not representative of the total cable loads since only one leg of each single or

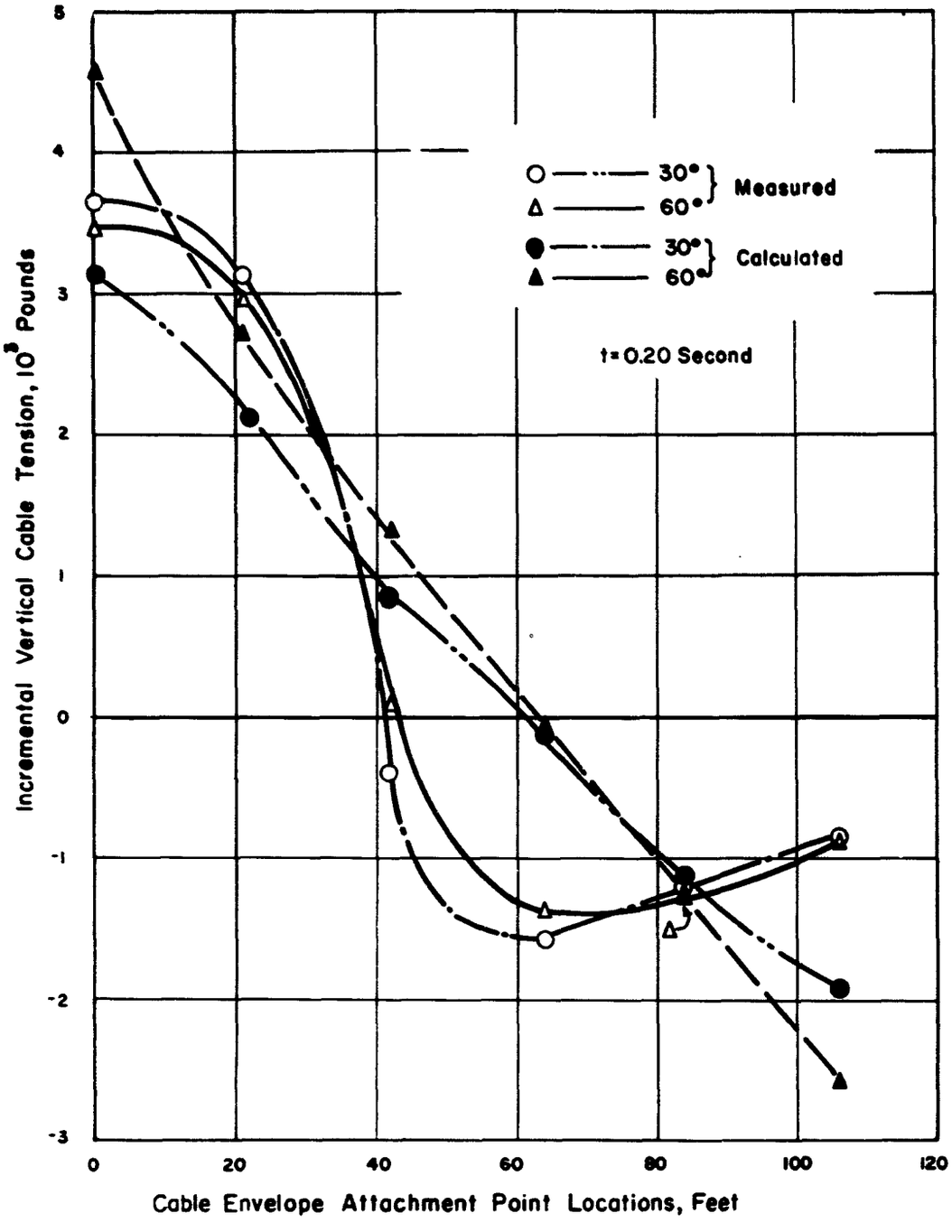

Figure 4.1 Internal cable-load distributions.

double loop was instrumented, and the elastic properties of the other legs may have been significantly different, which would probably result in load variations between the parts of the loop, particularly for dynamic conditions.

To satisfactorily calculate the distribution of loads in the surge and tie cable systems, it would be necessary to determine the longitudinal and vertical stiffness parameters of each component. Unlike the internal systems, where the most important flexibility is caused by envelope deformations, the relative stiffness of each part of the cable loops and the external catenary must be accurately defined. It appears that these parameters could not be adquately determined, except by an extensive series of static tests which would be beyond the scope of Project 5.2. It is assumed that the loads recorded in the external systems do not necessarily represent the maximum loads that might have occurred in portions of the cables which were not instrumented.

During Shot Stokes, in which no response measurements were obtained, a careful postshot inspection of the airship revealed no evidence of failures or overstressing of any of the components of the suspension systems, although the loads imposed were sufficient to rupture the envelope. Some implications of this result are discussed in Section 4.3.3.

4.3.3 Envelope Fabric Loads. Although it was considered desirable, it was not deemed feasible during the instrumentation of the test airships to provide suitable gages to record envelope fabric stresses. The maximum fabric tensions in both Shots Franklin and Stokes could be estimated only on a basis that was reasonably consistent with the available data, which was correlated with the calculated response characteristics.

The primary envelope stresses are normally caused by the pressure differential, aerodynamic forces, accelerations of the envelope, and local loads from the suspension catenaries. For the test conditions, aerodynamic forces may be neglected since the airships were stationary and the blast gust velocities were substantially parallel to the longitudinal axis. In view of the high longitudinal accelerations, it seems evident that the most critical area of the envelope would be at the bottom, immediately forward of the car, since the longitudinal forces carried by the external suspension system would be concentrated in this area.

The hoop tension stresses depend on the pressure differential, and the longitudinal stresses are related to accelerations and local suspension system loads, as well as to differential pressures. Consequently, the longitudinal and lateral stresses are not directly proportional. In fact, the hoop tension should be zero behind the incident shock for all cases in which the shock overpressure exceeds the sum of the transmitted and initial internal excess pressures. The maximum lateral and longitudinal tensions will not, in general, occur simultaneously; however, the fabric, which has essentially equal strength in both the lateral and longitudinal directions, is not isotropic, in the sense of more homogeneous materials, because of the perpendicular threads that act independently to a large degree. Accordingly, the lateral and longitudinal tensions are considered independently.

The maximum tensions have been calculated for Panel 33, Gore A, as follows:

Shot Franklin:	Hoop tension = 100 lb/in. at t = 0.18 second
	Longitudinal tension = 190 lb/in. at t = 0.22 second
Shot Stokes:	Hoop tension = 190 lb/in.
	Longitudinal tension = 427 lb/in.

The specification strength of the fabric involved is 225 lb/in. in either the lateral or longitudinal direction. In Shot Franklin, the calculated longitudinal tensions indicated a minimum safety factor of 1.18, based on the specified breaking strength, and the envelope fabric should not have failed under these conditions.

In Shot Stokes, the fabric strength would have been adequate for the calculated hoop tension; however, the longitudinal tension, based on the peak acceleration of 4.93 grams estimated in Section 4.3.1, was nearly twice the fabric breaking strength. Laboratory tests of fabric samples from various areas of the ruptured envelope indicated that its strength was equal to, or greater

than, the specified minimum of 225 lb/in. in both the warp and fill directions. Since the longitudinal tension should be directly proportional to the longitudinal acceleration, at least to a first approximation, the fabric failure would be expected to occur at an acceleration of 225/427 × 4.93 = 2.60 grams. If the acceleration time history for Shot Stokes was similar in shape to that for Shot Franklin, 2.60 grams would have occurred at about t = 0.16 second. If the incremental suspension cable loads recorded for Shot Franklin at t = 0.16 second are increased by the ratio of the peak longitudinal accelerations, 4.93/2.20 = 2.24, the resulting cable loads should be representative of those for Shot Stokes at the time of envelope failure. The suspension cable loads for Shot Stokes determined on this basis do not exceed the specified breaking strengths. The motion-picture sequences of Figures 3.14 and 3.16 are useful for a qualitative study of the variations of load distributions in the internal suspension systems; the indentations of the envelope at the catenary seams should be directly related to the associated cable tensions. The shift of peak cable tensions with time from the aft cables to the forward cables is clearly shown in Figure 3.14 for Shot Franklin. Although the catenary seam deflections are not as evident for the Shot Stokes sequence in Figure 3.16, it appears that, at the time of the initiation of the envelope rupture, the internal cable loads were almost uniformly distributed. This would probably correspond to times no later than 0.16 second, based on the load variations of Figures 3.6 and 3.7. Analysis appeared to support the probability of envelope failure prior to significant suspension system damage, although secondary effects (such as possible asymmetry of loads and local load variations) were neglected because of the somewhat approximate nature of the analysis. Results of this study of the limited test effects did tend to confirm that the envelope strength was the limiting factor for the test conditions.

No satisfactory explanation has been found for the ballonet failure in Shot Franklin. Since the ballonet was only about 50 percent full, it did not appear likely that the failure could be directly attributed to excess pressure. It may have been caused by local effects that might not be representative. Under normal flight conditions, a ballonet failure would not be catastrophic since the airship could probably be trimmed by use of the elevator controls.

4.4 RELIABILITY AND ADEQUACY OF DATA

In general, it is believed that the recorded data are reliable within ±10 percent. The few exceptions to this statement are briefly discussed below. The calibrations of all measuring systems were performed with the utmost care over ranges representative of the expected recordings. The external overpressure boom systems were recalibrated posttest in a Ballistic Research Laboratories (BRL) shock tube. The frequency response was found to be adequate, and the accuracy in pressure magnitudes was found to be excellent over the usable range of the pressure gage.

The reliability of the envelope differential pressure measurements was doubtful because of the acceleration sensitivity of the gages (see Section 3.1). Unfortunately, it was not possible to estimate whether any of these differential pressure measurements were realistic.

It is apparent that the measurement of tension in the starboard surge cable at Frame 6, Figure 3.10, is in error since the time history is completely out of phase with the loads in the associated cables.

Owing to the unfortunate circumstances encountered by Project 5.2 during Operation Plumbbob (Section 2.2), the desired scope of data was not obtained. The complexity of the airship structural system and the lack of adequate methods of response analysis required test data for a wide range of blast-wave orientations and input levels in order to substantiate any generally applicable technique for blast-response predictions. Since it was not possible to obtain the scope of data desired, the analysis of the results was limited to the single type of orientation tested with interpretations that seemed to be consistent with the data. To place a high degree of confidence in these deductions, additional full-scale response data would be necessary. However, the conclusions derived were considered to be reasonably valid and suitable to form at least a partial basis for further analytical work on the blast response of other airship models.

Chapter 5
CONCLUSIONS and RECOMMENDATIONS

5.1 CONCLUSIONS

It is concluded that the basic objective of Project 5.2 was not fulfilled since the scope of the data obtained was not adequate to define the response characteristics over a sufficient range of shock-wave orientations nor to satisfactorily justify techniques of analysis for predicting the critical-response parameters.

The following useful results were obtained despite the fact that the basic objective was not reached:

1. A method of relating the peak overpressures transmitted inside the envelope to the external overpressure was proposed and shown to correlate reasonably well with the limited test data.
2. A simple method for estimating the peak longitudinal acceleration of an airship subjected to a blast wave traveling parallel to the longitudinal axis was empirically derived.
3. A method of determining the internal suspension system loads, based on the elastic properties of the system, correlated favorably with the measured loads and may be satisfactory for a wider range of conditions if more adequate elastic parameters can be established.
4. The occurrence of the envelope failure in Shot Stokes was consistent with the response measurements from Shot Franklin, based on calculated fabric tensions.
5. The measured loads in the external suspension system were not necessarily representative of the total load in the cable loops.
6. The analysis of the Shot Franklin test data and the results of the Shot Stokes test tended to confirm that, for the ZSG-3 airship, the envelope strength was the limiting factor for the test conditions.
7. The overall test results were considered a suitable basis for further analytical studies of airship response to nuclear blast effects beyond the scope of this report.

5.2 RECOMMENDATIONS

Additional analytical studies should be conducted to determine airship response characteristics and structural limits for blast waves impinging at various incidence angles. These studies should be extended to other airship models for which blast limits are required since most of the data and analysis of this report are specific to the ZSG-3 airship.

Appendix A

METHODS OF PREDICTING WEAPON-EFFECT INPUT LEVELS

The procedures and data contained in Reference 1 were utilized for determining airship test positions (slant-range distance from Ground Zero (GZ) for a desired overpressure input) and for predicting the magnitude of other weapon effects at such positions. In all cases, test positions were considered to be in the region of reinforced shock (Mach stem); hence, the values of all yields used for computing test positions were multiplied by a factor of 2.

A complete set of sample calculations is given to illustrate how airship test positions were determined and how input levels of weapon effects were computed. For the sample case, it was desired to obtain a peak overpressure of 0.50 psi at the tail of the airship when moored to the mast in a tail-to attitude. Significant test conditions were as follows:

Yield (positioning), 2 kt
Height of burst, 4,800 feet (MSL)
Height of tower, 500 feet
Elevation of GZ, 4,300 feet (MSL)
Elevation of ground at test site, 4,200 feet (MSL)

A.1 CALCULATION OF SLANT-RANGE DISTANCE

The mean altitude between the burst height (4,800 feet) and the test position (4,200 feet) was 4,500 feet (MSL). From Figure 60 of Reference 1, the following altitude correction factors were obtained: pressure, 0.84; distance, 1.04; and time, 1.06.

By dividing 0.50 psi (desired overpressure at tail of airship) by 0.84, an overpressure value of 0.595 psi for sea level conditions was obtained. From Figure 6 of Reference 1, a slant-range distance of 1,725 yards was obtained for a 1-kt burst for an overpressure of 0.595 psi at sea-level conditions. Multiplying by the distance correction factor of 1.04, a slant-range distance of 1,795 yards was obtained for a 1-kt burst at 4,500 feet MSL. To determine the slant-range distance for a yield other than 1 kt for a given overpressure, the cube-root rule is applied as follows:

$$\frac{d_2}{d_1} = \frac{W_2^{\frac{1}{3}}}{W_1^{\frac{1}{3}}}$$

or

$$d_2 = d_1 \frac{W_2^{\frac{1}{3}}}{W_1^{\frac{1}{3}}}$$

where d_1 is the slant-range distance for yield W_1 and d_2 is the slant-range distance for yield W_2

Substituting values from tne sample case:

$$d_2 = 1{,}795\left(\frac{4^{\frac{1}{3}}}{1^{\frac{1}{3}}}\right) = 1{,}795\ (4^{\frac{1}{3}}) = 2{,}850 \text{ yards}$$

Since the airship was in the Mach-stem region, the yield, W_2, in this case was multiplied by a factor of 2 to obtain overpressure effects equivalent to a 4-kt burst. Owing to the small angle between the slant-range vector from the burst point and the horizontal-range vector from GZ to the airship test position, the slant-range and horizontal-range distances were considered equivalent, i.e., 2,850 yards.

A.2 CALCULATION OF SHOCK-ARRIVAL TIME

From the foregoing calculations, a slant-range distance of 1,725 yards was obtained for the sample case for a 1-kt burst at sea-level conditions. From Figure 9 of Reference 1, using a slant-range distance of 1,725 yards, a shock-arrival time of 3.93 seconds was obtained. From the previous calculations, a time-correction factor of 1.06 was determined for

the mean altitude of 4,500 feet MSL. For a 1-kt burst at 4,500 feet MSL, the shock-arrival time then becomes 3.93 seconds times 1.06, or 4.17 seconds. Since the time of shock arrival also scales in accordance with the cube-root rule, the shock-arrival time for the sample case is then

$$4.17\left(\frac{W_2^{\frac{1}{3}}}{W_1^{\frac{1}{3}}}\right) = 4.17\left(\frac{4^{\frac{1}{3}}}{1^{\frac{1}{3}}}\right) = 6.62 \text{ seconds}$$

A.3 CALCULATION OF POSITIVE-PHASE DURATION

Using Figure 7 of Reference 1, the duration of the positive-pressure phase was calculated in the same manner as the time of shock arrival. For a slant-range distance of 1,725 yards (1-kt burst in a homogeneous, sea-level atmosphere), a positive-phase duration of 0.40 second was read from Figure 7. Multiplying by the time-correction factor of 1.06 for altitude, a value of 0.424 second was obtained. Using the cube-root rule, the duration of the positive-pressure phase was then determined to be:

$$0.424\left(\frac{W_2^{\frac{1}{3}}}{W_1^{\frac{1}{3}}}\right) = 0.424\left(\frac{4^{\frac{1}{3}}}{1^{\frac{1}{3}}}\right) = 0.674 \text{ second}$$

A.4 CALCULATION OF PEAK PARTICLE OR WIND VELOCITY

From Section 4, Appendix 1, of Reference 1, the following relations are given:

$$\rho = \rho_0\left(\frac{7 + 6\ P/P_0}{7 + P/P_0}\right) \qquad (A.1)$$

$$q = \frac{5}{2} P_0 \frac{(P/P_0)^2}{7 + P/P_0} \qquad (A.2)$$

$$\mu^2 = \frac{2q}{\rho} \qquad (A.3)$$

Substituting the value of ρ in Equation A.1 and the value of q in Equation A.2 into Equation A.3 and simplifying, the following equation was obtained.

$$\mu = \left[\frac{5\ P_0\left(\frac{P}{P_0}\right)^2}{\rho_0\left(7 - 6\ \frac{P}{P_0}\right)}\right]^{\frac{1}{2}} \qquad (A.4)$$

where μ = peak particle velocity, ft/sec
P_0 = ambient pressure in front of the shock, lb/ft^2
P = peak overpressure behind the shock front, lb/ft^2
ρ_0 = ambient density in front of the shock, slugs/ft^3
ρ = peak density behind the shock front, slugs/ft^3
q = dynamic pressure, lb/ft^2

In calculating the peak particle velocity for the sample case, the following values are used:

P_0 = 1,794 lb/ft^2 (at 4,500 feet MSL)

P = 72 lb/ft^2

ρ_0 = 0.002080 slugs/ft^3 (at 4,500 feet MSL)

Substituting these values in Equation A.4 and solving for μ, the peak particle velocity behind the shock was determined to be 30.8 ft/sec.

A.5 CALCULATION OF INCIDENT THERMAL ENERGY

For conservative results, all detonations were considered to be air bursts in computing incident thermal energies. Using a yield of 2 kt, as defined for the sample case, a thermal yield of 0.85 kt was obtained (using Figure 19A of Reference 1). From Figure 20B, Reference 1, for a slant-range distance of 2,850 yards, a thermal energy of 0.87 cal/cm^2 was obtained for a thermal yield of 1 kt. Since the incident thermal energy for a given slant-range distance is proportional to the thermal yield, the incident thermal energy for the sample case then equals:

$$\frac{Q_2}{Q_1} = \frac{E_2}{E_1}$$

or

$$Q_2 = Q_1\left(\frac{E_2}{E_1}\right)$$

where Q_1 and E_1 are the incident thermal energy and thermal yield for a total yield of W_1 kt and Q_2 and E_2 are similar quantities for a total yield of W_2 kt.

Substituting the values from above

$$Q_2 = 0.87\left(\frac{0.85}{1.0}\right) = 0.74 \text{ cal/cm}^2$$

A.6 CALCULATION OF NUCLEAR RADIATION DOSE

From Figure 121, Appendix 1, of Reference 1, the relative air density, R, for a mean altitude of 4,500 feet MSL for the sample case was determined to be 0.835.

From Figure 23A of Reference 1, the scaling factor for determining the initial gamma radiation dose was 2 since a 1 to 1 ratio existed below 10 kt on the graph. From Figure 22A of Reference 1, the initial gamma radiation dose at a slant-range distance of 2,850 yards from a 1-kt burst with R = 0.835 was 0.17 r. Multiplying by the scaling factor of 2, the total initial gamma radiation dose was then equal to $2 \times 0.17 = 0.34$ r.

Added to the initial gamma radiation dose was the neutron radiation dose from the device, which was assumed to be a high-neutron-flux device. From Figure 24 of Reference 1, for a slant-range distance of 2,850 yards and with R = 0.835, the neutron radiation dose for a 1-kt burst was determined to be 0.06 rem. For a yield of 2 kt, the total neutron radiation dose was then $2 \times 0.06 = 0.12$ rem.

The overall total dose for the sample case was then equal to the total initial gamma radiation dose (0.34 r) plus the total neutron radiation dose (0.12 r), or 0.46 r.

Appendix B
OVERPRESSURE MEASUREMENTS

The peak overpressure of 0.40 psi, measured by means of the aft probe on the airship car during Shot Franklin, was considerably higher than the value of 0.06 psi calculated for the test position, based on the postshot yield estimate of 0.138 kt. The calculated overpressure of 0.06 psi was based on the procedures and data given in Reference 1, assuming a shock-reinforcement factor of 2 in the Mach-stem region. As shown in Figure B.2, the measured overpressure during Shot Franklin did not rise instantaneously to its peak value in the characteristic manner; instead, it had an initial low rise-time rate before rising sharply to the peak value.

In view of the foregoing results, it was considered a possibility that the overpressure-instrumentation installation on the airship was adversely affecting the validity of the measurements because of proximity of the envelope to the probe, adjacent structure, and other environmental conditions.

Accordingly, it was decided to obtain independent overpressure measurements at the planned airship test site on the next scheduled participation (Shot Wilson) by setting up instrumentation on the ground adjacent to the airship. In this manner, the effect of the installation arrangement on the airship could be evaluated by comparison of the overpressure records obtained at the ground station and on the airship. Although the airship did not participate during Shot Wilson, overpressure measurements were obtained using the ground station set up at the planned test location. Similar data was subsequently obtained using the ground station during Shots Kepler, Owens, and Stokes.

B.1 INSTRUMENTATION

Figure B.1 shows the instrumentation arrangement used to measure and record time histories of overpressure at selected ground stations during the various tests.

The overpressure probe and component parts removed from Airship K-77 after Shot Franklin were mounted on a plywood base, as shown. The probe was approximately 18 inches long and $1\frac{3}{4}$ inches in diameter. An orifice, 0.07 inch in diameter, was located on one side of the probe about $10\frac{1}{2}$ inches aft of the tip. A right-angled pressure tube inside the probe extended from the orifice to the diaphragm of the differential pressure pickup. The opposite side of the pickup was vented into a pressure-reference chamber, which was manually sealed at ambient pressure a few minutes before detonation.

Another differential pressure pickup, similar to the one in the probe, was mounted on top of the probe with the diaphragm normal (side-on) to the direction of the shock-wave propagation. For Shot Wilson, this pickup was vented to the reference chamber; for all other tests, the reference side was sealed at the pickup a few minutes before the tests.

For all tests, except Shot Wilson, an absolute pressure pickup was also mounted on top of the probe and oriented to measure side-on overpressure.

All pressure pickups were CEC Type 4-312. The differential pickups had a range of ±1.0 psi (plus 100-percent overshoot), and the absolute pickup had a range from 0 to 15 psi. Galvanometer 7-342 was used with the overpressure probe measuring system, giving a frequency response that was flat to 135 cps. With the exception of Shot Wilson, Galvanometer 7-339 was used in the differential and absolute pressure pickup recording system, resulting in a system response that was flat to 30 cps. All recording systems were 0.7 critically damped.

In addition to the Project 5.2 overpressure instruments, undamped very low pressure (VLP) gages furnished by Project 1.1 were installed on the plywood platform in an attempt to obtain data from an independent system for correlation.

On all tests, the plywood platform was weighted down on a table or platform, and all pickups were oriented side-on to the burst point. Pickups were located about 4 to 5 feet aboveground. Cleared areas, free of obstructions and uneven terrain, were selected at the test sites.

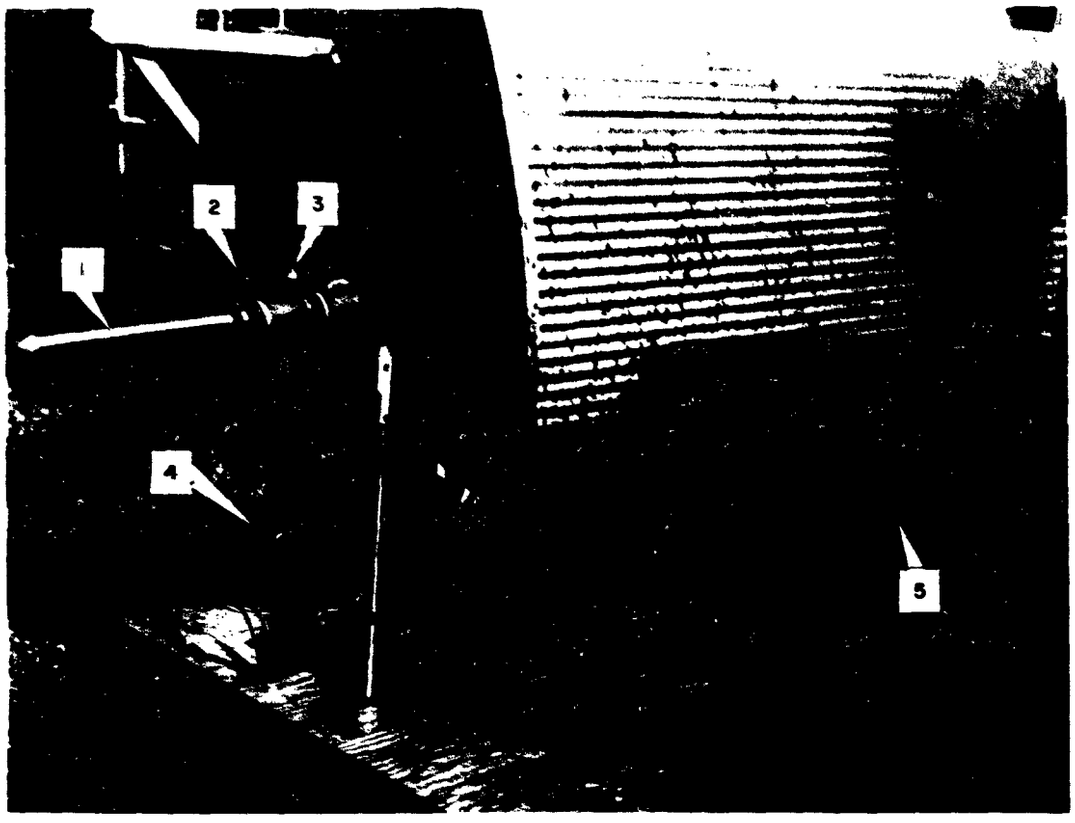

Figure B.1 Details of ground test setup for overpressure measurements. (1) Overpressure probe from aft end of airship, (2) differential pressure pickup, (3) absolute pressure pickup, (4) pressure reference chamber, and (5) recording oscillograph.

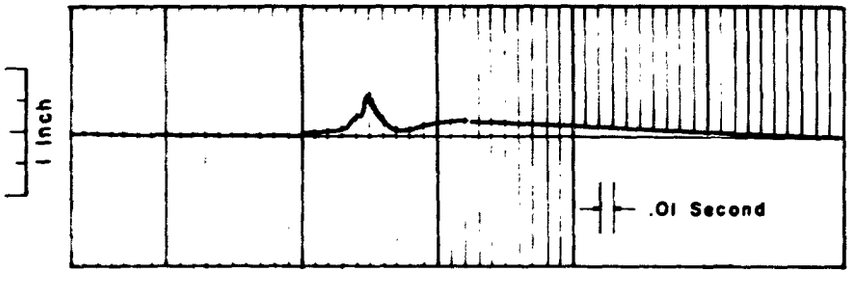

Figure B.2 Reproduction of oscillograph record of overpressure measurements, Shot Franklin. Differential pressure pickup inside probe installed on aft end of airship car. Galvanometer 7-342, 0.7 critically damped, 135 cps. Sensitivity, 1.29 psi per inch.

B.2 RESULTS

Peak overpressures measured with Project 5.2 instruments at the selected ground station during Shots Wilson, Kepler, Owens, and Stokes are listed in Table B.1, together with the pertinent conditions of each test. Also included is overpressure data recorded by the airship instrumentation during Shot Franklin. Calculated values of peak overpressure, based on the test conditions of each shot and the procedures given in Reference 1, are tabulated for comparison with corresponding measured values. On all tests, a second shock was received at the test station. The peak overpressure recorded and the time of arrival of the second shock following the first shock are tabulated for each shot. Reproductions of the oscillogram traces of overpressure time-history measurements for Shots Franklin, Wilson, Kepler, Owens, and Stokes are shown in Figures B.2 to B.6, respectively.

In Chapter 3 of Reference 3, preliminary results of the records obtained with the VLP gages installed adjacent to the Project 5.2 gages were reported for Shots Owens and Stokes. Two VLP gage records were reported for each of these shots; the peak pressures were 0.12 and 0.07 psi for Shot Owens and 0.17 and 0.13 psi for Shot Stokes. These peak pressures were much lower than the corresponding values obtained with the most reliable Project 5.2 gages, namely, 0.55 psi for Shot Owens and 0.75 psi for Shot Stokes. The VLP gage records were subject to question, however, since Reference 3 states that ringing of the gages occurred, and satisfactory interpretation of such records is usually impossible.

As stated in Section 4.4, Project 5.2 overpressure recording systems were calibrated posttest in a BRL shock tube, and the dynamic response characteristics were determined to be accurate within 2 per cent over a range of shock pressures from 0.4 to 1.5 psi. Similar shock-tube calibration tests of the undamped VLP gages at BRL demonstrated that an excessive amount of oscillation occurs when an abrupt shock pressure is imposed; and, at overpressures above 0.3 psi, the VLP records were so poor that they could not be read satisfactorily. Also, the technique of static calibration used for the VLP gages apparently did not provide a calibration that was suitable for sharp pressure gradients. Consequently, it is believed that the VLP results reported in Reference 3 are unreliable and cannot be used to confirm or deny the accuracy of the shock overpressures recorded by Project 5.2.

B.3 DISCUSSION

A comparison of the measured and calculated values of peak overpressure is shown in Figure B.7. As expected, the higher frequency response characteristics of the overpressure-probe system yielded the highest readings of peak overpressure since this system was more capable of following the instantaneous pressure rise in the shock front. Time-history measurements of overpressure obtained with this system were considered to be most representative of the actual shock phenomena during the tests. Owing to lag in the response of the 30-cps systems, the true values of peak overpressure in the shock front have been attenuated, and the rise time to indicated peak values has been extended as shown in Figures B.4 to B.6. In all cases where second shocks were received, the peak values of overpressure recorded by the 135-cps and 30-cps systems were in agreement because of the longer time required to reach peak value (reduced pressure-time gradient in shock front).

As shown in Figures B.4 and B.5, all overpressure records showed an initial low rate of pressure build-up before rising sharply to peak value. The same overpressure characteristics were obtained during measurements on the airship during Shot Franklin, which would indicate that the installation arrangement on the airship was not a contributing factor in producing this effect.

Measured values of peak overpressure were consistently higher than the corresponding calculated values for each of the shots, as shown in Figure B.7. After some investigation, it was believed that the higher values may have been caused by (1) ground effects on the instrumentation; (2) surface reflections from atmospheric temperature inversions, existing at the time of test and resulting in higher overpressure levels at the test site; and (3) envelope shock-refraction influences.

Since the recording instruments were located from 4 to 5 feet aboveground in unobstructed level areas, it was assumed that any terrain or ground-baffle effect would be negligible on overpressure readings. On the other hand, atmospheric inversions could have a marked effect on overpressure levels at different locations. On all the shots, such inversions were present at the time of test. An attempt was made to calculate the effects of these inversions on producing higher overpressure levels at given test locations, using a formula developed by Sandia Corporation which was based on experimental data and theoretical work on the problem. Material on this subject is given in Reference 4. Results of the calculations, based on actual test conditions for the shots, indicated that overpressure levels higher than those predicted through the calculations of Reference 1 could have been experienced at the different test locations. In general, however, measured peak overpressures exceeded the calculated values (based on inversion effects) by a factor of 2 or more.

Time histories of overpressure measurements obtained with the 135-cps instrumentation system more accurately recorded the initial shock wave during each test than the 30-cps system.

The difference between measured and calculated values of peak overpressure was due, in part, to the presence of atmospheric inversions existing at the time of each shot.

TABLE B.1 SUMMARY OF TEST CONDITIONS AND OVERPRESSURE DATA

Shot	Franklin*	Wilson	Kepler	Owens	Stokes*
Test Conditions:					
Date of test (1957)	2 June	18 June	24 July	25 July	7 August
Ground zero	T-3	B-9A	T-4	B-9A	B-7B
Type of test	300-ft tower	500-ft balloon	500-ft balloon	500-ft balloon	1,500-ft balloon
Zero time, PDST	0455	0445	0455	0630	0525
Estimated yield of shot, kt	0.138	10.3	10.3	9.6	19.0
Altitude of burst above MSL, ft	4,326	4,715	4,808	4,715	5,686
Altitude of ground zero above MSL, ft	4,026	4,215	4,308	4,215	4,186
Altitude of test station above MSL, ft	3,976	4,050	3,924	3,924	3,924
Height of burst above test station, ft	350	667	884	791	1,762
Mean altitude between burst point and test station, MSL	4,151	4,384	4,365	4,319	4,805
Horizontal range from ground zero to test station, yards	6,067	9,230	17,513	20,439	14,388
Bearing of test station from ground zero, degrees	200	185	150	172	172
Line of sight angle from test station to burst, degrees	1.0	1.5	1.0	0.75	2.5
Ambient temperature at zero time at test station, °C	11.6	12.5	9.3	15.5	8.0
Reduced horizontal range for 1 kt at mean altitude, yards†	9,330	3,400	6,450	7,280	4,210
Calculated and Measured Overpressure:					
Calculated peak overpressure based on Reference 1, psi	0.08	0.23	0.11	0.095	0.19
Measured peak overpressure (probe), psi	0.40	0.77	0.67	0.55	0.75
Measured peak overpressure (differential pressure pickup on probe), psi	—	0.77	0.49	0.40	0.55
Measured peak overpressure (absolute pressure pickup on probe), psi	—	—	0.53	0.44	0.55
Time of arrival of second shock after first, sec	0.67	2.09	2.15	2.43	3.78
Peak overpressure in second shock (all pickups), psi	0.14	0.15	0.05	0.08	0.19
Height above MSL of inversion, feet	5,000	4,200	4,300	4,330	4,300
Temperature of inversion, °C	23.6	21.0	21.0	23.5	19.2

*Airship exposed on these shots.

†Obtained by dividing true horizontal range by the cube root of two times the estimated yield.

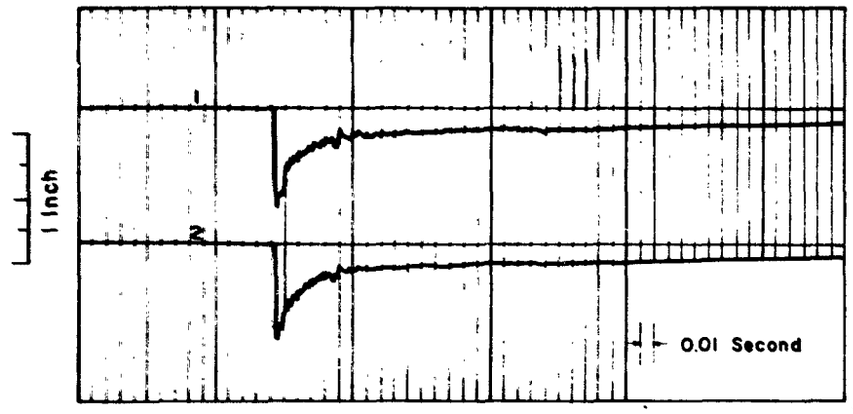

Figure B.3 Reproduction of oscillograph record of overpressure measurements, Shot Wilson. (1) Differential pressure pickup inside probe; Galvanometer 7-342, 0.7 critically damped, 135 cps; sensitivity, 1.11 psi per inch; (2) differential pressure pickup on top of probe; Galvanometer 7-342. 0.7 critically damped, 135 cps; sensitivity, 1.11 psi per inch

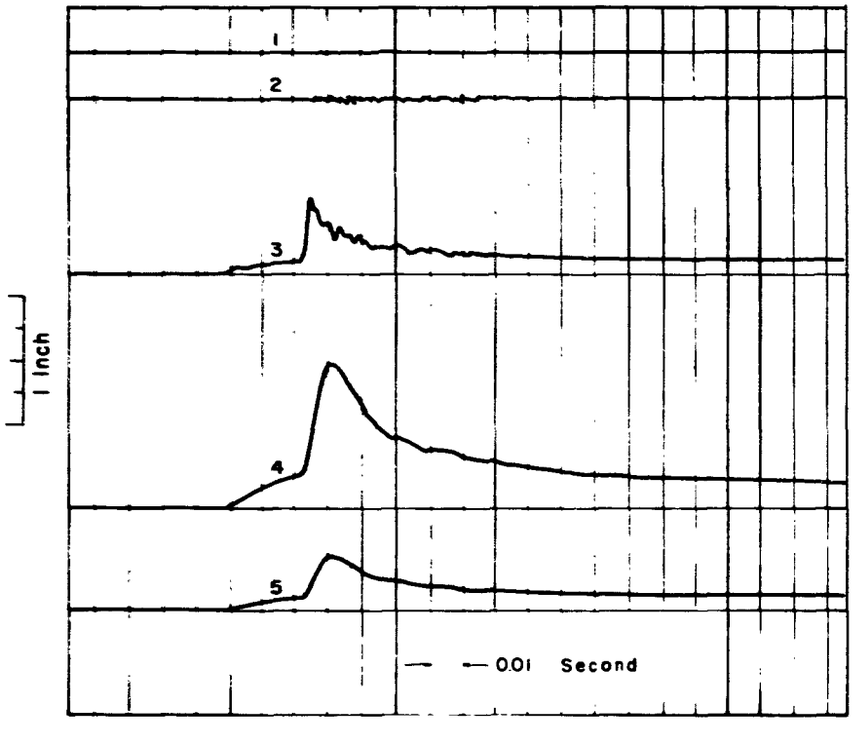

Figure B.4 Reproduction of oscillograph record of overpressure measurements, Shot Kepler. (1) Galvanometer 7-339. 0.7 critically damped, 30 cps; (2) Galvanometer 7-342, 0.7 critically damped, 135 cps; (3) differential pressure pickup inside probe; Galvanometer 7-342; sensitivity, 1.24 psi per inch; (4) differential pressure pickup on top of probe; Galvanometer 7-339; sensitivity, 0.45 psi per inch; (5) absolute pressure pickup on top of probe; Galvanometer 7-339; sensitivity, 1.26 psi per inch

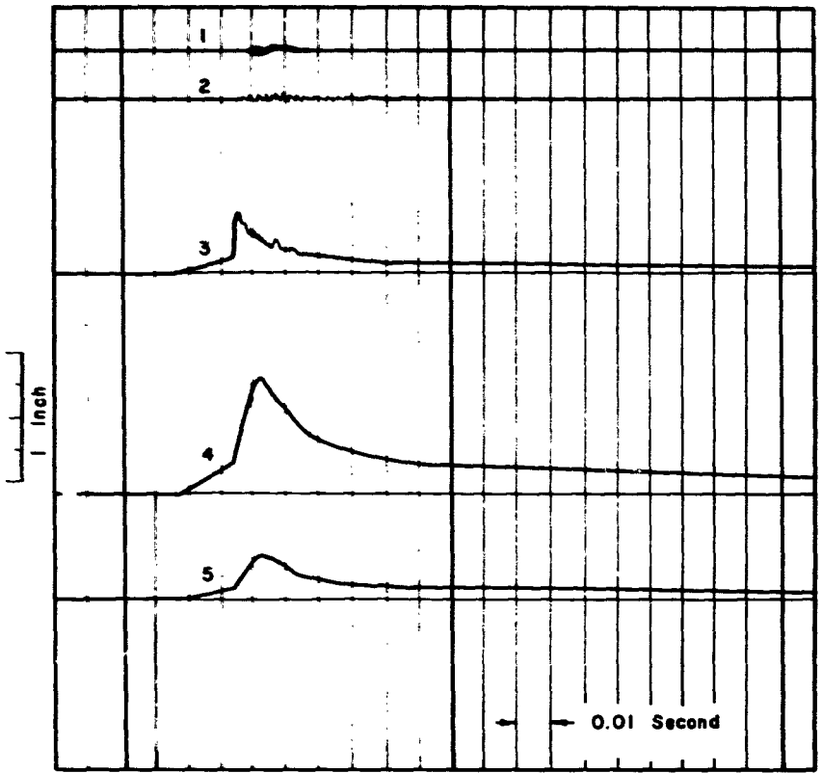

Figure B.5 Reproduction of oscillograph record of overpressure measurements, Shot Owens. (1) Galvanometer 7-339, 0.7 critically damped, 30 cps; (2) Galvanometer 7-342, 0.7 critically damped, 135 cps; (3) differential pressure pickup inside probe; Galvanometer 7-342; sensitivity, 1.23 psi per inch; (4) differential pressure pickup on top of probe; Galvanometer 7-339; sensitivity, 0.45 psi per inch; (5) absolute pressure pickup on top of probe; Galvanometer 7-339; sensitivity, 1.26 psi per inch.

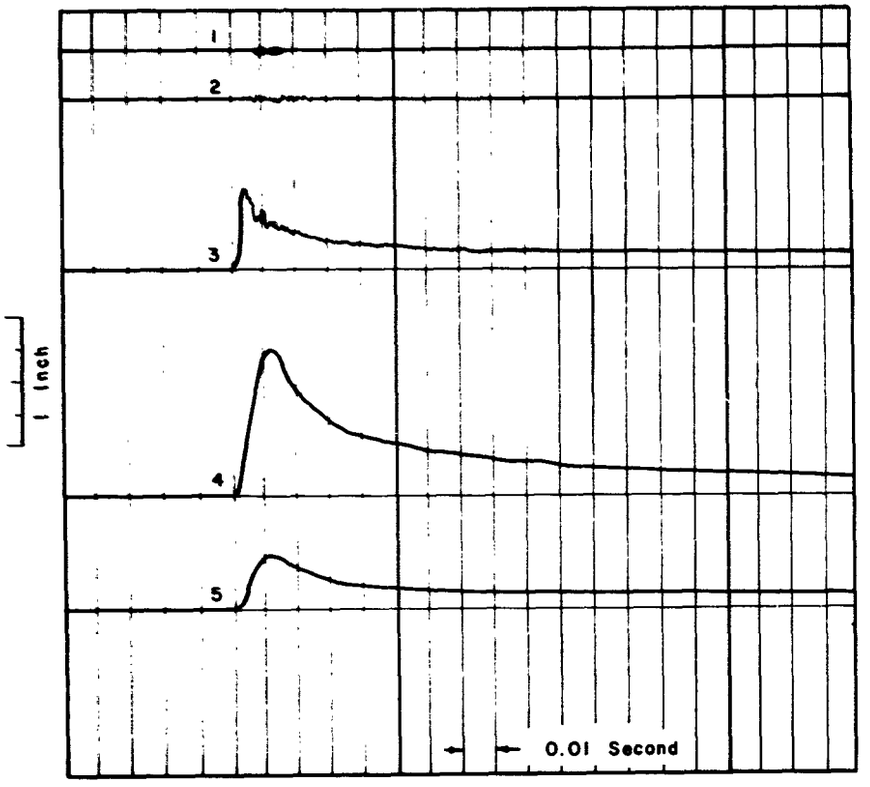

Figure B.6 Reproduction of oscillograph record of overpressure measurements, Shot Stokes. (1) Galvanometer 7-339, 0.7 critically damped, 30 cps; (2) Galvanometer 7-342, 0.7 critically damped, 135 cps; (3) differential pressure pickup inside probe; Galvanometer 7-342; sensitivity, 1.24 psi per inch; (4) differential pressure pickup on top of probe; Galvanometer 7-339; sensitivity, 0.45 psi per inch; (5) absolute pressure pickup on top of probe; Galvanometer 7-339; sensitivity, 1.27 psi per inch.

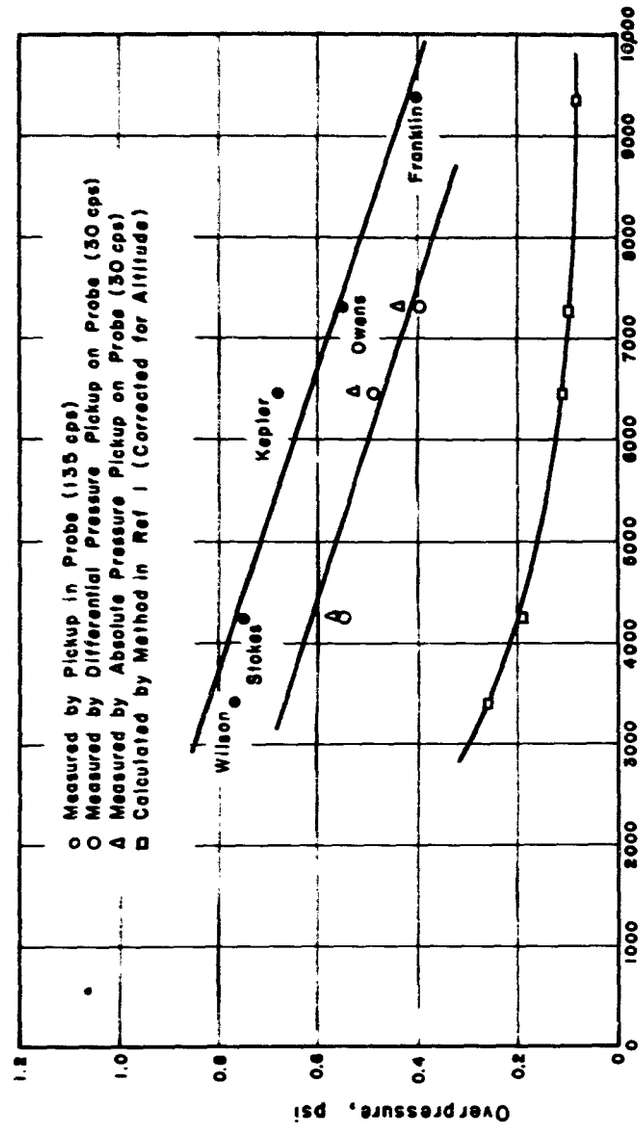

Figure B.7 Comparison of calculated and measured overpressures.

Additional measurements of overpressure versus time in the low overpressure region (below 1.0 psi) using instrumentation equipment and pickups with various frequency response ranges were desirable.

Studies and tests on the effects of atmospheric inversions on surface reflections should be continued, with emphasis on the effects within the low overpressure range (below 1.0 psi).

Appendix C

TRANSMISSION OF AIR-BLAST SHOCK INTO AN AIRSHIP ENVELOPE

C.1 BASIC AIR-HELIUM SHOCK-REFRACTION CHARACTERISTICS

To describe and correlate the effects of air-blast shock on an airship envelope, some degree of understanding of the nature of the air-helium shock-refraction process is necessary. The basic characteristics of the process of shock refraction and interaction are discussed in Reference 5, page 172; in References 6 and 7, the results of shock-tube tests and studies are reported. Considering a plane shock wave in air impinging on a helium region at an angle of incidence α, the two gases being separated by a film of zero mass, the shock patterns can be reasonably described. The refraction patterns vary with incidence angle, with the most significant change occurring at the critical angle α_j, as defined in Reference 6, i.e.:

$$\sin \alpha_j = \frac{a_1}{a_5}$$

where a_1 is the sound speed in air and a_5 is the sound speed in helium.

The resulting critical angle is of the order of 20 degrees for air and pure helium. At incidence angles below α_j, the shock pattern should be regular, as shown in Figure C.1. At incidence angles greater than α_j, the shock configuration changes to an irregular refraction pattern, as shown in Figure C.2. The transition from the regular pattern to the irregular pattern is primarily due to the fact that the physical conditions of the flow will not support an incidence angle of the transmitted shock of more than 90 degrees. Consequently, the transmitted shock will detach from its intersection with the incident shock when α_j is exceeded. The transmitted shock will then advance, parallel to the interface, at a speed that satisfies the shock conditions; for weak shocks, the transmitted wave should advance at approximately sonic speed in helium. The advance of the transmitted shock ahead of the incident shock results in a differential pressure between the helium and air in the region between the incident and transmitted shocks. This characteristic produces a retransmitted wave in air which is clearly seen in the interferograms of Reference 7. The retransmitted wave has been observed to consist of a shock front inclined at an angle β (defined by $\sin \beta = a_1/a_5$) and followed by a pressure gradient. As pointed out in Reference 6, page 36, as the incidence angle α is increased well beyond α_j, the inflow velocity in Region 5 becomes subsonic, and the transmitted shock may be expected to degenerate into a compression wave. This effect would probably weaken the retransmitted wave and decrease the pressure gradient in the affected region.

The quantitative parameter of primary interest in this shock-refraction problem is the relation between the strengths of the incident and transmitted shock waves. The theoretical strength of the transmitted shock in terms of the incident shock can be determined quite readily for a regular refraction pattern by the use of the procedures outlined in Reference 5, page 182, and further described in Reference 7, page 6. This method neglects any effects of the interface between gases, except that of physical separation in the sense of obviating mixing of the gases. Determination of the relative shock strengths for an irregular pattern, as described in the preceding paragraph, is a more difficult undertaking because of the complexity of the possible configurations and the multiple interaction between the two media. Since no adequate theoretical means appears to be available on which to base a quantitative estimate of the shock strengths in the irregular region, no attempt is made here to solve this problem. For cases in which the refraction is initiated at incidence angles in the regu-

lar region, followed by increasing angles into the irregular region, it may be anticipated that the primary transmitted shock strengths arise from the initial regular refraction and continue into the irregular region. This possibility seems quite likely for weak shocks in which overtaking of the primary transmitted wave by subsequent transmitted waves would be relatively slow.

The procedure for determining the peak pressure in the transmitted shock for regular refraction is taken from Reference 7. For air-helium refraction, the reflected wave should be a shock. The following equation relates all possible particle velocities and pressures behind the refracted wave (Figure C.3):

$$V_3 = V_2 - (P_3 - P_2)\sqrt{\frac{(1-\mu_2^2)\,\tau^2}{P_3 + \mu_2^2 P_2}} \qquad (C.1)$$

where V_3 = particle velocity behind reflected shock, ft/sec
V_2 = particle velocity behind incident shock, ft/sec
P_3 = pressure behind reflected shock, psf
P_2 = pressure behind incident shock, psf

$\mu_2^2 = (\gamma_2 - 1)/(\gamma_2 + 1)$
γ_2 (=γ_1) = ratio of specific heats in incident shock medium
$\tau_2 = 1/\rho_2$, slug/ft^3
ρ_2 = density behind incident shock, slug/ft^3

All possible velocities and pressures behind the transmitted wave are given by

$$V_4 = (P_4 - P_5)\sqrt{\frac{(1-\mu_5^2)\,\tau_5}{P_4 + \mu_5^2 P_5}} \qquad (C.2)$$

where V_4 = particle velocity behind transmitted shock
P_4 = pressure behind transmitted shock
P_5 = pressure ahead of transmitted shock
$\mu_5^2 = \frac{\gamma_5 - 1}{\gamma_5 + 1}$
γ_5 = ratio of specific heats in transmitted shock medium
τ_5(=$1/\rho_5$) = reciprocal of density ahead of transmitted shock

The condition arising from the assumption that the interface provides no resistance to pressure results in equality of the pressures and corresponding particle velocities in Regions 3 and 4. Equations C.1 and C.2 can then be solved, quite simply by graphical means, for the common pressures P_3 and P_4. From solutions for various values of P_2 corresponding to a range of incident overpressures, a relation between incident pressure ratios and transmitted pressure ratios can be established. Figure C.4 shows the resulting relations between the transmitted overpressures and the incident overpressures for helium purities from 90 to 98 percent. By expressing the overpressures as ratios of the ambient pressures, the relations given in Figure C.4 have been determined to apply for standard atmospheric conditions at all altitudes from sea level to at least 5,000 feet.

C.2 APPLICABILITY OF BASIC REFRACTION CHARACTERISTICS TO INTERACTION OF SHOCK WAVES WITH AN AIRSHIP ENVELOPE

The basic refraction characteristics discussed in Section C.1 relate to ideal conditions that are violated to some degree in the actual case of the airship. A primary assumption of the theory, as well as of the shock-tube studies, is that the interface offers no resistance to the pressures created, but only prevents material translation of the gases through the interface. Displacement of the boundary between gases is permitted for equilibrium. The airship envelope confines the helium at a pressure somewhat above atmospheric to maintain its shape and to support the distributed loads. Since the envelope is fully inflated, the deformation, or stretch, caused by increasing internal pressure is comparatively small; consequently, it may be expected that the transmission of excess pressure from the helium to air would be attenuated to some degree. For pressure transmission from the air to the envelope, the elastic resistance of the envelope fabric should be unimportant. The effects of the mass of the envelope fabric on transient interaction phenomena may be significant, but no means for estimating such effects appear to be practicable at the present time.

Considering a plane incident shock wave, the shock initially impinges at normal incidence at some point on the envelope. When the shock front is normal to the airship longitudinal axis, regular refraction would exist only for the initial 1 foot or less of shock travel. As the shock incidence angle exceeds α_j, the refraction pattern should change to a series of irregular patterns, as described in Reference 6, page 26. The interaction for the major portion of the shock-front travel over the envelope would conform to the configuration shown in Figure C.2. The effects of the interface mass and stiffness should attenuate the retransmitted wave but should have only a minor influence on the transmitted wave and the rarefaction wave.

The strength of the transmitted wave can be estimated from Figure C.4 since the refraction is initiated in the regular region, and the effects of the interface mass and stiffness should be small for conditions involving compression of the envelope. The characteristics of the transmitted wave would probably be those of a compression wave, i.e., no sharply defined shock front, for the reasons mentioned in Section C.1.

C.3 SIGNIFICANT EFFECTS OF SHOCK REFRACTION ON AIRSHIP ENVELOPE

The effects on an airship envelope resulting from the hypothesis set forth in Sections C.1 and C.2 may

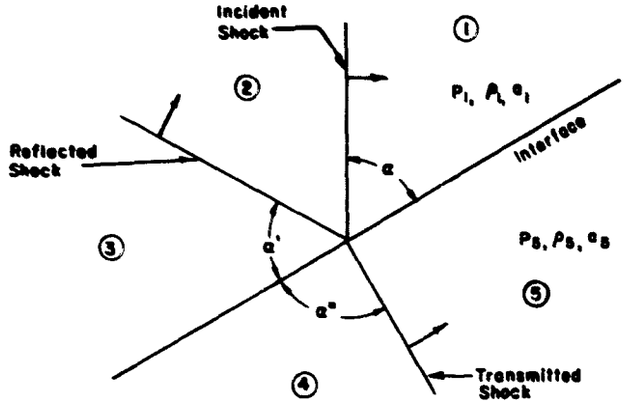

Figure C.1 Regular refraction pattern.

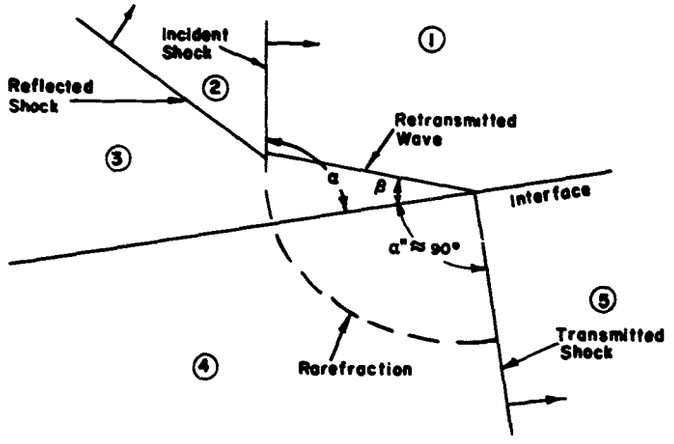

Figure C.2 Irregular refraction pattern.

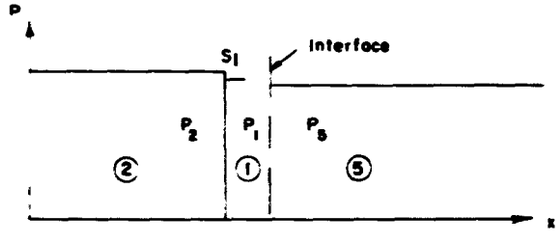

(a) Before Interaction

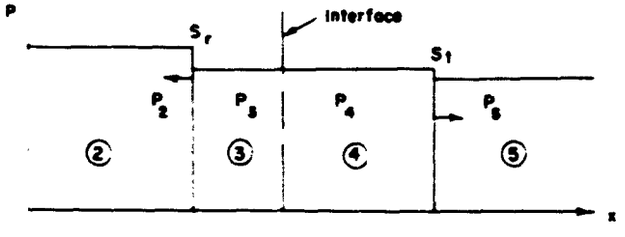

(b) After Interaction

Figure C.3 Schematic pressure diagrams for interaction of shock at normal incidence.

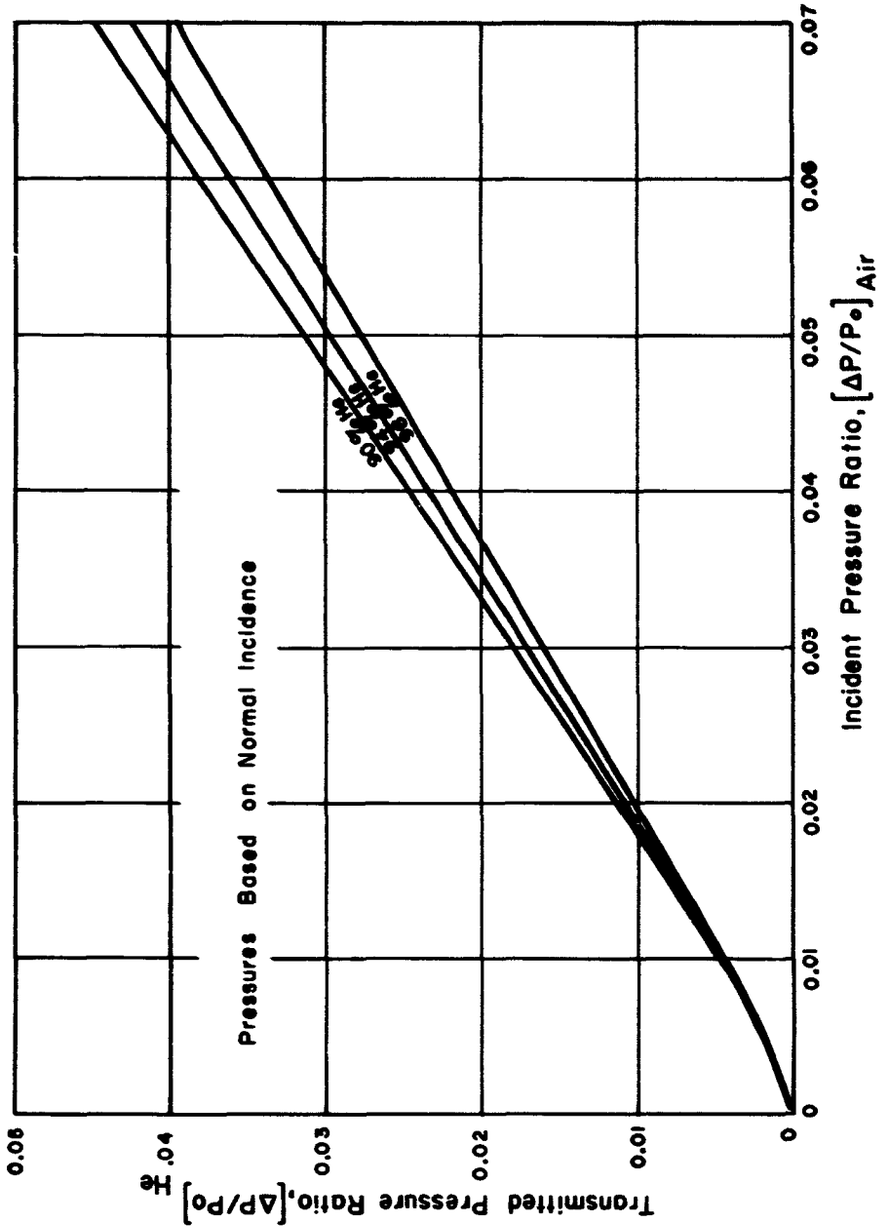

Figure C-4 Air-helium shock-refraction pressures.

form a reasonable basis for correlation with the experimental data and for further studies of airship response to shock waves for various conditions. If the envelope could be considered a rigid body, its response to pressure loads could be determined from appropriate integrations of the external pressure distributions. Since the envelope cannot be expected to support any appreciable tangential compressive forces, the rigid-body approach does not appear useful. The direct effects of the shock interaction should be (1) incremental stresses in the envelope fabric because of the advance of the transmitted wave inside the envelope ahead of the external shock creating a pressure differential across the fabric and (2) a net force in the general direction of the shock propagation because of the transmitted pressures acting on the inside surface of the envelope ahead of the external shock front. The local incremental pressures creating envelope fabric stresses cannot be adequately defined by the techniques discussed in Sections C.1 and C.2 because of the complex characteristics of the irregular refraction patterns and the extremely transient nature of these local pressures. It should be possible to estimate the peak forces on the envelope as a whole, however, by the use of the pressure ratios defined in Figure C.4. The time of occurrence of the peak translational force caused by pressure could be determined from the speed of sound in helium and the geometries involved if the transmitted wave exhibited a sharply defined shock front. With the transmitted wave characterized as a compression wave, the initial beginning of the pressure rise should correspond to sonic arrival time, but the peak pressure would lag because of slower pressure rise. Stipulation of such a pressure rise time for the general case does not appear possible.

Appendix D
SUSPENSION SYSTEM ANALYSIS

A theoretical method of analysis of airship suspension systems which represents the latest method of analyzing these redundant systems has been developed by the Goodyear Aircraft Corporation and is reported in Reference 8. Although the method is strictly applicable only to static-loading conditions, it considers the various elastic parameters of primary significance in establishing the distribution of loads among the components of the suspension system. By treating the blast-loading conditions as quasi-static, i.e., establishing equations of equilibrium for a particular time, it appeared that this method should provide a reasonable approximation for correlation with the test data.

The elastic properties of the external systems are more critically dependent on detailed characteristics of catenary fabrics, cable attachments, and similar construction factors than are the properties of the internal systems. The determination of these elastic parameters for the external systems would require experimental data that have not been obtained for the ZSG-3 airship. Consequently, the analysis as applied here considers only the flexibility of the internal suspension systems.

The car of the nonrigid ZSG-3 airship was suspended by two internal cable systems. The total number of cables was great and effected a high degree of structural redundancy.

Although a suitable set of rigging tensions can be calculated for a given basic or rigging condition, the determination of the cable loads for any other loading condition poses a rather complex problem, whose intricacy is aggravated by the fact that the relations between the cable loads and the deformation of the envelope produced by them are of a nonlinear nature.

The analytical method given in Table D.1 is a method of compatibility, which, in general, applies to any cable pair of either of the internal suspension systems. The method covers variations in all symmetrical load parameters, i.e., those which produce equal changes in the port and starboard cable of each cable pair. The equation of compatibility reflects the effect on the cable-load distribution of the following items:

1. Displacement of the theoretical cable-envelope attachment points in the vertical and lateral directions.
2. Vertical and angular displacement and acceleration of the airship car as a rigid body.
3. Elastic or inelastic bending and shear deformations of the envelope as a whole caused by the changes in its bending moments and shear forces.

TABLE D.1 INTERNAL CABLE-LOAD CALCULATIONS

1	2	3	4	5	6	7	8	9	10	11	12	13	14	15	16
Suspension Cable Number (30° and 60° Systems)	Number of Cables	Initial Tension Load (Sbd & Port Cables)	Z Factor for Vertical Load Components	Vertical Component of Resultant R of Initial Tension Load (Sbd & Port Cables)	Effective Carrying Envelope Length Per Cable Pair	Z Component of Curtain Load (Sbd & Port Side)	Slope of Curve of W vs. y (Lateral) Component of Envelope Deflection at Curtain to Envelope Attachment Point	Slope of Curve W vs. z (Vertical) Component of Envelope Deflection at Curtain to Envelope Attachment Point	β_i = Angle Between x-y Plane and Plane of Curtain	$m_{y_i} \cot \beta_i$	α = Angle of Inclination of R with the x-y Plane	$\bar{\lambda}/s_i$	Factor of Elastic Resistance Due to Cable Loading $\left(s_i = \frac{\bar{\lambda}_i}{(m_{z_i} - m_{y_i} \cot \beta) \csc \alpha_i}\right)$	Distance of Car Cable Attachment Point Aft of Frame 11	Elastic Resistance Due to Cable Loading
		V_{l_0}		R_z ③ × ④	$\bar{\lambda}_i$	W ⑧/⑥	m_{y_i}	m_{z_i}	$\cot \beta_i$	$m_{y_i} \cot \beta_i$ ⑧ × ⑩	$\csc \alpha_i$	[⑨ − ⑪] ⑫	s_i ⑥/⑬	x_i	$s_i x_i$ ⑭ × ⑮
		lbs		lbs	ft	lbs/ft	ft/lb/ft	ft/lb/ft		ft/lb/ft		ft/lb/ft	lb/ft	ft	lb
1_{30}	1	1030	0.857	0.875	44.8	19.5	−0.00267	0.00425	+0.577	−0.00154	1.2265	0.00710	6310	38.30	241,700
3_{30}	2	1377	0.911	0.1253	42.4	29.6	−0.00274	0.00439	+0.577	−0.00158	1.0877	0.00649	6533	30.70	200,600
5_{30}	2	1736	0.970	0.1682	42.4	39.7	−0.00281	0.00452	+0.577	−0.00162	1.0134	0.00622	6617	22.80	150,400
7_{30}	2	1809	0.980	0.1770	42.4	41.7	−0.00282	0.00455	+0.577	−0.00163	1.0065	0.00622	6617	15.45	105,300
9_{30}	2	2286	0.941	0.2150	42.0	50.7	−0.00369	0.00340	+0.577	−0.00213	1.0680	0.00591	7107	7.50	53,300
11_{30}	2	1290	0.894	0.1153	46.8	24.6	−0.00270	0.00432	+0.577	−0.00156	1.1890	0.00699	6695	0	0
1_{60}	2	1661	0.734	0.1220	48.8	25.0	−0.00230	0.00315	+0.500	−0.00115	1.2804	0.00551	8887	38.30	339,200
3_{60}	2	1913	0.815	0.1560	41.2	37.8	−0.00246	0.00325	+0.552	−0.00136	1.0959	0.00505	8156	30.70	250,500
5_{60}	2	2082	0.886	0.1845	42.0	44.0	−0.00254	0.00330	+0.485	−0.00123	1.0192	0.00462	9091	22.80	207,300
7_{60}	2	2070	0.895	0.1855	41.6	44.5	−0.00255	0.00330	+0.483	−0.00123	1.0079	0.00457	9103	15.45	140,600
9_{60}	2	1567	0.847	0.1342	41.6	32.3	−0.00346	0.00285	+0.500	−0.00174	1.0714	0.00492	6485	7.50	63,400
11_{60}	2	1722	0.769	0.1325	49.6	26.7	−0.00232	0.00328	+0.467	−0.00108	1.2146	0.00530	9358	0	0
		Σ = 20,045		Σ = 18,030									Σ = 93,301		Σ = 1,737,300

(Columns 17 to 31 are continued on the next page.)

TABLE D.1 — (Continued)

17	18	19	20	21	22	23	24	25	26	27	28	29	30	31
Elastic Resistance Moment			Internal Absolute Pressure Referenced to Internal Ambient Helium Pressure	Internal Absolute Pressure Referenced to Internal Ambient Air Pressure	Envelope Deflection in the z (Vertical) Direction Due to Change in Envelope Pressure	Envelope Deflection in the y (Lateral) Direction Due to Change in Envelope Pressure		Elastic Resistance Due to Pressure Loading (Q_i = [−ΔZ_{p_i} + ΔY_{p_i} cot β_i csc α_i] a_i)	Elastic Resistance Pressure Moment	Factor of Elastic Resistance (a_i) × Displacement of Car (V) (in the z direction)	Factor of Elastic Resistance ($a_i x_i \theta$) × Car Angle of Rotation (θ) (about y axis)	ΔV_i, Vertical Component of Cable Loads (Calculated at 0.2 Second	ΔV_i, Vertical Component of Cable Loads (Measured at 0.2 Second	Distance of Cable–Envelope Attachment Point Aft Most Forward Cable
$a_i \Sigma_i^j$	cot α_i	a_i cot α_i	ΔP_h	ΔP_a	ΔZ_{p_i}	ΔY_{p_i}	ΔY_{p_i} cot β_i	Q_i	Q_{x_i}	$a_i V$	$a_i x_i \theta$	ΔV_i	ΔV_i	X
(18) × (19)		(14) × (18)	lb_h/ft^2	lb_a/ft^2			(19) + (23)	[(25) + ((24) × (18))] (14)	(26) × (19)	(14) × 0.8433	(19) × (−0.0221)	(28) + (27) + (26)		
lb/ft		lb/ft			ft	ft	ft	lb	lb/ft	lb	lb	lb	lb	ft
9,257,000	0.7100	4480	−1.94	0	0	0	0	0	0	3428	−5242	−1914	− 887	136
6,180,000	0.4280	2796	0.22	2.22	−0.067	0.051	0.029	−229	−7030	3549	−4433	−1113	−1302	84
3,843,000	0.1640	1118	1.72	3.72	−0.104	0.078	0.045	−395	−9006	2704	−3434	− 128	−1971	64
1,627,000	−0.1140	− 777	3.32	5.32	−0.134	0.100	0.058	−516	−8003	2704	−2327	899	− 392	42
400,000	−0.3760	−2672	4.43	6.43	−0.147	0.109	0.063	−569	−4268	3661	−1178	2114	2140	22
0	−0.6430	−4305	5.00	7.00	−0.151	0.112	0.065	−495	0	3637	0	3142	3665	0
12,991,000	0.7997	7083	−1.94	0	0	0	0	0	0	4812	−7496	−2684	− 880	106
7,680,000	0.4480	3685	0.22	2.22	−0.052	0.042	0.023	−220	−6784	4432	−5536	−1234	−1297	84
4,726,000	0.1968	1789	1.72	3.72	−0.080	0.067	0.032	−427	−9736	4939	−4861	− 69	−1374	64
2,172,000	−0.1297	−1144	3.32	5.32	−0.101	0.088	0.043	−526	−8158	4945	−3107	1310	90	42
475,000	−0.3880	−3355	4.43	6.43	−0.110	0.098	0.049	−490	−3675	4593	−1401	2702	2965	22
0	−0.6890	−6448	5.00	7.00	−0.112	0.101	0.047	−515	0	5064	0	4569	3455	0
Σ = 49,039,000		Σ = 2320						Σ = −4386	Σ = −56,630	Σ = 50,688	Σ = 38,835	Σ = 7,467	Σ = 5,752	

$V\Sigma(14) = -\theta\Sigma(16) - \Sigma(24) + (\text{Vert. Accel.} \times \text{Car Wt.})$

$V\Sigma x_i = -\theta\Sigma x_i \Sigma_i^j - \Sigma Q_{x_i} + \Delta Z$

93,201 $V = -1{,}787{,}300\,\theta + 4{,}386 + 0.4\ g\ (18{,}665)$

93,201 $V = -1{,}787{,}300\,\theta + 11{,}852$

$V = -18.835\,\theta + 0.1270$

$V = 0.4163 + 0.1270$

$V = 0.8433$ feet

$$V\Sigma(16) = -\theta\Sigma(17) - \Sigma(26) + \left\{\left(\begin{matrix}\text{Hor. Dist. C.G. to}\\ \text{Car Fwd. Attach. Pt.}\end{matrix}\right) \times \left(\begin{matrix}\text{Vert.}\\ \text{Accel.}\end{matrix}\right) \times \left(\begin{matrix}\text{Car}\\ \text{Wt.}\end{matrix}\right)\right\} + \left\{\left(\begin{matrix}\text{Vert. Dist. C.G. to}\\ \text{Car Cable Attach. Pt.}\end{matrix}\right) \times \left(\begin{matrix}\text{Hor.}\\ \text{Accel.}\end{matrix}\right) \times \left(\begin{matrix}\text{Car}\\ \text{Wt.}\end{matrix}\right)\right\}$$

$V\Sigma x_i x_i = -\theta\Sigma x_i \Sigma_i^j - \Sigma Q_{x_i} + m_{y_i}$

1,787,300 $V = -49{,}039{,}000\,\theta + 56{,}630 + 25.08\ (0.4\ g)\ (18{,}665) - 373{,}300$

$V = -27.906\,\theta - 129{,}470$

$27.906\,\theta - 18.835\,\theta = -0.1270 - 0.0727$

$9.071\,\theta = -0.2007$

$\theta = -0.0221$ radian, or -1.27 degrees

REFERENCES

1. "Capabilities of Atomic Weapons"; TM 23-200, Revised Edition; prepared by Armed Forces Special Weapons Project, 1 June 1955; Secret Restricted Data.

2. Charles P. Burgess; "Airship Design"; 1927; The Ronald Press Company, New York; Unclassified.

3. E. J. Bryant and J. H. Keefer; "Basic Air-blast Phenomena, Part 2"; Project 1.1, Operation Plumbbob, ITR-1481, December 1957; Ballistic Research Laboratories, Aberdeen Proving Ground, Maryland; Confidential. Formerly Restricted Data.

4. E. F. Cox and J. W. Reed; "Long-distance Blast Predictions, Microbarometric Measurements, and Upper-atmosphere Meteorological Observations for Operations Upshot-Knothole, Castle, and Teapot"; WT-9003; September 1957; Sandia Corporation, Albuquerque, New Mexico; Secret Restricted Data.

5. R. Courant and K. O. Friedricks; "Supersonic Flow and Shock Waves"; 1948; Interscience Publishers, Incorporated, New York; Unclassified.

6. W. Bleakney and R. G. John; "The Refraction of Shock Waves at a Gaseous Interface. III. Irregular Refraction"; Technical Report II-19, April 1955; Princeton University, Department of Physics, Princeton, New Jersey; Unclassified.

7. R. G. Stoner and D. C. Hock; "Interaction of Shock Waves at a Plane Gaseous Interface at Grazing Incidence"; Technical Report 445-1, September 1955; Pennsylvania State University, Department of Physics; Unclassified.

8. A. F. Foerster; "A Method of Analysis of the Car Suspension Systems of Nonrigid Airships"; GER-6954, July 1958; Goodyear Aircraft Corporation, Akron, Ohio; Unclassified.

DISTRIBUTION

Military Distribution Categories 52 and 54

ARMY ACTIVITIES

1 Deputy Chief of Staff for Military Operations, D/A, Washington 25, D.C. ATTN: Dir. of SW&R
2 Chief of Research and Development, D/A, Washington 25, D.C. ATTN: Atomic Div.
3 Assistant Chief of Staff, Intelligence, D/A, Washington 25, D.C.
4 Chief of Engineers, D/A, Washington 25, D.C. ATTN: ENGTB
5- 6 Office, Chief of Ordnance, D/A, Washington 25, D.C. ATTN: ORDTX
7 Chief Signal Officer, D/A, Plans, Programs, and Ops. Div., Washington 25, D.C. ATTN: SIGOP-7A
8 Chief of Transportation, D/A, Office of Planning and Int., Washington 25, D.C.
9- 11 Commanding General, U.S. Continental Army Command, Ft. Monroe, Va.
12 Director of Special Weapons Development Office, Headquarters CONARC, Ft. Bliss, Tex. ATTN: Capt. Chester I. Peterson
13 President, U.S. Army Artillery Board, Ft. Sill, Okla.
14 President, U.S. Army Air Defense Board, Ft. Bliss, Tex.
15 President, U.S. Army Aviation Board, Ft. Rucker, Ala. ATTN: ATBG-DG
16 Commandant, U.S. Army Command & General Staff College, Ft. Leavenworth, Kansas. ATTN: ARCHIVES
17 Commandant, U.S. Army Air Defense School, Ft. Bliss, Tex. ATTN: Command & Staff Dept.
18 Commandant, U.S. Army Artillery and Missile School, Ft. Sill, Okla. ATTN: Combat Development Department
19 Commandant, U.S. Army Aviation School, Ft. Rucker, Ala.
20 Commandant, U.S. Army Ordnance School, Aberdeen Proving Ground, Md.
21 Commandant, U.S. Army Ordnance and Guided Missile School, Redstone Arsenal, Ala.
22 Commanding General, U.S. Army Chemical Corps, Research and Development Comd., Washington 25, D.C.
23- 24 Commanding Officer, Chemical Warfare Lab., Army Chemical Center, Md. ATTN: Tech. Library
25 Commanding Officer, Diamond Ord. Fuze Labs., Washington 25, D.C. ATTN: Chief, Nuclear Vulnerability Br. (230)
26- 27 Commanding General, Aberdeen Proving Grounds, Md. ATTN: Director, Ballistics Research Laboratory
28- 29 Commanding General, U.S. Army Ord. Missile Command, Redstone Arsenal, Ala.
30 Commander, Army Rocket and Guided Missile Agency, Redstone Arsenal, Ala. ATTN: Tech Library
31 Commanding General, White Sands Proving Ground, Las Cruces, N. Mex. ATTN: ORDBS-OM
32 Commander, Army Ballistic Missile Agency, Redstone Arsenal, Ala. ATTN: ORDAB-HT
33 Commanding General, Ordnance Ammunition Command, Joliet, Ill.
34 Commanding General, USA Combat Surveillance Agency, 1124 N. Highland St., Arlington, Va.
35 Commanding Officer, USA Transportation Research Command, Ft. Eustis, Va. ATTN: Chief, Tech. Info. Div.
36 Commanding Officer, USA Transportation Combat Development Group, Ft. Eustis, Va.
37 Director, Operations Research Office, Johns Hopkins University, 6935 Arlington Rd., Bethesda 14, Md.
38 Commander-in-Chief, U.S. Army Europe, APO 403, New York, N.Y. ATTN: Opot. Div., Weapons Br.

NAVY ACTIVITIES

39 Chief of Naval Operations, D/N, Washington 25, D.C. ATTN: OP-03EG
40 Chief of Naval Operations, D/N, Washington 25, D.C. ATTN: OP-75
41 Chief of Naval Operations, D/N, Washington 25, D.C. ATTN: OP-92D1
42- 43 Chief of Naval Research, D/N, Washington 25, D.C. ATTN: Code 811
44- 45 Chief, Bureau of Aeronautics, D/N, Washington 25, D.C.
46- 50 Chief, Bureau of Aeronautics, D/N, Washington 25, D.C. ATTN: AER-AD-41/20
51 Chief, Bureau of Ordnance, D/N, Washington 25, D.C.
52 Chief, Bureau of Ordnance, D/N, Washington 25, D.C. ATTN: S.P.
53 Director, U.S. Naval Research Laboratory, Washington 25, D.C. ATTN: Mrs. Katherine H. Cass
54- 55 Commander, U.S. Naval Ordnance Laboratory, White Oak, Silver Spring 19, Md.
56 Director, Material Lab. (Code 900), New York Naval Shipyard, Brooklyn 1, N.Y.
57 Commanding Officer, U.S. Naval Mine Defense Lab., Panama City, Fla.
58- 59 Commanding Officer, U.S. Naval Radiological Defense Laboratory, San Francisco, Calif. ATTN: Tech. Info. Div.
60 Commanding Officer, U.S. Naval Schools Command, U.S. Naval Station, Treasure Island, San Francisco, Calif.
61 Superintendent, U.S. Naval Postgraduate School, Monterey, Calif.
62 Commanding Officer, Nuclear Weapons Training Center, Atlantic, U.S. Naval Base, Norfolk 11, Va. ATTN: Nuclear Warfare Dept.
63 Commanding Officer, Nuclear Weapons Training Center, Pacific, Naval Station, San Diego, Calif.
64 Commanding Officer, U.S. Naval Damage Control Trng. Center, Naval Base, Philadelphia 12, Pa. ATTN: ABC Defense Course
65 Commanding Officer, Air Development Squadron 5, VX-5, China Lake, Calif.
66 Director, Naval Air Experiment Station, Air Material Center, U.S. Naval Base, Philadelphia, Pa.
67 Commander, Officer U.S. Naval Air Development Center, Johnsville, Pa. ATTN: NAS, Librarian
68 Commanding Officer, Naval Air Sp. Wpns. Facility, Kirtland AFB, Albuquerque, N. Mex.
69 Commander, U.S. Naval Ordnance Test Station, China Lake, Calif.
70 Commandant, U.S. Marine Corps, Washington 25, D.C. ATTN: Code A03H
71 Director, Marine Corps Landing Force, Development Center, MCS, Quantico, Va.
72 Commanding Officer, U.S. Naval CIC School, U.S. Naval Air Station, Glynco, Brunswick, Ga.

AIR FORCE ACTIVITIES

73 Assistant for Atomic Energy, HQ, USAF, Washington 25, D.C. ATTN: DCS/O
74 Hq. USAF, ATTN: Operations Analysis Office, Office, Vice Chief of Staff, Washington 25, D. C.
75- 76 Air Force Intelligence Center, HQ. USAF, ACS/I (AFCIN-3V1) Washington 25, D.C.
77 Director of Research and Development, DCS/D, HQ. USAF, Washington 25, D.C. ATTN: Guidance and Weapons Div.
78 The Surgeon General, HQ. USAF, Washington 25, D.C. ATTN: Bio.-Def. Pre. Med. Division
79 Commander, Tactical Air Command, Langley AFB, Va. ATTN: Doc. Security Branch
80 Commander, Air Defense Command, Ent AFB, Colorado. ATTN: Assistant for Atomic Energy, ADLDC-A
81 Commander, Hq. Air Research and Development Command, Andrews AFB, Washington 25, D.C. ATTN: RDSWA
82 Commander, Air Force Ballistic Missile Div. HQ. ARDC, Air Force Unit Post Office, Los Angeles 45, Calif. ATTN: WDSOT

83- 84 Commander, AF Cambridge Research Center, L. G. Hanscom Field, Bedford, Mass. ATTN: CRQST-2
85- 89 Commander, Air Force Special Weapons Center, Kirtland AFB, Albuquerque, N. Mex. ATTN: Tech. Info. & Intel. Div.
90- 91 Director, Air University Library, Maxwell AFB, Ala.
92 Commander, Lowry Technical Training Center (TW), Lowry AFB, Denver, Colorado.
93 Commandant, School of Aviation Medicine, USAF, Randolph AFB, Tex. ATTN: Research Secretariat
94 Commander, 1009th Sp. Wpns. Squadron, HQ. USAF, Washington 25, D.C.
95- 97 Commander, Wright Air Development Center, Wright-Patterson AFB, Dayton, Ohio. ATTN: WCOSI
98- 99 Director, USAF Project RAND, VIA: USAF Liaison Office, The RAND Corp., 1700 Main St., Santa Monica, Calif.
100 Commander, Air Defense Systems Integration Div., L. G. Hanscom Field, Bedford, Mass. ATTN: SIDE-S
101 Chief, Ballistic Missile Early Warning Project Office, 220 Church St., New York 13, N.Y. ATTN: Col. Leo V. Skinner, USAF
102 Commander, Air Technical Intelligence Center, USAF, Wright-Patterson AFB, Ohio. ATTN: AFCIN-4Bla, Library
103 Assistant Chief of Staff, Intelligence, HQ. USAFE, APO 633, New York, N.Y. ATTN: Directorate of Air Targets
104 Commander-in-Chief, Pacific Air Forces, APO 953, San Francisco, Calif. ATTN: PFCIE-MB, Base Recovery

OTHER DEPARTMENT OF DEFENSE ACTIVITIES

105 Director of Defense Research and Engineering, Washington 25, D.C. ATTN: Tech. Library
106 Chairman, Armed Services Explosives Safety Board, DOD, Building T-7, Gravelly Point, Washington 25, D.C.
107 Director, Weapons Systems Evaluation Group, Room 1E880, The Pentagon, Washington 25, D.C.
108-111 Chief, Defense Atomic Support Agency, Washington 25, D.C. ATTN: Document Library
112 Commander, Field Command, DASA, Sandia Base, Albuquerque, N. Mex.
113 Commander, Field Command, DASA, Sandia Base, Albuquerque, N. Mex. ATTN: FCTG
114-118 Commander, Field Command, DASA, Sandia Base, Albuquerque, N. Mex. ATTN: FCWT
119 Administrator, National Aeronautics and Space Administration, 1520 "H" St., N.W., Washington 25, D.C. ATTN: Mr. R. V. Rhode
120 Commander-in-Chief, Strategic Air Command, Offutt AFB, Neb. ATTN: OAWS
121 Commander-in-Chief, NORAD, APO 128, New York, N.Y.

ATOMIC ENERGY COMMISSION ACTIVITIES

122-124 U.S. Atomic Energy Commission, Technical Library, Washington 25, D.C. ATTN: For DMA
125-126 Los Alamos Scientific Laboratory, Report Library, P.O. Box 1663, Los Alamos, N. Mex. ATTN: Helen Redman
127-131 Sandia Corporation, Classified Document Division, Sandia Base, Albuquerque, N. Mex. ATTN: H. J. Smyth, Jr.
132-134 University of California Lawrence Radiation Laboratory, P.O. Box 808, Livermore, Calif. ATTN: Clovis G. Craig
135 Essential Operating Records, Division of Information Services for Storage at AEC-H. ATTN: John E. Hans, Chief, Headquarters Records and Mail Service Branch, U.S. AEC, Washington 25, D.C.
136 Weapon Data Section, Technical Information Service Extension, Oak Ridge, Tenn.
137-170 Technical Information Service Extension, Oak Ridge, Tenn. (Surplus)